R89-917704-1

(4)

CARBON FIBER REINFORCED GLASS MATRIX COMPOSITES FOR STRUCTURAL SPACE BASED APPLICATIONS

Prepared by

W. K. Tredway
K. M. Prewo

FINAL REPORT

Contract N00014-85-C-0332

for

Department of the Navy
Office of Naval Research
Arlington, VA 22217

July 31, 1989

UNITED TECHNOLOGIES RESEARCH CENTER
East Hartford, Connecticut 06108

REPORT DOCUMENTATION PAGE

Form Approved OMB No. 0704-0188

1a. REPORT SECURITY CLASSIFICATION: Unclassified	1b. RESTRICTIVE MARKINGS: None
2a. SECURITY CLASSIFICATION AUTHORITY	3. DISTRIBUTION/AVAILABILITY OF REPORT: Unlimited
2b. DECLASSIFICATION/DOWNGRADING SCHEDULE	
4. PERFORMING ORGANIZATION REPORT NUMBER(S): R89-917704-1	5. MONITORING ORGANIZATION REPORT NUMBER(S)
6a. NAME OF PERFORMING ORGANIZATION: United Technologies Research Center; 6b. OFFICE SYMBOL (If applicable)	7a. NAME OF MONITORING ORGANIZATION: Office of Naval Research
6c. ADDRESS (City, State, and ZIP Code): East Hartford, CT 06108	7b. ADDRESS (City, State, and ZIP Code): Arlington, VA 22217
8a. NAME OF FUNDING/SPONSORING ORGANIZATION: Office of Naval Research; 8b. OFFICE SYMBOL (If applicable)	9. PROCUREMENT INSTRUMENT IDENTIFICATION NUMBER: N00014-85-C-0332
8c. ADDRESS (City, State, and ZIP Code): Arlington, VA 22217	10. SOURCE OF FUNDING NUMBERS: PROGRAM ELEMENT NO. / PROJECT NO. / TASK NO / WORK UNIT ACCESSION NO.

11. TITLE (Include Security Classification)
CARBON FIBER REINFORCED GLASS MATRIX COMPOSITES FOR STRUCTURAL SPACE BASED APPLICATIONS

12. PERSONAL AUTHOR(S)
W. K. Tredway and K. M. Prewo

13a. TYPE OF REPORT	13b. TIME COVERED	14. DATE OF REPORT (Year, Month, Day)	15. PAGE COUNT
Final	FROM 7/1/87 TO 5/31/89	1989 July 31	104

16. SUPPLEMENTARY NOTATION

17. COSATI CODES			18. SUBJECT TERMS (Continue on reverse if necessary and identify by block number)
FIELD	GROUP	SUB-GROUP	Glass Matrix Composites Carbon Fiber Reinforced Composites Glass-Ceramic Matrix Composites

19. ABSTRACT (Continue on reverse if necessary and identify by block number)

A variety of ultra-high elastic modulus pitch-based carbon fibers were combined with several different glass and glass-ceramic matrix compositions to produce unidirectionally reinforced composites. Composite performance was evaluated in several different areas, including tensile stress-strain behavior, flexural properties at both room and elevated temperature, thermal expansion, and fracture behavior. Pitch fiber reinforced glass matrix composites demonstrated high tensile strength (540-790 MPa), high elastic modulus (300-350 GPa), and high specific stiffness (135-165 x 10^7 cm). Residual matrix tensile stress resulting from differential thermal contraction between fiber and matrix was shown to have a strong influence on composite behavior. Pitch/Glass composites were found to exhibit fairly linear coefficient of thermal expansion behavior in the longitudinal direction over the temperature range of -150°C to +100°C. High temperature matrix compositions were developed which maintained the excellent tensile properties of pitch fiber reinforced composites while giving them the capability to preserve structural integrity up to temperatures of at least 800°C. Composition was found to have a strong influence on the wetting behavior of glasses on carbon fibers. Oxycarbide glasses demonstrated enhanced wetting behavior on carbon fibers as well as resisting devitrification at temperatures as high as 1100°C.

20. DISTRIBUTION/AVAILABILITY OF ABSTRACT: ☒ UNCLASSIFIED/UNLIMITED ☐ SAME AS RPT. ☐ DTIC USERS	21. ABSTRACT SECURITY CLASSIFICATION: None
22a. NAME OF RESPONSIBLE INDIVIDUAL: Dr. S. Fishman,ONR	22b. TELEPHONE (Include Area Code): (202) 696-4401; 22c. OFFICE SYMBOL: ONR/1131

R89-917704-1

Carbon Fiber Reinforced Glass Matrix Composites for Structural Space Based Applications

FINAL REPORT

Contract N00014-85-C-0332

REPORTED BY William K. Tredway

William K. Tredway

Karl M. Prewo

Karl M. Prewo

APPROVED BY Earl R. Thompson

Earl R. Thompson

DATE July 31, 1989

TABLE OF CONTENTS

I. INTRODUCTION

The carbon fiber reinforced glass matrix composite system provides a unique opportunity for the basic investigation of mechanisms controlling ceramic matrix composites behavior and at the same time develop a material eminently suited to structural space based applications. The United Technologies Research Center and Pennsylvania State University have joined in the herein reported activity to characterize, understand, and improve the performance of carbon fiber reinforced glass. Carbon fiber reinforced glass composites have been fabricated and studied by several investigators over the past years in an attempt to develop a composite having performance superior to that of carbon reinforced resins and metals [1-10]. This investigation, which was begun in mid-1985, focused during the first two years on understanding the behavior in glass matrix composites reinforced with Hercules HMU carbon fiber [11, 12]. Use of this fiber allowed for reliable interpretation of the mechanisms controlling the tensile stress-strain behavior and resulted in unidirectionally reinforced composites possessing excellent tensile strength and stiffnesses in the range of 160-180 GPa [10, 11]. Currently, the focus of the investigation has shifted to composites exhibiting higher moduli as a result of SDI requirements for increased specific stiffness in space structures. To this end, ultra-high modulus pitch-based carbon fibers possessing stiffnesses greater than 690 GPa have been incorporated as the reinforcement for glass and glass-ceramic matrix composites with considerable success.

In the herein described investigation, the performance of glass and glass-ceramic matrix composites containing ultra-high modulus pitch-based carbon fibers is discussed. The nature of the fiber-matrix interface and the effect of fiber-matrix adhesion on composite properties is emphasized throughout the investigation. The tensile stress-strain behavior of these high modulus composite systems is described and related to that of HMU reinforced glass matrix composites. Flexural behavior, thermal expansion, and fracture behavior are also discussed. The development of high temperature matrices for these high modulus composite systems and the resulting mechanical behavior of these composites is also included. In addition, studies conducted at Penn State University concerning fiber-matrix interfacial wetting and the development of oxycarbide glass matrices and carbon fiber reinforced composites containing these matrices are described.

This program supported by the Strategic Defense Initiative Office/Innovative Science and Technology under ONR contract N00014-85-C-0332.

The program participants are:

William K. Tredway	UTRC
Karl M. Prewo	UTRC
Carlo G. Pantano	Penn State University
Dongxin Qi	Penn State University
G. Chen	Penn State University
Hanxi Zhang	Penn State University

REFERENCES

1. I. Crivelli-Visconti and G. A. Cooper, "Mechanical Properties of a New Carbon Fiber Material," *Nature*, **221** (1969) 754-755.

2. R. A. J. Sambell, et al., "Carbon Fibre Composites With Ceramic and Glass Matrices - Part 2. Continuous Fibres," *J Mater. Sci.*, **7** (1972) 676-681.

3. R. A. J. Sambell, D. H. Bowen and D. C. Phillips, "Carbon Fibre Composites With Ceramic and Glass Matrices - Part 1. Discontinuous Fibres," *J. Mater. Sci.*, **7** (1972) 663-675.

4. D. C. Phillips, R. A. J. Sambell and D. H. Bowen, "The Mechanical Properties of Carbon Fibre Reinforced Pyrex Glass," *J. Mater. Sci.*, **7** (1972) 1454-1464.

5. D. C. Phillips, "Interfacial Bonding and the Toughness of Carbon Fibre Reinforced Glass and Glass-Ceramics," *J. Mater. Sci.*, **9** (1974) 1847-1854.

6. K. M. Prewo and J. F. Bacon, "Glass Matrix Composites - I - Graphite Fiber Reinforced Glass," *Proceedings of ICCM/2 - The 1978 International Conference on Composite Materials*, Toronto, Canada, 1978, pp. 64-74.

7. K. M. Prewo, J. F. Bacon and D. L. Dicus, "Graphite Fiber Reinforced Glass Matrix Composites," *SAMPE Quart.*, **10** (1979) .

8. K. M. Prewo, "A Compliant, High Failure Strain, Fibre-Reinforced Glass-Matrix Composite," *J. Mater. Sci.*, **17** (1982) 3549-3563.

9. K. M. Prewo, "Carbon Fibre Reinforced Glass Matrix Composite Tension and Flexure Properties," *J. Mater. Sci.*, **23** (1988) 2745-2752.

10. V. C. Nardone and K. M. Prewo, "Tensile Performance of Carbon-Fibre-Reinforced Glass," *J. Mater. Sci.*, **23** (1988) 168-180.

11. K. M. Prewo and V. C. Nardone, "Carbon Fiber Reinforced Glass Matrix Composites for Space Based Applications," UTRC Report R86-917161-1, ONR Annual Report, September 15, 1986.

12. W. K. Tredway and K. M. Prewo, "Carbon Fiber Reinforced Glass Matrix Composites for Space Based Applications," UTRC Report R87-917470-1, ONR Annual Report, August 30, 1987.

II. EXPERIMENTAL PROCEDURE

A. Composite Fabrication

All composites were fabricated utilizing the tape winding and hot pressing procedure described in Figure II-1. The matrices were all obtained as -325 mesh size glass powders which were combined with water and an organic binder to produce slurries through which the carbon tows could be pulled. The infiltrated carbon fiber tows were then wound onto a mandrel, dried, the binder burned out in air, and the final composite densified under a pressure of 6.9 MPa at temperatures of 1100 to 1450°C.

This procedure was used to fabricate composites consisting of various combinations of the carbon fibers and the glass and glass-ceramic matrices listed in Table II-1.

B. Composite Testing and Characterization

1. *Tensile Testing*

Tensile tests were performed using parallel sided specimens (see Figure II-2). In all cases the gauge length was 2.5 cm and the loads were applied at a strain rate of 0.127 $cm \cdot cm^{-1} \cdot min^{-1}$. Strain measurements were made using glued-on strain gauges.

2. *Flexural Testing*

Three-point flexural tests were performed only on unidirectionally reinforced composites. High temperature testing was performed in an inert atmosphere. Flexural specimen geometry was varied to permit the ratio of maximum flexural stress to shear stress to be altered. These stresses were calculated using the formulae for simple beam bending as follows, where P is the maximum load applied, b is the specimen width, and L and h are as shown in Figure II-2.

$$\sigma_{max} = \frac{3}{2}\frac{PL}{bh^2} \qquad \text{(II-1)}$$

$$\tau_{max} = \frac{3}{4}\frac{P}{bh} \qquad \text{(II-2)}$$

$$\frac{\sigma_{max}}{\tau_{max}} = 2\frac{L}{h} \qquad \text{(II-3)}$$

3. *Thermal Expansion Behavior*

Composite coefficient of thermal expansion (CTE) was measured in an inert atmosphere against a fused SiO_2 standard within the temperature range of -150°C to +300°C. Samples were heated from room temperature to the upper temperature, cooled to the lower temperature, and then heated back up to room temperature at a rate of 2°C/min. At least two thermal cycles were always employed. Specimen dimensions were 2.54 cm x 0.51 cm x 0.25 cm.

4. *Microstructural Characterization*

Composite microstructures were examined using optical microscopy methods. Specimen cross-sections were prepared using standard metallographic techniques. Carbon fibers and composite fracture surfaces were observed in a scanning electron microscope (SEM). Fracture surfaces were sputtered with a gold film to eliminate charging effects in the microscope.

5. *Crystalline Phase Identification*

Crystalline phases present in the glass-ceramic matrix composites after heat-treatment were identified using x-ray diffraction (XRD). Crystallized composite samples were crushed in a mortar and pestle to -200 mesh powder prior to being loaded in the diffractometer. A monochromator was used to ensure that only Cu K_α radiation struck the powdered sample. Samples were scanned from 10° to 60° 2θ at a rate of 2° 2θ/min.

Table II-1

Materials Used in Composite Fabrication

Fiber	Manufacturer	Density (g/cc)	Elastic Modulus (GPa)	Tensile Strength (MPa)	Fiber Dia. (μm)	Precursor
HMU	Hercules	1.84	380	2760	8	PAN
UHM	Tonen	2.15	682	3410	10	Pitch
P-100	Amoco	2.16	758	2240	10	Pitch
P-120	Amoco	2.17	827	2067	10	Pitch
E-130-X	DuPont	2.19	894	3445	9.2	Pitch

UTRC Matrix Designation	Report Matrix Designation	Density (g/cc)	Elastic Modulus (GPa)	Glass Transition Temperature (°C)	CTE (10^{-6}/°C)	
UT2-4	BSG-1*	2.23	63	560	3.2	
UT2-3	BSG-2*	2.13	51	496	3.2	
UT2-5	BSG-3*	2.19	66	~900	1.3	
UT4-1002	LAS-I**	-	-	765	~3.0	(glass)
		2.45	88	-	~1.0	(ceramed)
UT6-1001	BMAS+	-	-	835	~3.8	(glass)
		2.66	-	-	~2.8	(ceramed)

* BSG = borosilicate glass

** LAS = lithium aluminosilicate (glass-ceramic)

+ BMAS = barium-magnesium aluminosilicate (glass-ceramic)

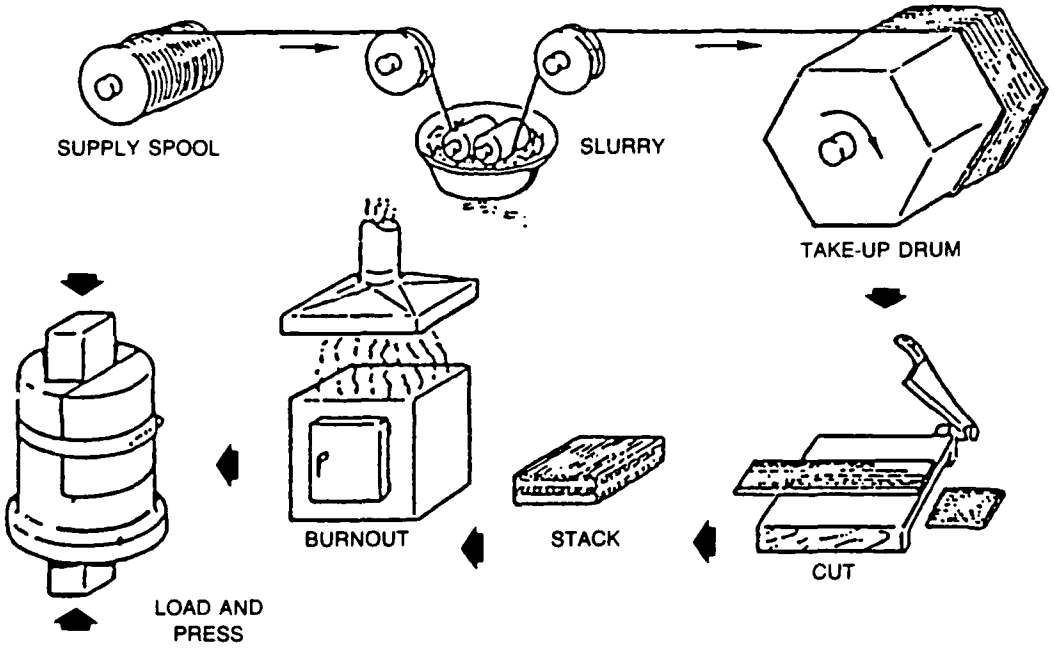

Fig. II-1. Composite Fabrication Procedure

86-7-99-1

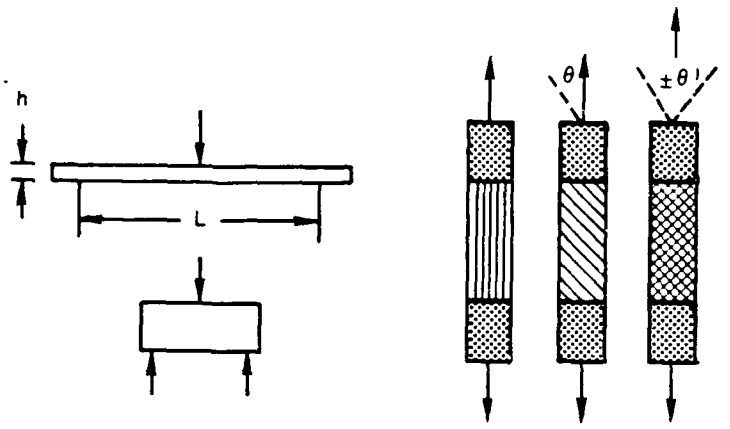

Fig. II-2. Mechanical Test Techniques

III. MECHANICAL PROPERTIES OF PITCH FIBER REINFORCED GLASS MATRIX COMPOSITES

A. Introduction

The reinforcement of ceramics with fibers has proven to be a successful means of improving the toughness of these inherently brittle materials. The incorporation of carbon fibers into glasses to produce high strength, tough composite materials was demonstrated more than a decade ago by researchers in the U. K. [1-4]. Development of the carbon fiber reinforced glass (C/Glass) composite system was then continued in the U. S. [5-8], with the most recent studies focusing on the use of Hercules HMU carbon fiber in borosilicate glass matrices [9-11]. The unique combination of properties demonstrated by C/Glass composites (high strength and stiffness, excellent toughness, low density, dimensional stability, excellent tribological characteristics, high impact resistance, environmental stability) makes them likely candidates for structural applications previously reserved for polymer and metal matrix composites, such as gas turbine engine components and structural members in space-based applications. Perhaps the more exotic of these applications is as structural components in satellites and other space-oriented systems. Materials suited for these roles must be structurally sound, lightweight, and able to withstand the severe conditions imposed by the space environment.

One of the critical requirements of materials for space structures is that they demonstrate high specific stiffness (stiffness divided by density). In order to meet this demand, researchers have had to utilize ultra-high modulus carbon fibers made from mesophase pitch precursors [12]. These fibers, which exhibit a high degree of graphitization in their internal structure, typically possess tensile elastic moduli in the range of 690-900 GPa. Implementation of these ultra-high modulus fibers in C/Glass composites, which is the subject of this study, has met with reasonably good success; however, the nature of the tensile stress-strain behavior and the fracture behavior have been found to differ significantly from that of C/Glass composites reinforced with HMU carbon fiber [11]. The cause of these variations is thought to be related to differences in the nature of the fiber-matrix interface, primarily in the degree of fiber-matrix adhesion displayed in the two composite systems [13]. Matrix microcracking strain, fiber pullout length, and work of fracture are all known to be strong functions of fiber-matrix interfacial strength .

This chapter describes the results of an effort to investigate the mechanical performance and fracture behavior of glass matrix composites reinforced with ultra-high modulus pitch-based carbon fiber. The tensile stress-strain characteristics, flexural behavior, and fracture morphology of C/Glass composites reinforced with several types of pitch-based carbon fiber will be discussed and compared to those characteristics of HMU reinforced C/Glass composites. The influence of fiber-matrix interfacial adhesion on these properties will be emphasized.

B. Experimental Procedure

All composites were fabricated utilizing the tape winding and hot pressing procedure described in Figure III-1. The matrix was obtained as -325 mesh size glass powder which was combined with water and an organic binder to produce a slurry through which the carbon tows could be pulled. The infiltrated carbon fiber tows were then wound onto a mandrel, dried, the binder burned out in air, and the final composite densified under a pressure of 6.9 MPa at a temperature of ~1250°C. This procedure was used to fabricate composites consisting of the carbon fibers and the glass matrix composition listed in Table III-1. All the composites in this study were unidirectional in fiber orientation.

Tensile tests were performed using parallel sided specimens (see Figure III-2). In all cases the gauge length was 2.5 cm and the loads were applied at a strain rate of 0.127 $cm \cdot cm^{-1} \cdot min^{-1}$. Strain measurements were made using glued-on strain gauges.

Three-point flexural tests were performed on unidirectionally reinforced composites. Flexural specimen geometry was varied to permit the ratio of maximum flexural stress to shear stress to be altered. These stresses were calculated using the formulae for simple beam bending as follows, where P is the maximum load applied, b is the specimen width, and L and h are as shown in Figure III-2.

$$\sigma_{max} = \frac{3}{2}\frac{PL}{bh^2} \qquad \text{(III-1)}$$

$$\tau_{max} = \frac{3}{4}\frac{P}{bh} \qquad \text{(III-2)}$$

$$\frac{\sigma_{max}}{\tau_{max}} = 2\frac{L}{h} \qquad \text{(III-3)}$$

Composite microstructures were examined using optical microscopy methods. Specimen cross-sections were prepared using standard metallographic techniques. Carbon fibers and composite fracture surfaces were observed in a scanning electron microscope (SEM). Fracture surfaces were sputtered with a gold film to eliminate charging effects in the microscope.

C. Results and Discussion

C. 1. Carbon Fiber Structure and Morphology

Dissimilarities in the amount of adhesion between carbon fibers and glass matrices are

related to a number of factors, including internal fiber structure, surface structure, and surface chemistry. Carbon fibers derived from polyacrylonitrile (PAN) and mesophase pitch precursors are typically characterized by differences in all three of these characteristics [14, 15]. Hercules HMU fiber, which is an intermediate modulus PAN-derived carbon fiber, is typified by an internal fiber structure which resembles a 'rolled-up newspaper' in appearance (Figure III-3(a)). The graphite planes are aligned parallel to the fiber axis, but the degree of graphitization in the fiber results in planes which are somewhat curled and bent. The outer skin of HMU fiber consists of a thin layer of graphite planes which are oriented parallel to the surface of the fiber [16]. This results in a smooth fiber surface with a surface energy characteristic of that of graphite basal planes, which is typically quite low.

In contrast to HMU, the degree of graphitization displayed in ultra-high modulus pitch-derived fiber results in a highly oriented structure characterized by radial alignment of the graphite planes about the fiber axis. Figures III-3(b), (c), and (d) illustrate the structures of P-100, UHM, and E-130 pitch-based carbon fibers, respectively. Like HMU fiber, the outer layer of pitch-based fiber also consists to some degree of graphite planes which are oriented parallel to the fiber surface; however, a portion of the surface also consists of planes from the interior of the fiber whose edges intersect the outer fiber surface. These edge planes possess a very high surface energy, consequently resulting in a surface chemistry that differs from that of HMU fiber. Another distinction between pitch-based and HMU fiber is the corrugated surface of the pitch-based fiber. This increase in surface roughness results in a higher specific surface area, which translates directly to increased interfacial area in composites reinforced with pitch-based carbon fiber.

C. 2. Tensile Stress-Strain Behavior

Borosilicate glass matrix composites unidirectionally reinforced with four different types of ultra-high modulus pitch-based carbon fiber were fabricated (see Table III-1 for specific fibers used). The tensile stress-strain behavior of all of the composites was very similar, with ultimate tensile strengths (UTS), elastic moduli, and failure strains as reported in Table III-2. Composite UTS values varied from 540-790 MPa, which is in part due to the differences in fiber volume and fiber strength. These UTS values represent only 50-75% of the strength that would be expected based on single fiber strengths and fiber volume; however, this amount of translation is consistent with that displayed by other C/Glass composite systems (e.g., the UTS of the HMU/Glass composite listed in Table III-2 represents 65% translation of fiber strength). There are a number of possible explanations for this lack of full translation, including damage to the fibers during fabrication or slight misalignment of the fibers in the tensile samples. In fact, it has been shown that as little as 1° of misalignment, either through an error in layup or in machining of the tensile samples from the composite coupon, can reduce measured strengths of carbon fiber reinforced polymers by more than 30% [17].

However, in this case misorientation is not believed to be the cause of the lower composite strengths since the degree of strength translation from the fibers is fairly consistent among all the composites fabricated. A more likely explanation is that fiber bundle strength plays a more important role in determining ultimate composite failure stress than does single fiber strength. Models employing this concept [18-21] consider the statistical nature of fiber strength, with composite failure resulting from an accumulation of single fiber breaks. As the weaker fibers fail, the load is carried by an increasingly fewer number of fibers, with the effective stress borne by these remaining fibers increasing as more fibers break. Intact fibers in the vicinity of a fiber break are subjected to a higher load intensity than those farther away from the fracture site. Also playing a role is the "critical transfer length" (l_c), or the ineffective length over which load cannot be transferred after fiber failure. This accumulation of breaks usually leads to failure of the composite at loads below those predicted based on average single fiber strength; however, small values of l_c can actually lead to higher composite strengths than those predicted based on single fiber strength. This model has been successfully used to explain tensile behavior in Nicalon reinforced glass-ceramic composites [22]. More information on the bundle strengths of pitch-based carbon fibers is required before a similar analysis can be performed.

Composite elastic moduli were all in the range of 300-350 GPa, with corresponding specific elastic moduli of 135-165 x 10^7 cm (refer to Table III-2). These values are a significant increase from those obtained using HMU fiber (Table III-2) and are in a range of values that can be considered for use in the design of structural components for space systems. The elastic moduli are near those predicted based on a "rule of mixtures" (ROM) approach. This differs somewhat from the behavior observed in C/Glass composites reinforced with HMU fiber, where the fiber appears to contribute only about 80% of its reported stiffness to the composite [10]. This apparent loss in fiber stiffness could be caused by damage to the HMU fiber during tape fabrication, specifically in the sizing removal step. The oxidative stability of carbon fibers is known to be directly proportional to fiber elastic modulus, which is a reflection of the degree of graphitization of the fiber structure. The lower degree of graphitization in HMU carbon fiber makes it inherently less oxidation resistant than ultra-high modulus pitch-based fiber, which should give the pitch-based fiber greater stability during burn-off of the sizing. If any material were removed from the fiber surface during sizing burn-off, it would be more detrimental to the performance of HMU fiber than to that of ultra-high modulus pitch-based carbon fiber due to the structural dissimilarities that exist between HMU fiber and pitch-based fiber (described earlier). As a result of these dissimilarities, most of the stiffness in HMU fiber is concentrated in the outer layer, where the graphite basal planes are highly oriented parallel to the fiber surface, whereas in the pitch-based carbon fiber the uniform internal structure results in constant stiffness across the fiber cross-section. Therefore, the removal of only a small percentage of the HMU fiber surface results in a large decrease in fiber stiffness [16]. Pitch-based carbon fiber, on the other hand, can tolerate some surface removal with no sacrifice to fiber stiffness [23].

A tensile stress-strain curve representative of the characteristic behavior displayed by all the

pitch fiber reinforced glasses is shown in Figure III-4. This curve was obtained from a composite containing approximately 40 vol% P-100 fiber. It is instructive to examine the tensile behavior of the P-100/Glass composite by first comparing it with that displayed by the well-characterized HMU/Glass composite system [11]. Several characteristics are shared by the two types of composites, while others are quite dissimilar. Figure III-5 shows a typical stress-strain curve for a unidirectionally reinforced HMU/Glass composite containing approximately 40 vol% fiber. The composite displays linear elastic behavior up to a strain level of about 0.2%. In this initial linear region, the composite elastic modulus is predictable based on a combination of stiffness from the carbon fibers and the glass matrix. At the upper level of this initial linear region, the stress-strain curve deviates significantly from linearity, passing through a 'plateau' region of increasing strain with very little increase in stress. The point where the curve deviates from linearity is commonly referred to as the proportional limit (PL). In the HMU/Glass composite system, it has been assumed that the PL corresponds to the onset of matrix microcracking and probable fiber-matrix debonding [11]. In the plateau region, the degree of microcracking of the matrix and fiber-matrix debonding increases rapidly, resulting in a large and sudden increase in transverse strain when the fiber tows 'broom out' (allowed by the constraining force of the matrix being reduced through microcracking and debonding. Cyclic tensile testing of this composite system has indicated that the matrix no longer contributes to the overall composite stiffness once the composite has been strained past the plateau region [11]). The curve then again exhibits linear behavior representative of the fibers carrying the load alone after matrix microcracking. The mechanism of fiber-matrix debonding prior to this stage is critical to the fibers being able to carry the load until they reach their inherent failure strain of 0.6 to 0.7%. If significant debonding did not occur, matrix cracks would propagate directly through the fibers and the composite would fail in a brittle manner.

The tensile stress-strain behavior of the P-100/Glass composite shows some similarity to the HMU/Glass composite, but also differs in several ways. The initial portion of the curve is again representative of linear elastic behavior which is predictable based on a knowledge of fiber and matrix moduli. The curve experiences a PL at a strain of about 0.05%, followed by a secondary region of steadily decreasing slope. The fibers continue to carry the load until they reach their failure strain of approximately 0.2%. The stress-strain curves of the two materials differ in two main respects: 1) the P-100/Glass composite does not exhibit the 'plateau' region following the PL, and; 2) the secondary region representative of fibers carrying the load alone in the P-100/Glass composite is not linear, but instead exhibits a negative curvature with increasing strain. These dissimilarities between the two composite systems most likely result from a number of factors, including a variation in the nature of the fiber-matrix interface caused by the differing surface structure and surface chemistry of HMU and P-100 carbon fiber.

It does not appear that the PL in the P-100/Glass composite is simply the result of the matrix no longer contributing to the overall composite stiffness. This was assessed by

comparing the theoretical matrix contribution to composite stiffness with the difference between the slope of the initial linear region of the curve (E_1) and the modulus corresponding to the initial portion of the secondary region of the curve (E_2); *viz.*, that portion of the curve immediately following the PL. This value of $E_1 - E_2$ is equal to about 30 GPa for the P-100/Glass composite, which is very close to the value of 38 GPa corresponding to the contribution of the matrix to composite stiffness. However, cyclic tensile testing of this system gives indications that the mechanism by which this transient loss in stiffness occurs in the P-100/Glass composite is different from that in the HMU/Glass composite, *i.e.* it does not appear that the matrix experiences severe microcracking at the PL in the P-100/Glass composite. Figure III-6 shows the stress-strain curves for one of the cyclic tensile tests performed on the P-100/Glass composite, with the tensile data summarized in Table III-3. During the first cycle, the composite was loaded just past the PL to a stress of 50 MPa, with the composite exhibiting an initial elastic modulus of 334 GPa. On unloading, the curve traced over the loading curve exactly, with no permanent strain being introduced. The second cycle resulted in the composite being loaded well past the PL to a stress of 99 MPa. The initial elastic modulus was slightly lower for the second cycle (318 GPa), which may indicate some permanent loss of the matrix contribution to stiffness; however, the amount lost (16 GPa) represents only 40% of the total matrix contribution, *i.e.* the matrix still possesses 60% of its stiffness. During the third cycle, the composite experienced a stress up to 166 MPa (significantly beyond the PL), and on unloading exhibited a permanent strain of 0.004%. The initial elastic modulus during this cycle was again 318 GPa, indicating no further loss in matrix contribution from the loading of the second cycle. The fourth and final cycle loaded the composite to the point of ultimate failure, with the initial elastic modulus again being 318 GPa.

This cyclic behavior differs from that of HMU/Glass composites in two significant respects: 1) the P-100/Glass composite system exhibits a proportional limit during cycles subsequent to those in which the loading exceeded the PL by a significant amount, and; 2) the initial elastic modulus demonstrated in these cycles remains fairly constant and is indicative of the matrix contributing more than 50% of its stiffness to the composite. These two factors imply that the matrix in P-100/Glass composites does not experience the severe microcracking at the PL as it does in the HMU/Glass composite system. This seems reasonable in light of the fact that the level of strain where the PL occurs in HMU/Glass composites (~ 0.20%) is well above the PL strain in P-100/Glass composites (0.05%). In fact, the PL strain for HMU/Glass composites is at or above the failure strain regime of P-100/Glass composites, indicating that severe matrix microcracking may occur in the P-100/Glass composite system only on ultimate failure of the composite. This behavior is important when considering the possibility of designing structural components from P-100/Glass composites. Normally, the PL is considered to be the maximum stress to which a structure can be loaded in order for it to retain its properties during subsequent cycles. The repetitive tensile nature of the P-100/Glass composite system after being loaded well past the PL would seem to relax this criterion. Further analysis is underway to determine the

mechanism(s) responsible for the PL in the P-100/Glass composite system.

C. 3. Flexural Behavior

Three-point flexural testing was performed on all the C/Glass composites reinforced with pitch-based carbon fiber, with the results presented in Table III-4. The span-to-depth ratio was in all cases greater than 23, since it has been reported that span-to-depth ratios less than 20 lead to a shear mode of failure [10, 24]. All of the flexural strengths were in the range of 700-840 MPa, with corresponding Flexural Strength:Tensile Strength (FS:TS) ratios falling between 1.1 and 1.3. This is in contrast to the HMU/Glass composite system, which typically exhibits much higher flexural strengths (refer to Table III-4) and greater FS:TS ratios, usually around 2 (as in the example given in Table III-4). Most of the pitch fiber reinforced composites exhibited primarily a tensile failure mode, with little evidence of shear failure, although the composite samples reinforced with E-130 fiber failed in compression. Some composite samples exhibited mixed failure modes of both tension and compression.

Composite interlaminar shear strength (ILSS) values were obtained via short beam shear testing. Span-to-depth ratios were held constant at a value of 4 so that all the composite samples failed in shear. The values of ILSS for all of the pitch fiber reinforced composites as well as that for an HMU/Glass composite are included in Table III-4. Shear strengths for the composites reinforced with pitch-based fiber were in the range of 40-50 MPa, while that for the HMU/Glass composite was considerably less at 22 MPa. It has been shown [10] that short beam shear strength in C/Glass composites is directly related to fiber-matrix interfacial debond shear strength, τ_{max} (this value represents the shear stress necessary to initiate debonding between fiber and matrix). The average maximum interfacial shear stress (τ_{max}) in HMU/Glass composites has been found to be approximately 10 MPa using a fiber push-test technique [25]. While values of τ_{max} have not been obtained for the composites containing pitch-based fiber via a direct measurement (*e.g.* a fiber push test), it may be inferred based on the aforementioned relationship between ILSS and τ_{max} that fiber-matrix interfacial adhesion is greater in composites reinforced with pitch-derived carbon fibers than in HMU/Glass composites.

The increased fiber-matrix adhesion exhibited in the Pitch/Glass composites is most likely due in part to increased mechanical interlocking created by the corrugated surface of the pitch-based carbon fibers (as described previously). The corrugated surface translates directly to an increase in fiber-matrix interfacial area, as illustrated in Figure III-3(b). In this micrograph of a fracture surface in a P-100/Glass composite, the matrix surrounding the "holes" where fibers have pulled out has replicated the corrugated surface of the pitch-based carbon fiber. It seems clear that the mechanical interlocking of this type of interface would be greater than that of the "smooth" interface existing in HMU/Glass composites. Another factor that may contribute partially to the increased fiber-matrix adhesion in Pitch/Glass composites is the inherently higher

wettability of the glass on the pitch-based carbon fibers compared to HMU fiber. Micro-sessile drop experiments have shown that the contact angle between the borosilicate glass used in this study and P-100 fiber is significantly less than that between the glass and HMU fiber [26], demonstrating that the glass wets the P-100 fiber more easily. It can be assumed that similar behavior would exist with the other two pitch-based fibers used in this investigation. Although it seems reasonable that increased wettability leads to greater values of interfacial adhesion, a direct relationship between the two has not yet been demonstrated. Work is currently underway to verify this relationship. Reasons for the increased wettability of pitch-based fibers are speculative at this point. However, it is believed that two of the most probable causes are: (1) the rougher surface of the pitch-based fibers makes it easier for the glass to spread by providing more surface sites, and; (2) the surface energy of the pitch-based carbon fibers is higher than that of HMU fiber due to differences in the internal fiber structure (described previously).

The observed differences in ILSS and fiber-matrix adhesion in HMU/Glass composites and Pitch/Glass composites can be used to explain the difference between the FS:TS ratio in these two composite systems. During flexural testing of a composite in the HMU/Glass system, the relatively low values of ILSS and τ_{max} allow the load to be redistributed throughout the sample via shear deflection of the laminae relative to one another, thus allowing the composite to carry higher loads and fail at a higher level of stress. On the other hand, the higher values of ILSS and τ_{max} in the Pitch/Glass composite system make it more difficult for the load to be redistributed in a similar manner. This prevents the composite from carrying higher loads and results in failure at lower stress levels. Failure in these pitch-based fiber reinforced composites occurs once the tensile strength of the composite has been exceeded by a small amount, as evidenced by the FS:TS ratio of 1.1-1.3.

C. 4. Composite Fracture Behavior

Tensile fracture surfaces of composites in the HMU/Glass and P-100/Glass systems are illustrated in Figure III-7. The average fiber pullout length, l_f, is noticeably higher in the HMU/Glass composite than in the P-100/Glass composite. The well-known equation relating critical transfer length (l_c) to fiber radius (R), fiber strength (σ_f), and interfacial shear stress (τ), given as [27]

$$l_c = \frac{R\sigma_f}{\tau} \quad , \qquad \text{(III-4)}$$

can be applied to these cases if it is assumed that the fiber pullout length l_f is equal to the critical transfer length. This is a reasonable assumption for the purposes of this discussion. By inserting the values of R and σ_f for HMU and P-100 fiber given in Table III-1, it can be seen that

for comparison between these two systems, equation III-4 simplifies approximately to

$$\frac{l_{f,\,HMU}}{l_{f,\,P\text{-}100}} \approx \frac{\tau_{P\text{-}100}}{\tau_{HMU}} \qquad \text{(III-5)}$$

Equation III-5 indicates that the ratio of fiber pullout lengths in these two composite systems is approximately equal to the inverse ratio of fiber-matrix interfacial shear strengths, implying that $\tau_{P\text{-}100}$ is significantly greater than τ_{HMU}. This is in agreement with the results presented earlier relating τ_{max} to ILSS, where the short beam shear strength of Pitch/Glass composites was found to be about twice that of HMU/Glass composites.

Flexural fracture behavior followed a similar trend to the tensile fracture behavior, with the Pitch/Glass composites exhibiting much shorter fiber pullout lengths than the HMU/Glass composite. As above, this was expected based on the relative magnitudes of τ_{max} in the two composite systems. These short pullout lengths were of some concern, since the work of fracture and the associated composite toughness are directly related to l_f. In an attempt to engineer additional toughness into Pitch/Glass composites, a"microstructural toughening" approach was adopted. This approach involved the addition of a thin layer of carbon "scrim cloth" between laminae in the composite. The presence of the scrim cloth provides a glass-rich region between plies, as shown in Figure III-8. These glass-rich regions lower the ILSS of the composite by providing an easy path for shear deflection of advancing cracks. Results of tensile and flexural testing of Pitch/Glass composites containing scrim cloth are summarized in Table III-5. Tensile and flexural strengths are somewhat lower in the composites containing scrim when compared against the data in Tables III-4 and III-5. However, when taking into account the decrease in load-bearing cross-section in the composites containing scrim (assuming that the scrim cloth bears very little of the total load), the effective strengths of the axial plys of the composites with and without scrim are similar.

The property that shows a real change is the ILSS, which experienced a 25-35% decrease in the composites containing scrim. This decrease in ILSS had very little effect on the tensile fracture behavior of the scrim-containing composites. To the contrary, however, the flexural fracture behavior was significantly affected, as shown in Figure III-9. In the standard Pitch/Glass composite, the crack that initiated on the tensile surface propagated about midway through the composite, deflected once between laminae, and then ran through the remainder of the composite thickness. On the other hand, the composite containing scrim exhibited a much more tortuous path for the crack during propagation through the composite. After initiation on the tensile surface, the crack experienced a shear deflection at each successive layer of scrim that it encountered. This more graceful mode of failure resulted in an increase in the area under the load-deflection curve, translating to an increase in the work of fracture for the composites

containing scrim.

D. Summary

Glass matrix composites possessing higher specific stiffness were successfully fabricated utilizing ultra-high modulus pitch-based carbon fibers. Elastic stiffnesses obtained in these Pitch/Glass composites were predictably high; however, only 50-75% translation of fiber strength was demonstrated. This behavior is similar to other C/Glass composite systems and is believed to be related to the control of fiber bundle strength over composite strength. The tensile stress-strain behavior of Pitch/Glass composites was found to differ in several respects to that of the well-characterized HMU/Glass composite system. The cyclic stress-strain behavior was especially interesting when considering the repetitive nature of the stress-strain curve after loading well past the proportional limit. Composite interlaminar shear strength and fiber-matrix interfacial shear strength (τ_{max}) were found to be significantly higher in Pitch/Glass composites than in HMU/Glass composites, with subsequent effects on fiber pullout length and fracture behavior. The increase in τ_{max} is caused by differences in fiber surface structure and surface chemistry. Work of fracture during flexure of Pitch/Glass composites was improved by introducing a layer of carbon scrim cloth between plies, which lowered interlaminar shear strength without significantly affecting composite strength and stiffness.

ACKNOWLEDGEMENTS

The authors gratefully acknowledge the support of the Innovative Science and Technology branch of the Strategic Defense Initiative Organization through the Office of Naval Research (Contract N00014-85-C-0332) with Dr. Steven Fishman as contract monitor. They would also like to recognize Mr. William Kelley for composite fabrication, Ms. Judy Whitehead for carrying out for the SEM portions of the investigation, and the Mechanical Testing group at UTRC for performing the tensile and flexural testing.

REFERENCES

1. R. A. J. Sambell, D. H. Bowen and D. C. Phillips, "Carbon Fibre Composites With Ceramic and Glass Matrices - Part 1. Discontinuous Fibres," *J. Mater. Sci.*, **7** (1972) 663-675.

2. R. A. J. Sambell, et al., "Carbon Fibre Composites With Ceramic and Glass Matrices - Part 2. Continuous Fibres," *J. Mater. Sci.*, **7** (1972) 676-681.

3. D. C. Phillips, R. A. J. Sambell and D. H. Bowen, "The Mechanical Properties of Carbon Fibre Reinforced Pyrex Glass," *J. Mater. Sci.*, **7** (1972) 1454-1464.

4. D. C. Phillips, "Interfacial Bonding and the Toughness of Carbon Fibre Reinforced Glass and Glass-Ceramics," *J. Mater. Sci.*, **9** (1974) 1847-1854.

5. K. M. Prewo and J. F. Bacon, "Glass Matrix Composites - I - Graphite Fiber Reinforced Glass," *Proceedings of ICCM/2 - The 1978 International Conference on Composite Materials*, Toronto, Canada, 1978, pp. 64-74.

6. K. M. Prewo, J. F. Bacon and D. L. Dicus, "Graphite Fiber Reinforced Glass Matrix Composites," *SAMPE Quart.*, **10** (1979) 42.

7. K. M. Prewo, "A Compliant, High Failure Strain, Fibre-Reinforced Glass-Matrix Composite," *J. Mater. Sci.*, **17** (1982) 3549-3563.

8. K. M. Prewo and E. J. Minford, "Graphite Fiber Reinforced Thermoplastic Glass Matrix Composites for Use at 1000°F," *SAMPE J.*, (1985) 26-33.

9. K. M. Prewo and J. A. Batt, "The Oxidative Stability of Carbon Fibre Reinforced Glass-Matrix Composites," *J. Mater. Sci.*, **23** (1988) 523-527.

10. K. M. Prewo, "Carbon Fibre Reinforced Glass Matrix Composite Tension and Flexure Properties," *J. Mater. Sci.*, **23** (1988) 2745-2752.

11. V. C. Nardone and K. M. Prewo, "Tensile Performance of Carbon-Fibre-Reinforced Glass," *J. Mater. Sci.*, **23** (1988) 168-180.

12. V. C. Nardone, et al., "Carbon Fiber Reinforced Metal and Glass Matrix Composites for Space Based Applications," presented at the 19th International SAMPE Technical Conference, Arlington, Virginia, October 13-15, 1987 (sponsored by SAMPE).

13. W. K. Tredway and K. M. Prewo, "Performance of Glass Matrix Composites Reinforced With PAN and Pitch-Derived Carbon Fibers," presented at the 13th Annual Conference on Composite Materials and Structures, Cocoa Beach, Florida, January 18-20, 1989 (sponsored by United States Advanced Ceramics Association).

14. W. Johnson, "The Structure of PAN Based Carbon Fibres and Relationship to Physical Properties"; pp. 389-473 in Handbook of Composites, Volume 1 - Strong Fibres. Edited by W. Watt and B. V. Perov. Elsevier Science Publishers B. V., Amsterdam, 1985.

15. B. Rand, "Carbon Fibres from Mesophase Pitch"; pp. 495-575 in Handbook of Composites, Volume 1 - Strong Fibres. Edited by W. Watt and B. V. Perov. Elsevier Science Publishers B. V., Amsterdam, 1985.

16. K. J. Chen and R. J. Diefendorf, "Residual Stresses in High Modulus Carbon Fibers," Proceedings of Progress in Science and Engineering of Composites, ICCM-IV, Tokyo, Japan, 1982, pp. 97-105.

17. P. W. Manders and I. M. Kowalski, "The Effect of Small Angular Fiber Misalignments and Tabbing Techniques on the Tensile Strength of Carbon Fiber Composites," *Proceedings of 32nd International SAMPE Symposium*, 1987, pp. 985-996.

18. B. W. Rosen, "Tensile Failure of Fibrous Composites," *AIAA J.*, **2** (1964) 1985-1991.

19. B. W. Rosen, "Mechanics of Composite Strengthening"; pp. 37-75 in Fiber Composite Materials. American Society for Metals, Metals Park, Ohio, 1965.

20. C. Zweben, "Tensile Failure of Fiber Composites," *AIAA J.*, **6** (1968) 2325-2331.

21. C. Zweben and B. W. Rosen, "A Statistical Theory of Material Strength With Application to Composite Materials," *J. Mech. Phys. Solids*, **18** (1970) 189-206.

22. K. M. Prewo, "Tension and Flexural Strength of Silicon Carbide Fibre-Reinforced Glass Ceramics," *J. Mater. Sci.*, **21** (1986) 3590-3600.

23. M. Aoki, Tonen Energy International Corp., 1989, personal communication.

24. K. M. Prewo and V. C. Nardone, "Carbon Fiber Reinforced Glass Matrix Composites for Space Based Applications," UTRC Report R86-917161-1, ONR Annual Report, September 15, 1986.

25. D. H. Grande, J. F. Mandell and K. C. C. Hong, "Fibre-Matrix Bond Strength Studies of Glass, Ceramic, and Metal Matrix Composites," *J. Mater. Sci.*, **23** (1988) 311-328.

26. C. G. Pantano, G. Chen and D. Qi, "Interface Reactions and Wetting in Carbon Fiber Reinforced Glass Matrix Composites," submitted for publication, 1989.

27. A. Kelly, "Microstructural Parameters of an Aligned Fibrous Composite," *The Properties of Fibre Composites*, National Physical Laboratory, 1971, pp. 5-14.

Table III-1

Materials Used in Composite Fabrication

FIBERS

Fiber	Manufacturer	Density (g/cc)	Elastic Modulus (GPa)	Tensile Strength (MPa)	Fiber Dia. (μm)	Precursor
HMU	Hercules	1.84	380	2760	8	PAN
UHM	Tonen	2.15	682	3410	10	Pitch
P-100	Amoco	2.16	758	2240	10	Pitch
P-120	Amoco	2.17	827	2067	10	Pitch
E-130-X	DuPont	2.19	894	3445	9.2	Pitch

MATRIX COMPOSITION

Matrix Designation	Density (g/cc)	Elastic Modulus (GPa)	Glass Transition Temperature (°C)	CTE (ppm/°C)
BSG-1*	2.23	63	560	3.2

* BSG = borosilicate glass

Table III-2. Tensile Properties of Pitch Fiber Reinforced Glass Matrix Composites

Matrix	Fiber	Vol % Fiber	Ultimate Tensile Strength (MPa)	Elastic Modulus (GPa)	Failure Strain (%)	Density (g/cm^3)	Specific Modulus (10^7 cm)
7740	P-100	39	537	324	0.19	2.21	150
	P-120	41	647	356	0.21	2.19	166
	UHM	45	792	296	0.31	2.21	137
	E-130	37	668	345	0.23	2.22	159
	HMU *	44	785	169	0.60	2.06	84

* Reference 11.

Table III-3. Cyclic Tensile Properties of Pitch Fiber Reinforced Glass Matrix Composites

Cycle	Maximum Stress (MPa)	Initial Elastic Modulus (GPa)	Proportional Limit Stress (MPa)
1	50	334	37
2	99	318	41
3	166	318	41
4	274	318	33

Table III-4. Flexural Properties of Pitch Fiber Reinforced Glass Matrix Composites

Matrix	Fiber	Vol % Fiber	3-Point Flexural Strength (MPa)	Failure Mode	Interlaminar Shear Strength (MPa)
7740	P-100	39	720	T	49
	P-120	41	700	T/C	41
	UHM	45	840	C/T	39
	E-130	37	730	C	39
	HMU *	44	1160	T	22

* Reference 10.

Table III-5. Tensile and Flexural Properties of Pitch/Glass Composites Containing Scrim Cloth

			Tensile Properties			*Flexural Properties*	
Matrix	Fiber	Vol % Fiber	Ultimate Tensile Strength (MPa)	Elastic Modulus (GPa)	Failure Strain (%)	3-Point Flexural Strength (MPa)	Interlaminar Shear Strength (MPa)
7740	P-100	36	432	285	0.18	641	31
	Scrim	4					
	P-120	40	555	355	0.19	631	31
	Scrim	5					

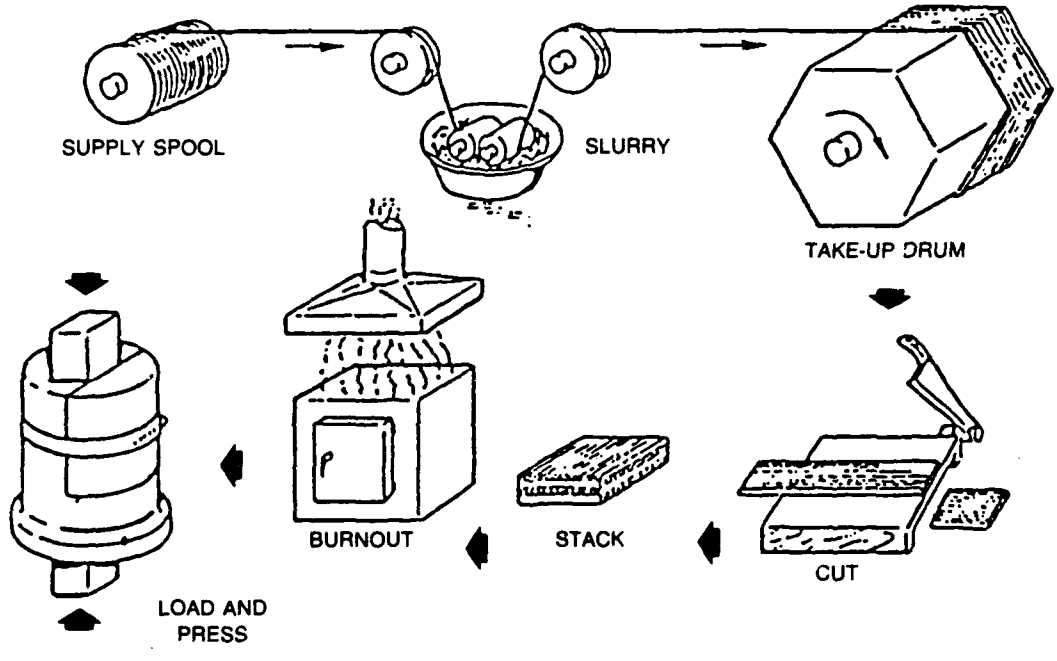

Fig. III-1. Composite Fabrication Procedure

89—7—50—1

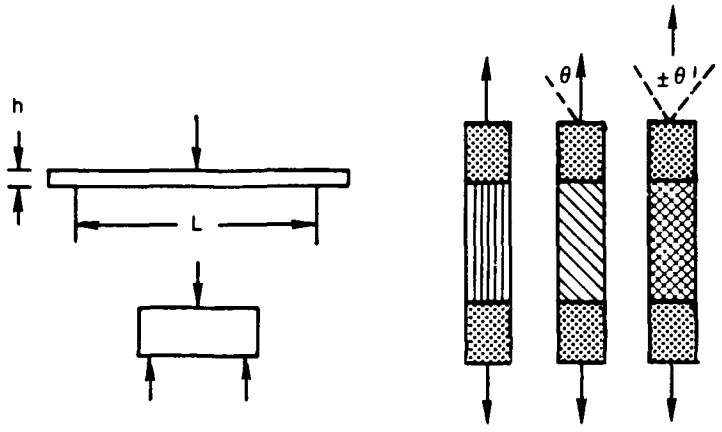

Fig. III-2. Mechanical Test Techniques

89—7—50—2

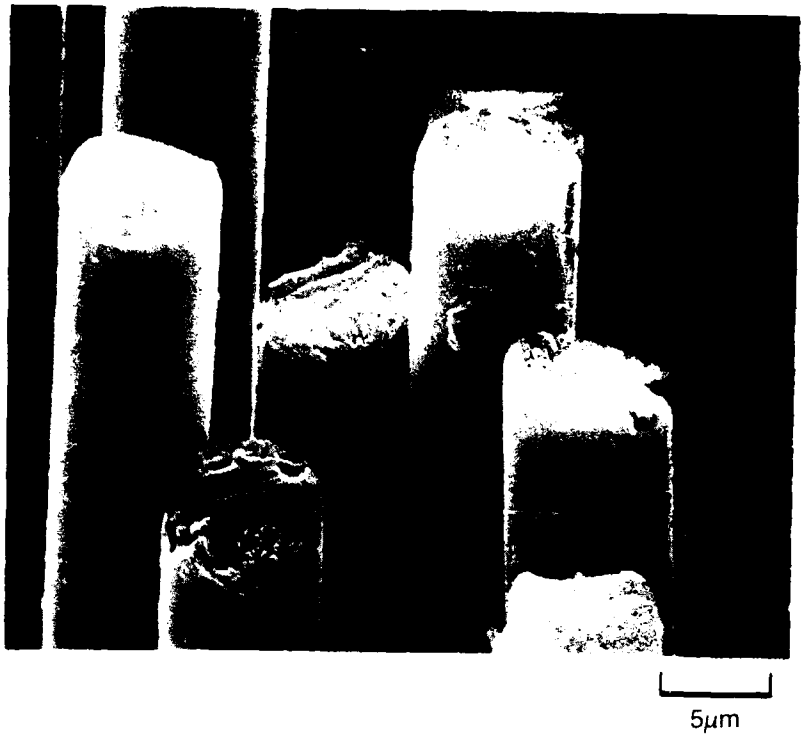

Fig. III-3 (a). Structure of Hercules HMU Carbon Fiber

Fig. III-3 (b). Structure of Amoco P-100 Carbon Fiber

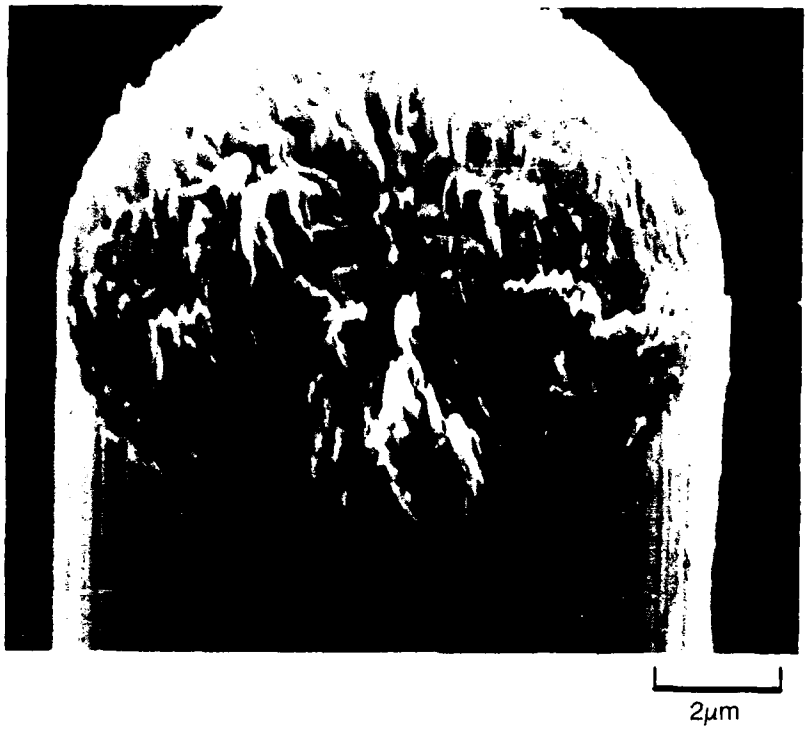

Fig. III-3 (c). Structure of Tonen UHM Carbon Fiber

Fig. III-3 (d). Structure of DuPont E-130 Carbon Fiber

89—7—50—15

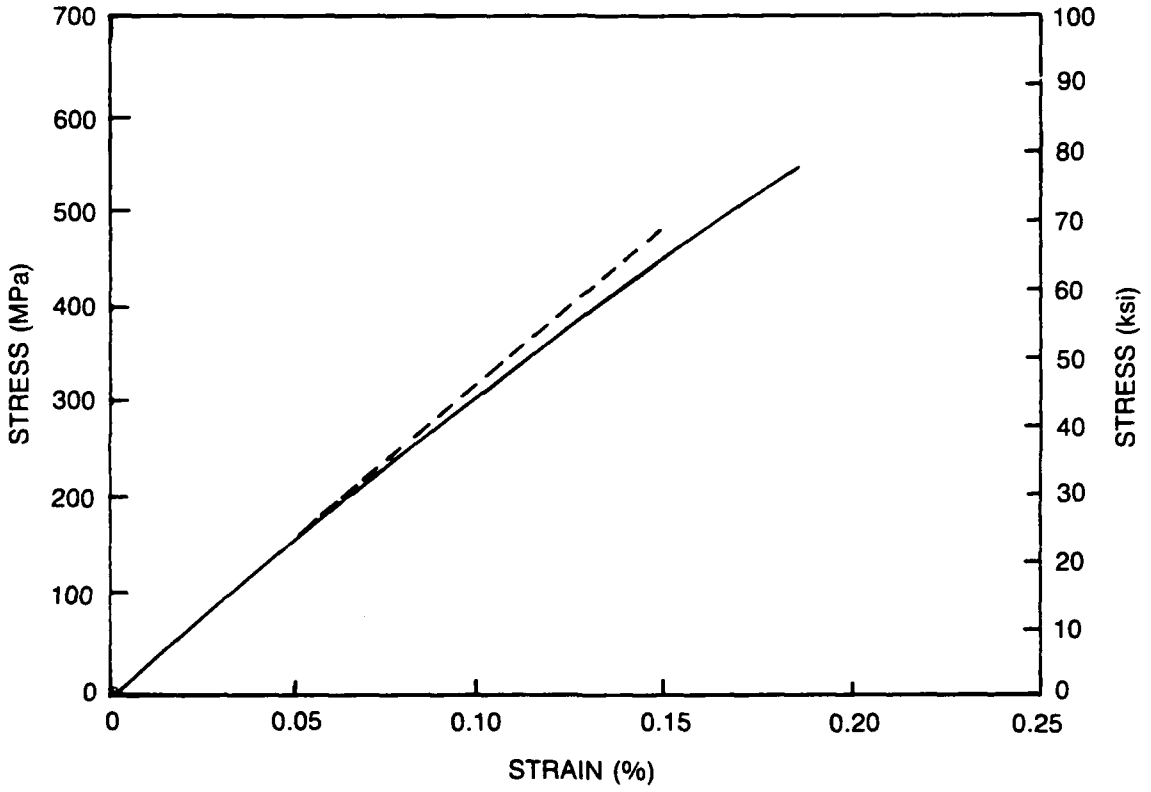

Fig. III-4. Longitudinal Strain vs Applied Tensile Load for 0°-39 v/o P-100/BSG-1

89—7—50—3

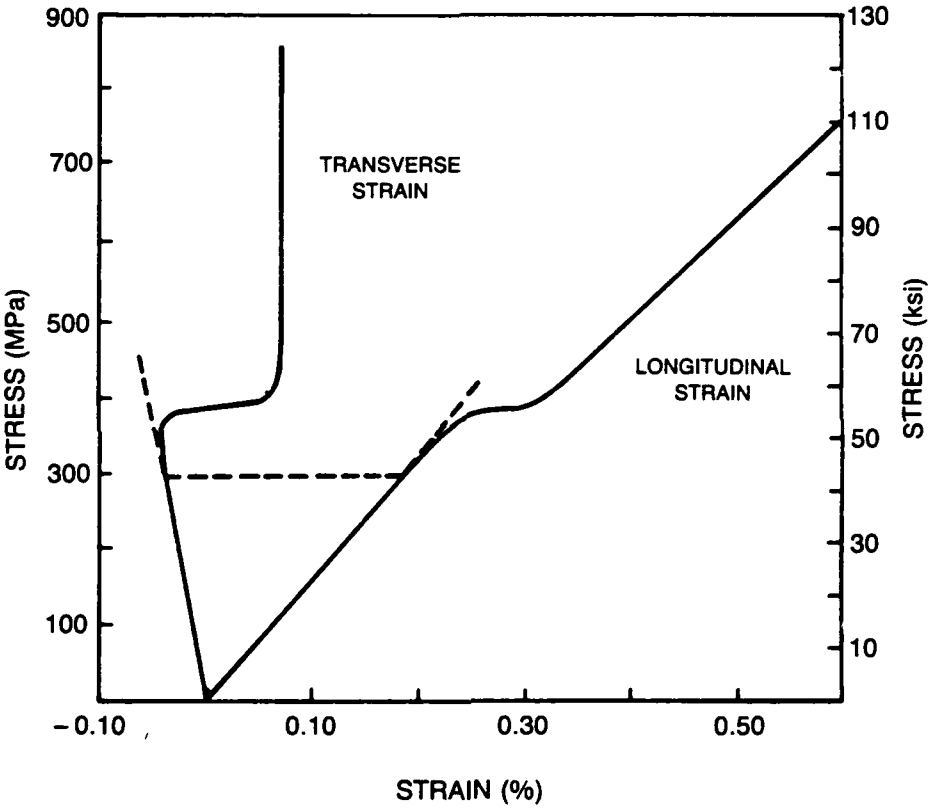

Fig. III-5. Longitudinal and Transverse Strain Versus Applied Tensile Load for 0°-43 v/o HMU/7740

86-7-54-3

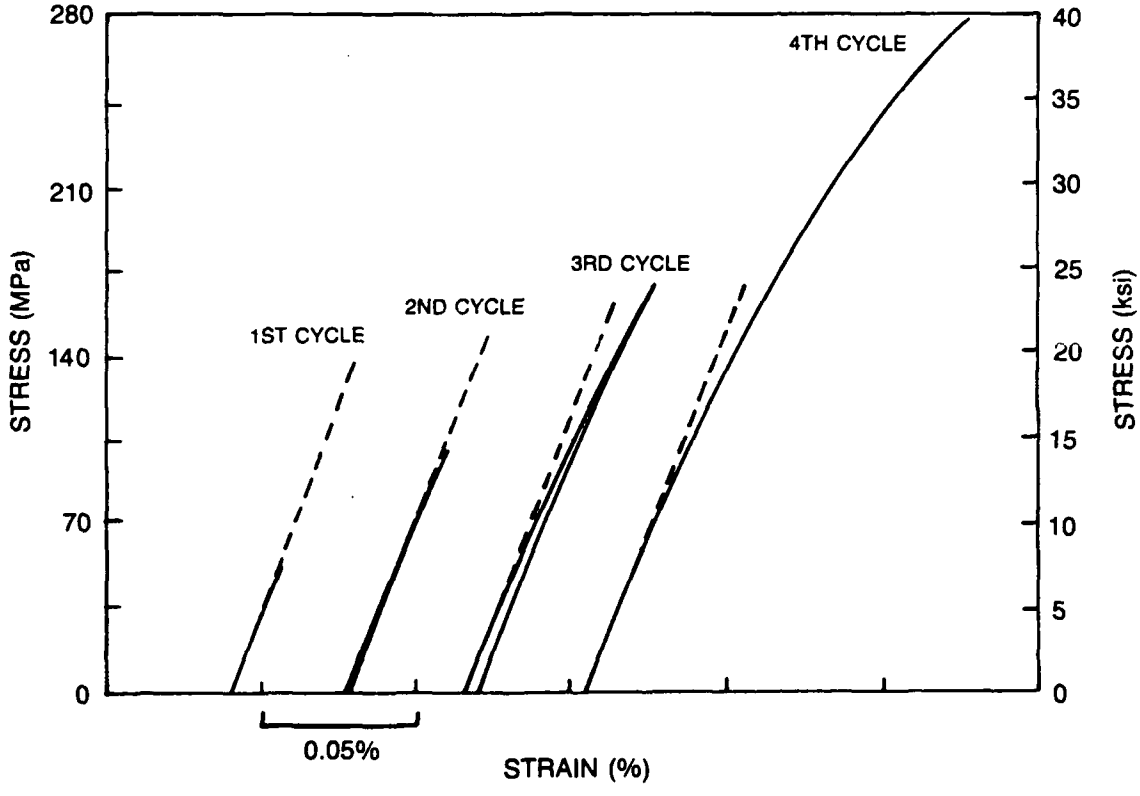

Fig. III-6. Cyclic Tensile Stress-Strain Behavior for 0°-38 v/o P-100/BSG-1

89—7—50—4

100μm

100μm

Fig. III-7. Tensile Fracture Surfaces of HMU/BSG-1 (top) and P-100/BSG-1 (bottom) Composites

200μm

100μm

Fig. III-8. Microstructure of a Pitch/BSG-1 Composite Containing Scrim

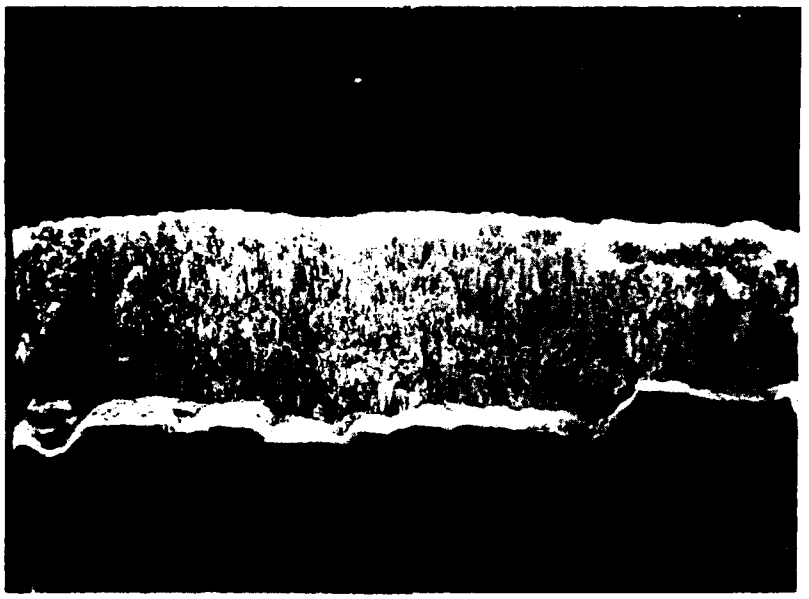

1 mm

1 mm

Fig. III-9. Flexural Fracture Surfaces of Pitch/BSG-1 Composites Without Scrim (top) and With Scrim (bottom)

89—7—50—18

IV. IMPROVED MECHANICAL BEHAVIOR IN PITCH FIBER REINFORCED GLASS MATRIX COMPOSITES THROUGH MATRIX MODIFICATION

The previous chapter discussed the tensile and flexural behavior of glass matrix composites reinforced with pitch-based carbon fiber where the matrix was the BSG-1 composition. While these composites demonstrated respectable levels of strength and stiffness, the proportional limit (PL) stress and strain values were somewhat low, with PL stresses of ~100 MPa and PL strains of 0.03-0.04%. These PL values represent less than 20% of the ultimate composite tensile stress and failure strain, which can be of great concern from a design standpoint. This chapter summarizes work conducted to improve PL behavior in Pitch/Glass composites by making modifications to matrix composition that result in less residual tensile stress in the matrix after composite fabrication.

A. Residual Stresses in Carbon Fiber Reinforced Glass Matrix Composites

Carbon fiber reinforced glass matrix (C/Glass) composites are characterized by a complex stress state as a result of coefficient of thermal expansion (CTE) mismatch between the carbon fiber and the glass matrix. Complicating the matter even further is the highly anisotropic nature of carbon fiber. This large degree of anisotropy in the axial and transverse fiber directions results from the graphitic microcrystalline structure of the fiber (for a more complete discussion of carbon fiber structure, refer to section III. C. 1.). Examples of properties that vary greatly in the two directions are CTE and elastic modulus, as summarized in Table IV-1 for HMU and P-100 fibers. The negative CTE of the fiber and the positive CTE of the glass results in the matrix being placed in residual tension in a direction parallel to the fibers. The magnitude of the tensile stress is determined by several factors other than the difference in CTE ($\Delta\alpha$) between fiber and matrix, including the fiber and matrix volume fractions, fiber and matrix moduli, and viscosity characteristics of the glass. The viscosity characteristic that is most important is the strain temperature (or strain point) of the glass, which is defined as the temperature below which the viscosity is so high that any further strain can be removed only after several hours at or above that temperature [1]. As the composite begins to cool from the fabrication temperature, the viscosity of the glass is low enough that the matrix can relax and relieve any accumulated stress until it reaches the strain temperature. After that, relaxation cannot occur and stress builds up as the composite continues to cool to room temperature.

The residual matrix stress existing at any temperature below the strain point can be calculated using a simple expression relating fiber and matrix CTE, fiber and matrix moduli, fiber volume fraction, and the change in temperature below the strain point. This expression can be given as

$$\sigma_m = \frac{(\alpha_f - \alpha_m)\,\Delta T\, E_f V_f}{1 + V_f\left(\frac{E_f}{E_m} - 1\right)} \quad , \qquad \text{(IV-1)}$$

where σ_m is the residual matrix stress, α_f and α_m are the fiber and matrix thermal expansion coefficients, respectively, ΔT is the temperature difference below the strain point ($T - T_{strain}$, where T is the temperature of the composite and T_{strain} is the strain point), V_f is the fiber volume fraction, and E_f and E_m are the fiber and matrix moduli, respectively. This expression makes several assumptions regarding the composite system, namely: (1) the problem is one-dimensional, which implies that stresses generated due to transverse CTE mismatch are negligible in comparison and therefore do not significantly affect the longitudinal stresses, and; (2) the CTE's and moduli of the fiber and matrix are independent of temperature over the ΔT range. The first assumption is fairly reasonable for the C/Glass composite system given the large difference in the longitudinal and transverse stiffness of carbon fiber. The second assumption, on the other hand, is rather bold since CTE and modulus are known to be functions of temperature for both the fiber and matrix. However, by using room temperature values of CTE and stiffness for each of the components, it is believed that approximations of residual matrix stress can be obtained so that relative comparisons can be made between different composite systems.

B. Tensile Stress-Strain Behavior

Equation IV-1 describing residual matrix stress in a C/Glass composite provides useful insight into approaches that can be taken to reduce this stress. Less residual tensile stress in the matrix should allow the composite to be loaded to a higher level of stress before matrix microcracking ensues. Assuming constant values of V_f, E_f, and α_f, it becomes clear that matrix stress can be reduced by using a glass with either: (1) a lower elastic modulus; (2) a lower CTE, or; (3) a lower strain point. Unfortunately, it is not a simple matter to change only one of these parameters without affecting the other two. However, one glass composition has been identified which results in a 25% decrease in residual matrix tensile stress in C/Glass composites containing pitch-based carbon fiber, placing them very close to the level of matrix stress in HMU/BSG-1 composites (which demonstrate excellent levels of PL stress and strain). Table IV-2 summarizes the results of calculations for composites containing these two types of fiber with both matrix compositions, assuming a constant fiber volume fraction of 0.40.

In order to evaluate the effect of lower residual tensile stress, several composites were fabricated using this different matrix composition (BSG-2) and three different types of pitch-based carbon fiber. The tensile stress-strain behavior of these composites is summarized in Table IV-3, including PL stress and strain and the corresponding residual matrix stress calculated

for each composite. Also included in the table for comparison are data for the composites fabricated using BSG-1 as the matrix (presented in Chapter III) and a composite in the HMU/BSG-1 system. The moduli of the Pitch/BSG-2 composites correspond closely to those predicted based on the rule of mixtures. Composite strengths are respectable for the composites containing P-100 and UHM fiber; however, the composite reinforced with E-130 fiber exhibited a rather low tensile strength. The reason for this low strength is unclear. Comparison of PL stresses and strains between the two matrix compositions reveals an outstanding increase in these parameters, even in the low-strength E-130/BSG-2 composite. This increase in PL stress and strain correlates well with the reduction in residual matrix stress resulting from the use of the BSG-2 matrix composition.

The stress-strain curves of P-100/BSG-2 and P-100/BSG-1 composites are compared in Figure IV-1. While the general shape of the curves is similar, it is clear that the linear portion of the curve (up to the PL) is much larger in the P-100/BSG-2 composite. Cyclic tensile testing of a P-100/BSG-2 composite was performed to assess the effect of repeated loading to successively higher stresses on the stress-strain behavior. The cyclic stress-strain curves are shown in Figure IV-2, with the results being summarized in Table IV-4. During the first cycle, the composite was loaded to a maximum stress of 220 MPa, with an initial elastic modulus of 315 GPa, and demonstrated linear behavior throughout the entire range. No permanent strain was introduced on the unloading portion of the cycle. In the subsequent second and third cycles, during which the maximum loads were 367 and 449 MPa, respectively, the composite also exhibited linear behavior and an elastic modulus of 315 GPa. No proportional limit was observed up to a stress of 449 MPa, where failure occurred at the doublers. The repetitive nature of the elastic modulus and the lack of a PL confirmed that there was no damage accumulation in the matrix, indicating that matrix microcracking was not taking place during loading of the composite.

The stress-strain curve of the UHM/BSG-2 composite was somewhat unusual in that the elastic modulus of the composite *increased* after going through the PL, as shown in Figure IV-3. The elastic modulus of carbon fibers is known to increase with an increase in strain due to the greater alignment of the graphite planes at higher strain levels [2]. However, the reason for the increase in composite stiffness only in the UHM/BSG-2 system is not clear. This behavior is believed to be a true characteristic of this composite system since it has been repeated several times among separate composites. Further investigation into this behavior is currently underway at UTRC.

The fracture behavior of all the Pitch/BSG-2 composites was very similar to that of the Pitch/BSG-1 composites described previously in Chapter III. As with the Pitch/BSG-1 composites, pullout lengths in the Pitch/BSG-2 composites were considerably shorter than those observed in the HMU/BSG-1 composite system. The similarity in fracture behavior correlates well with the interlaminar shear strengths that were observed in the Pitch/BSG-2 composites,

which were all in the range of 50 MPa. These values are slightly higher than those observed in the Pitch/BSG-1 system and imply that fiber-matrix interfacial shear strength may also be somewhat higher.

REFERENCES

1. P. W. McMillan, Glass-Ceramics, Academic Press, New York, 1979.

2. R. J. Diefendorf, RPI, 1988, personal communication.

3. V. C. Nardone and K. M. Prewo, *J. Mater. Sci.*, **23** (1988) 168-180.

Table IV-1

Anisotropic Properties Displayed by Carbon Fibers

	*CTE (ppm/°C)**		*Elastic Modulus (GPa)**	
Fiber	Axial	Transverse	Axial	Transverse
HMU	-0.7	13.1	380	10
P-100	-1.6	21.1	758	4

* Room temperature values

Table IV-2. Calculated Residual Matrix Stress σ_m for C/Glass Composites

		Fiber Properties			Matrix Properties			
Fiber	Matrix	V_f	α_f (ppm/°C)	E_f (GPa)	Strain Point (°C)	α_m (ppm/°C)	E_m (GPa)	σ_m (Calculated) (MPa)
P-100	BSG-1	0.40	-1.6	758	510	3.2	63	130
P-100	BSG-2	0.40	-1.6	758	456	3.25	51	97
HMU	BSG-1	0.40	-0.7	380	510	3.2	63	95

Table IV-3. Tensile Properties and Calculated Residual Matrix Stresses for Pitch/BSG-2 Composites

Matrix	Fiber	Fiber Vol %	Ultimate Tensile Strength (MPa)	Elastic Modulus (GPa)	Failure Strain (%)	*Proportional Limit* Stress (MPa)	*Proportional Limit* Strain (%)	σ_m (Calculated) (MPa)
BSG-2	P-100	33	661	289	0.25	412	0.14	94
	UHM	43	523	296	0.17	441	0.15	97
	E-130	36	317	317	0.11	248	0.08	97
BSG-1	P-100	39	537	324	0.19	104	0.03	130
	UHM	45	792	296	0.31	96	0.03	132
	E-130	37	668	345	0.23	97	0.03	131
	HMU*	44	785	169	0.60	290	0.19	98

* Reference [3]

Table IV-4

Cyclic Tensile Properties for P-100/BSG-2 Composite

Cycle	Maximum Stress (MPa)	Initial Elastic Modulus (GPa)	Proportional Limit Stress (MPa)
1	220	315	Linear to 220
2	367	315	Linear to 367
3	449	314	Linear to failure at 449

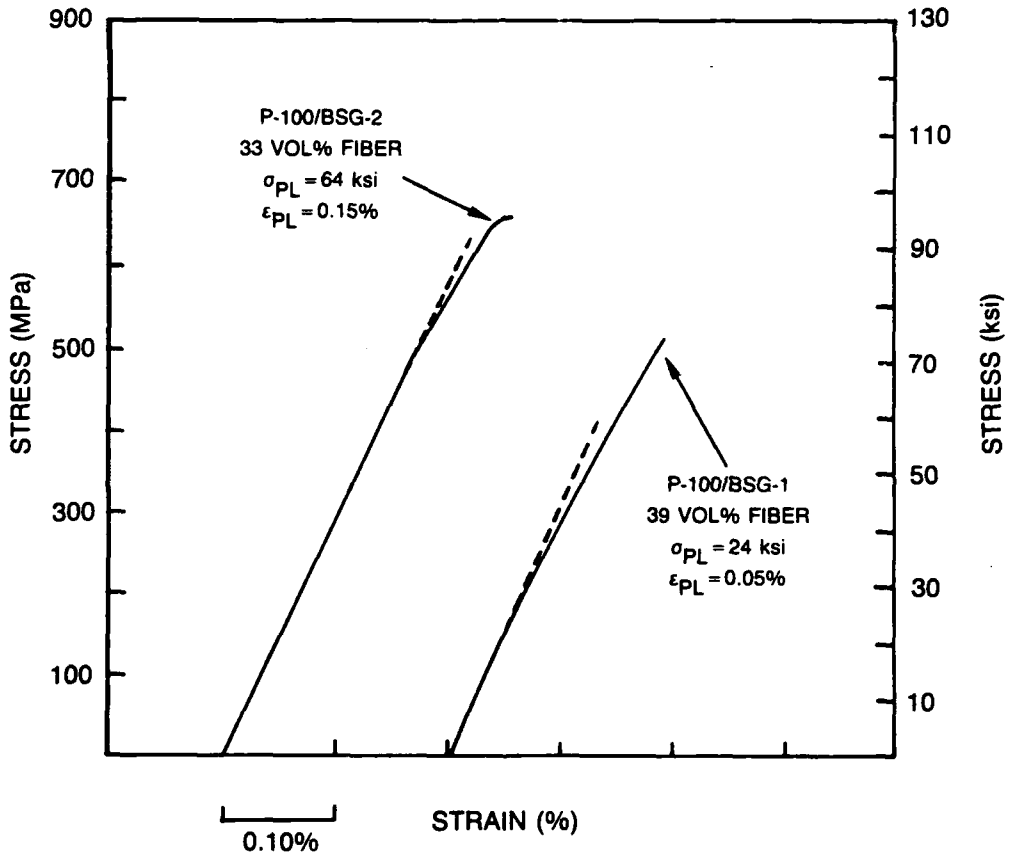

Fig. IV-1. Longitudinal Tensile Stress-Strain Behavior for 0° P-100/BSG-1 and 0° P-100/BSG-2 Composites

89—7—50—5

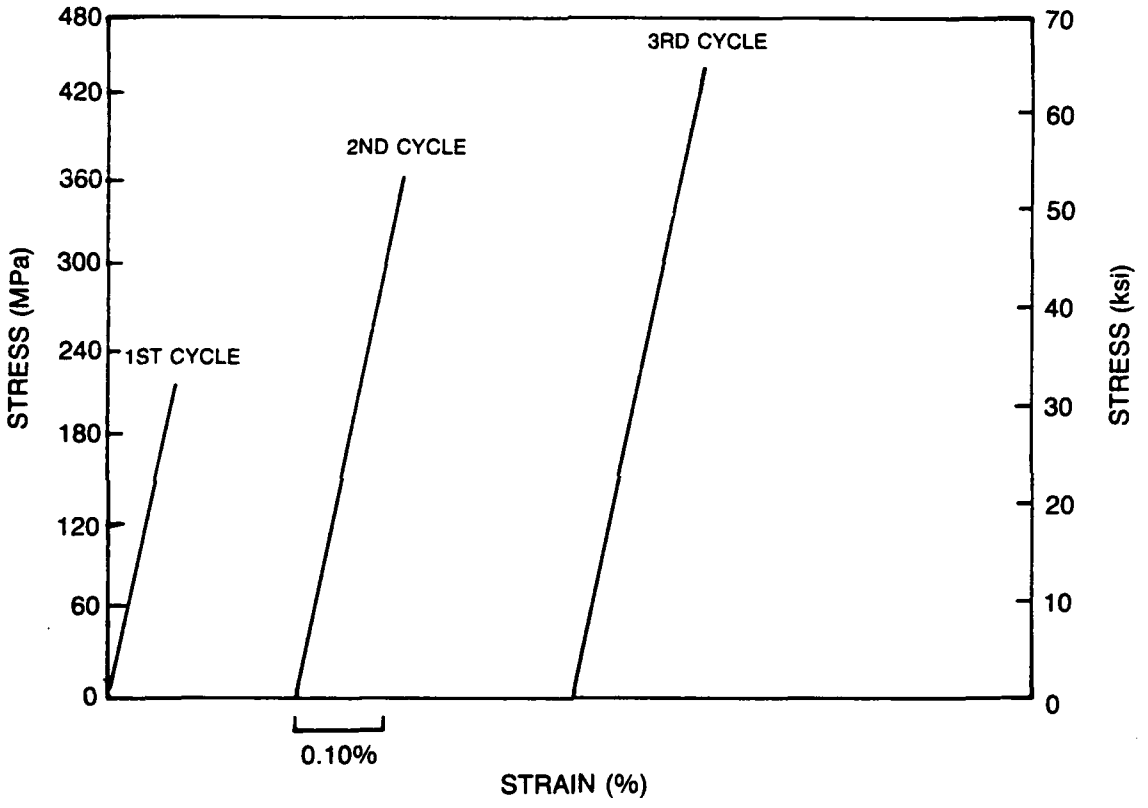

Fig. IV-2. Cyclic Tensile Stress-Strain Behavior for 0°-36 v/o P-100/BSG-2 Composite

89—7—50—6

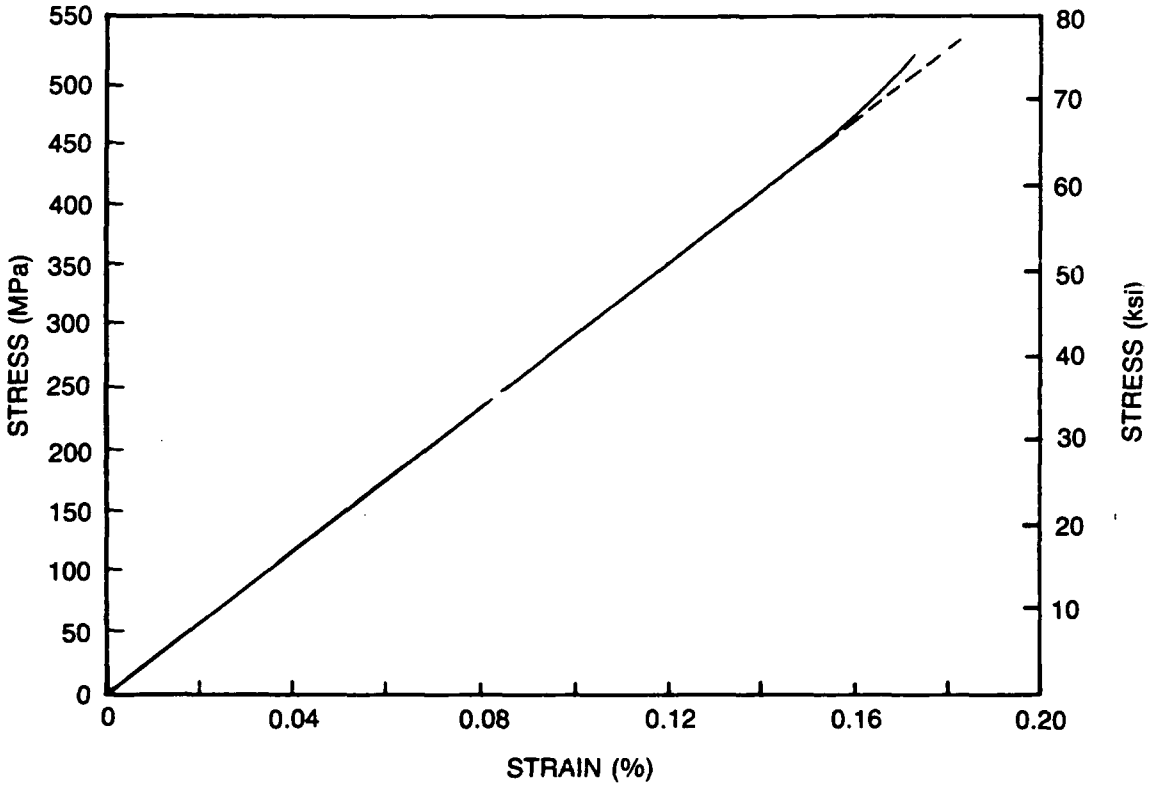

Fig. IV-3. Longitudinal Tensile Stress-Strain Curve for 0°-43 v/o UHM/BSG-2 Composite

89—7—50—7

V. THERMAL EXPANSION BEHAVIOR OF PITCH FIBER REINFORCED GLASS MATRIX COMPOSITES

Axial coefficient of thermal expansion (CTE) behavior for the P-100/BSG-1, E-130/BSG-1, UHM/BSG-2, and E-130/BSG-2 composites was evaluated over the temperature range of -150°C to +300°C. The thermal cycle was initiated at room temperature, followed by heating to 300°C, cooling to -150°C, and re-heating back to room temperature. At least two thermal cycles were always imposed. The CTE behavior of all the composite systems was found to be very similar. Typical thermal strain curves for the first and second cycles are shown in Figure V-1, representing the P-100/BSG-1 composite system. For both cycles, the hysteresis was fairly low, with values of ~25 ppm or less over the entire second cycle. This represents the maximum displayed by all the Pitch/Glass composites, with other systems exhibiting less than 10 ppm over the second thermal cycle. The initial cycle always exhibited a negative offset of 20-40 ppm at the end of the cycle; however, subsequent cycling was characterized by closed loop behavior. The offset is believed to be associated with matrix microcracking resulting from differential thermal expansion between fiber and matrix and/or "settling" of the dilatometer during the first thermal cycle.

Composite CTE over the -150°C to +300°C temperature range was derived from the thermal strain curves by approximating the closed loop of the second thermal cycle with a 5th-order polynomial curve that was fit using least squares analytical techniques. The resulting CTE curve for the P-100/BSG-1 composite is representative of all the composites and is presented in Figure V-2. From -150°C to +100°C, the CTE curve is relatively flat, varying from approximately -0.75 ppm/°C to -1.0 ppm/°C. From 100°C to 300°C, the CTE increases linearly from -0.75 ppm/°C to zero. The temperature range from -150°C to +100°C is probably of the most interest for space-based applications. The near linear CTE behavior and low hysteresis in this region is encouraging since it is believed that there are applications which can tolerate negative CTE behavior as long as it is reproducible.

Table V-1 compares the measured values of composite CTE for the P-100/BSG-1 composite with calculated values of CTE at several different temperatures. Calculated CTE's were derived from the expression shown in the table. The temperature range extends only to 50°C since data on fiber CTE was not readily available for higher temperatures. The calculated and measured values of α_c are in close agreement over the temperature range shown in the table, suggesting that even though the matrix may experience some degree of microcracking during thermal cycling, it maintains a large portion of its structural integrity and contributes stiffness to the composite.

Table V-1

Calculated and Measured Values of Composite CTE for the P-100/BSG-1 Composite System

		Composite CTE (10^{-6}/°C)	
Temperature (°C)	α_f (10^{-6}/°C)	Calculated*	Measured
-150	-1.09	-0.69	-0.82
-100	-1.415	-0.99	-1.01
-50	-1.57	-1.13	-1.08
0	-1.49	-1.06	-1.05
25	-1.395	-0.97	-1.00
50	-1.29	-0.88	-0.94

* Calculated values of composite CTE were derived from the expression

$$\alpha_c = \frac{\alpha_f E_f V_f + \alpha_m E_m V_m}{E_f V_f + E_m V_m} \quad ,$$

where α is CTE, E is modulus, V is volume fraction, and the subscripts c, f, and m denote composite, fiber, and matrix, respectively.

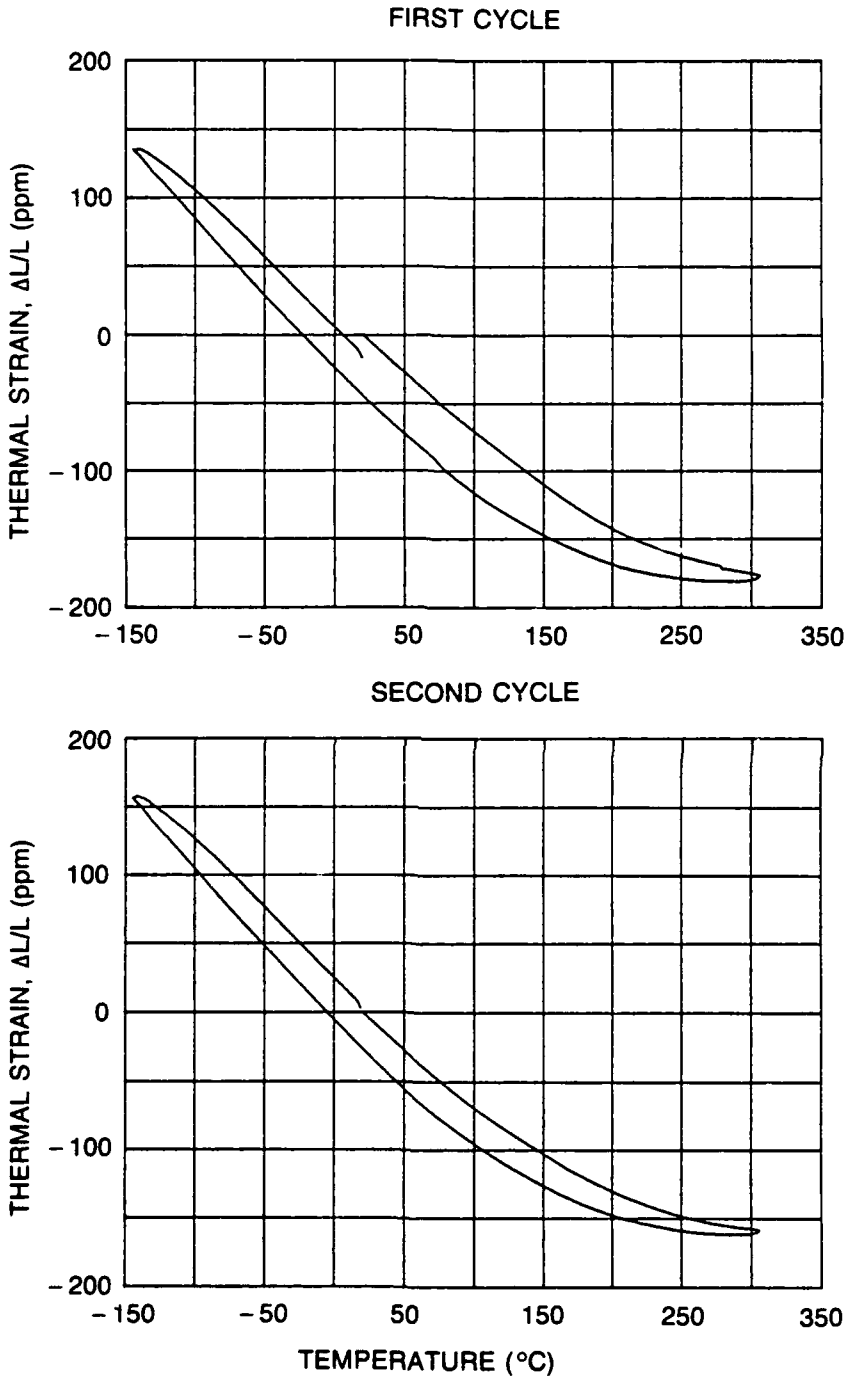

Fig. V-1. Axial Thermal Strain vs Temperature for 0°-45 v/o P-100/BSG-1 Composite: First Cycle (Top); Second Cycle (Bottom)

89—7—50—8

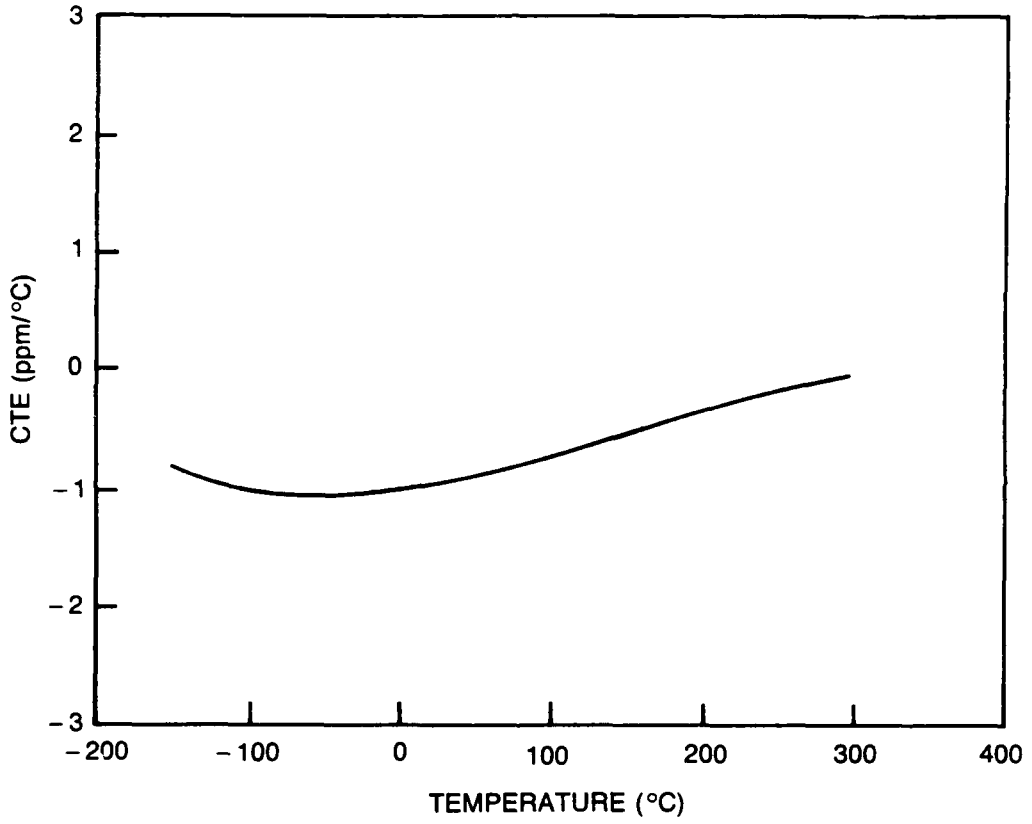

Fig. V-2. Average Axial Coefficient of Thermal Expansion for 0°-45 v/o P-100/BSG-1 From −150°C to 300°C

89—7—50—9

VI. DEVELOPMENT OF HIGH TEMPERATURE MATRICES FOR CARBON FIBER REINFORCED GLASSES

High modulus composites utilizing pitch-based carbon fibers and borosilicate glass matrices have been successfully developed with the hope that they will prove to be useful materials for structural applications in space. However, in certain applications where the potential exists for a large increase in temperature as the result of a thermal threat, borosilicate glass matrices may not provide suitable structural integrity, particularly once the temperature exceeds 500-600°C. For this reason, the development of matrices capable of withstanding temperatures of 800-1200°C was undertaken in order to improve the survivability of C/Glass composites being utilized in space-based systems. This chapter summarizes the initial work conducted in this development, including a description of the matrix materials used, room temperature tensile behavior, the relationship between fracture behavior and composite microstructure, and high temperature flexural testing.

A. Matrix Compositions

Several matrix compositions were evaluated in this study and are listed in Table II-1 (located in the Experimental Procedure section). One composition, designated as BSG-3, was a glass containing a large fraction of SiO_2, which is the most refractory of the glass-forming oxides. This composition was chosen because it had demonstrated good high temperature capability in Nicalon®-reinforced composites [1]. The other two compositions, designated as LAS-I and BMAS, were glass-ceramics from the lithium aluminosilicate and barium magnesium aluminosilicate systems, respectively. Glass-ceramics are materials that have the characteristics of glasses at elevated temperatures (so that they can be easily deformed and fabricated) but can be crystallized through a suitable heat treatment to initiate nucleation and crystal growth (this heat treatment will be referred to hereafter as "ceraming"). By choosing the proper matrix composition, the crystalline phases that form during this ceraming treatment can be quite refractory.

The primary crystalline phase that forms in the LAS-I composition when ceramed at ~900°C is β-quartz solid solution [2], which is comprised of β-eucryptite ($LiAlSiO_4$) and β-quartz (SiO_2). In the BMAS composition, the primary crystalline phase that precipitates when ceramed at ~1140°C is the totally-stuffed form of barium osumilite ($BaMg_2Al_6Si_9O_{30}$). β-quartz solid solution and barium osumilite are both highly refractory crystalline phases, with temperature capability above 1000°C. In both of these glass-ceramic compositions, the amount of amorphous material that converts to the crystalline phase is greater than 75%. It is desirable to have as little amorphous material remaining after ceraming as possible, since the residual glass is the temperature limiting phase in the glass-ceramic matrix. Large amounts of residual glass can

lead to a decrease in temperature capability through viscous relaxation mechanisms. (For a more complete discussion of glass-ceramics, Reference [3] is an excellent source of general information.)

B. Composite Fabrication

Pitch fiber reinforced composites were fabricated using the BSG-3, LAS-I, and BMAS matrix compositions as detailed in Table VI-1. The ceraming cycle temperatures for the LAS-I composites were ~780°C for nucleation followed by crystallization at ~900°C, while the temperatures used for the BMAS composites were ~870°C for nucleation and~1150°C for crystal growth. These ceraming temperatures were derived from differential thermal analysis traces of the starting glass powders. Ceraming was performed in a flowing argon atmosphere to minimize oxidation of the carbon fibers. X-ray diffraction of the ceramed composites confirmed that the primary crystalline phases were β-quartz solid solution in the LAS-I composites and barium osumilite in the BMAS composites. Traces of mullite ($3Al_2O_3 \cdot 2SiO_2$) and hexacelsian ($BaAl_2Si_2O_8$) were also identified.

C. Tensile Stress-Strain Behavior

The tensile stress-strain behavior of the composites is summarized in Table VI-1. The P-100/BSG-3 composite demonstrated excellent strength and stiffness, with a high proportional limit (PL) stress. These properties are comparable to those of the best Pitch/BSG-1 and Pitch/BSG-2 composites (described previously in Chapters III and IV), with the added benefit of increased temperature capability (to be discussed in a subsequent section). The shape of the stress-strain curve for the P-100/BSG-3 composite is similar to that of the Pitch/BSG-2 composite discussed earlier.

The stress-strain behavior of the composites containing glass-ceramic matrices varied greatly between the LAS-I and BMAS systems and also within each system between the as-fabricated and ceramed conditions. The LAS-I composites exhibited much lower tensile strengths and stiffnesses than the BMAS composites, with correspondingly low PL stress and strain. The shape of the stress-strain curves was also quite unusual (Figure VI-1), with very flat regions of increasing strain at constant stress just prior to failure. These regions would seem to be associated with a large amount of fiber slippage and pullout; however, the fracture surfaces did not exhibit these characteristics, as shown in Figure VI-2. The ceramed sample possesses a large degree of fiber pullout compared to P-100/BSG-1 composites (refer to Figure III-7), but certainly not to the extent suggested by the stress-strain curve. The fracture surface of the as-fabricated sample was very similar to that of P-100/BSG-1 composites, with very little fiber pullout. This lack of correlation between the stress-strain curves and the fracture surfaces has not yet been explained.

The low values of tensile strength and modulus in the LAS-I composite can be explained based on weak interfacial adhesion resulting from the large difference in transverse fiber and matrix CTE. The transverse CTE of P-100 fiber is ~21ppm/°C, compared to a matrix CTE of 3 ppm/°C in the amorphous state and 1 ppm/°C after ceraming. It is likely that the matrix CTE in the as-fabricated condition is between 1 and 3 ppm/°C due to partial devitrification during cooling from the hot-pressing temperature. The large degree of differential shrinkage that occurs during cooling results in a fiber-matrix interface that is under high tensile stress, which probably weakens interfacial adhesion to the point that load transfer from the matrix to the fiber is not as efficient. Ceraming degrades the interfacial adhesion even further due to the larger difference in CTE, resulting in even less efficient load transfer and lower values of composite stiffness. Also contributing to the drop in modulus after ceraming was an increase in matrix porosity associated with a volume decrease during crystallization of β-quartz solid solution from the matrix glass (Figure VI-3). This increase in porosity effectively decreases the interfacial contact area, thus reducing load transfer efficiency. This factor was believed to play a minor role in the stiffness decrease compared with the transverse CTE mismatch. As a result of the overall poor performance demonstrated by the LAS-I matrix composition when used in combination with pitch-based carbon fibers, further investigation of this composition was discontinued.

The tensile performance of both the P-100/BMAS and the E-130/BMAS composites was excellent, with high values of strength and stiffness in the as-fabricated condition. In fact, these values were the highest obtained among all the composites reinforced with pitch-based carbon fiber studied in this investigation. The shape of the stress-strain curves was similar to that of P-100/BSG-1 composites. Ceraming was found to degrade the strength and modulus of both composites somewhat, with the magnitude of the strength decrease being greater in the P-100/BMAS composite. The loss in stiffness is thought to primarily result from an increase in matrix porosity resulting from a slight shrinkage that takes place during crystallization of barium osumilite from the glass. An increase in matrix porosity was observed in optical micrographs of both systems after ceraming (Figure VI-4), with measured increases in apparent porosity ranging from 2.5 to 5 % (apparent porosity, which is the surface-connected porosity in a material, was determined using liquid displacement density measurements). As described previously, it is believed that the increased porosity results in less interfacial contact area, slightly reducing the load transfer efficiency. Associated with this reduction in interfacial contact in the ceramed BMAS composites was a 25-50% decrease in interlaminar shear strength (implying lower values of τ_{max}) and an increase in fiber pullout, as shown in Figure VI-5. This suggests that while ceraming may lead to small reductions in composite stiffness, it may also result in composites with improved fracture toughness in addition to increased temperature capability

D. High Temperature Performance

Three-point flexural testing was performed on the BSG-3, LAS-I, and BMAS composites

reinforced with P-100 fiber at room temperature and at 800°C in an inert atmosphere. The results are presented in Table VI-2 and in Figure VI-6. It can be seen that all the composites demonstrated full retention of strength at the upper temperature of 800°C. It is expected that the LAS-I and BMAS composites should maintain structural integrity up to at least 1000°C based on the refractory nature of the matrix compositions. It is interesting to note that the flexural strength in the LAS-I and BMAS ceramed composites exhibited a substantial increase in strength at 800°C compared to room temperature. This can be explained by again considering the difference in transverse CTE between fiber and matrix. As the composite is heated to 800°C, the differential transverse expansion results in greater fiber-matrix adhesion as the fiber expands more rapidly than the matrix, thereby increasing load transfer efficiency.

REFERENCES

1. K. M. Prewo, "Silicon Carbide Yarn Reinforced Glass Matrix Composites," UTRC Report R79-111330-6, UTRC Internal Report, October, 1979.

2. W. K. Tredway and K. M. Prewo, "Carbon Fiber Reinforced Glass Matrix Composites for Space Based Applications," UTRC Report R87-917470-1, ONR Annual Report, August 30, 1987.

3. P. W. McMillan, Glass-Ceramics, Academic Press, New York, 1979.

Table VI-1. Mechanical Behavior of High Temperature Matrix Composites

Fiber	Matrix	Fiber Vol %	Condition	Ultimate Tensile Strength (MPa)	Elastic Modulus (GPa)	Failure Strain (%)	*Proportional Limit* Stress (MPa)	*Proportional Limit* Strain (%)	Interlaminar Shear Strength (MPa)
P-100	BSG-3	49	As-fabricated	641	386	0.17	418	0.11	30
P-100	LAS-I	42	As-fabricated	214	262	0.43	43	0.02	39
			Ceramed	83	193	0.87	21	0.01	23
P-100	BMAS	46	As-fabricated	689	358	0.24	130	0.04	33
			Ceramed	393	331	0.13	143	0.04	18
E-130	BMAS	49	As-fabricated	820	413	0.23	186	0.05	33
			Ceramed	620	386	0.17	261	0.07	25

Table VI-2

High Temperature Strength of Pitch Fiber Reinforced Composites

			3-Point Flex Strength (MPa)	
Fiber	Matrix	Condition	25°C	800°C
P-100	BSG-3	As-fabricated	626	660
P-100	LAS-I	As-fabricated	510	--
		Ceramed	181	485
P-100	BMAS	As-fabricated	633	--
		Ceramed	428	642

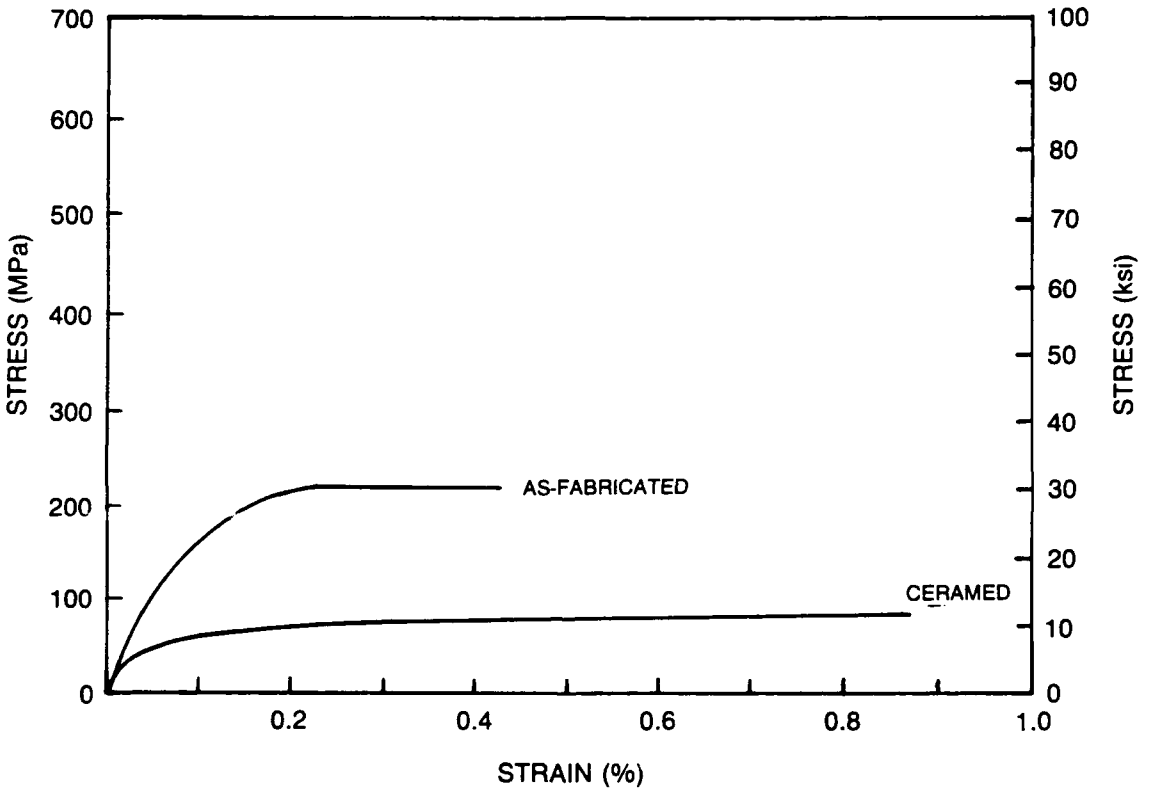

Fig. VI-1. Longitudinal Tensile Stress-Strain Curves for 0°-42 v/o P-100/LAS-I Composite in As-Fabricated and Ceramed Condition

89—7—50—10

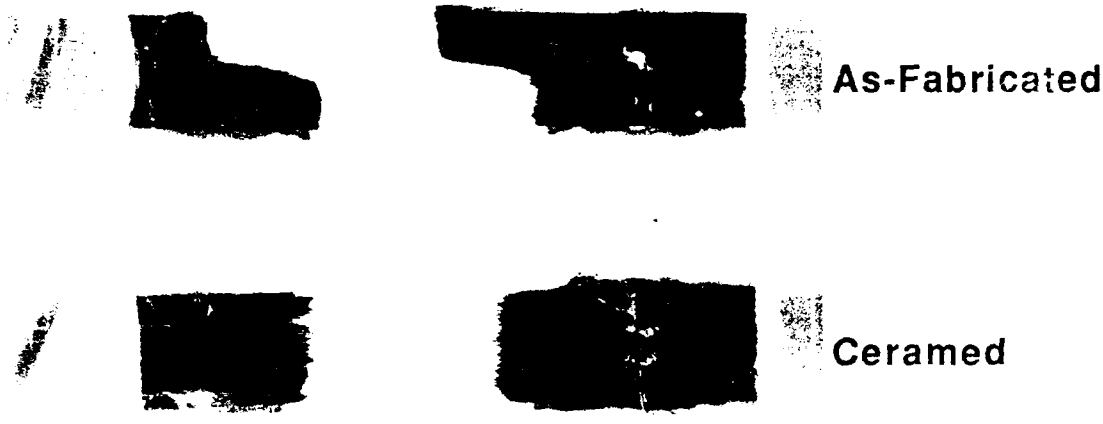

Fig. VI-2 (a). **Fracture Morphology of P-100/LAS-I Composites**

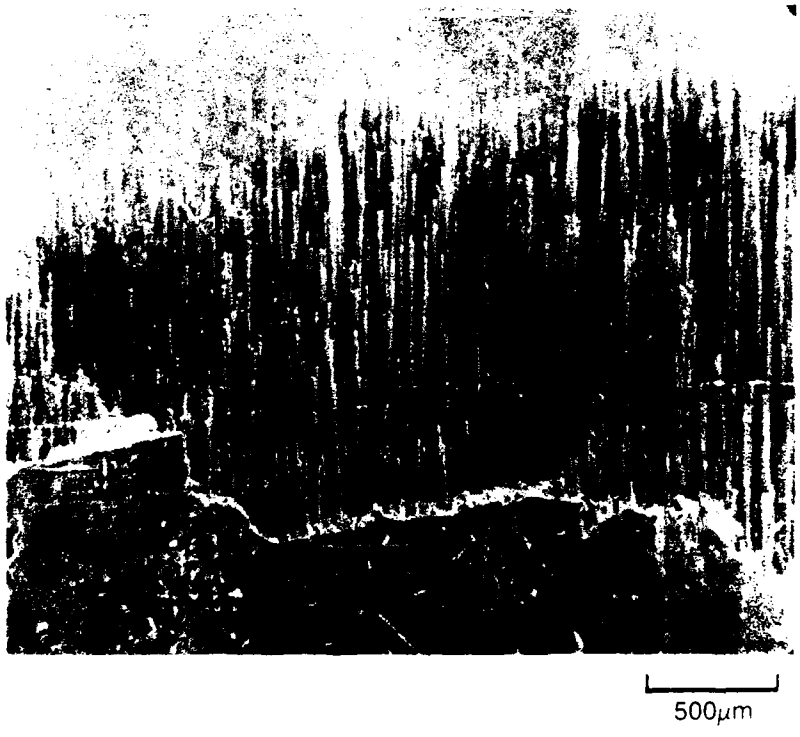

Fig. VI-2 (b). **Tensile Fracture Surface of Ceramed P-100/LAS-I Composite**

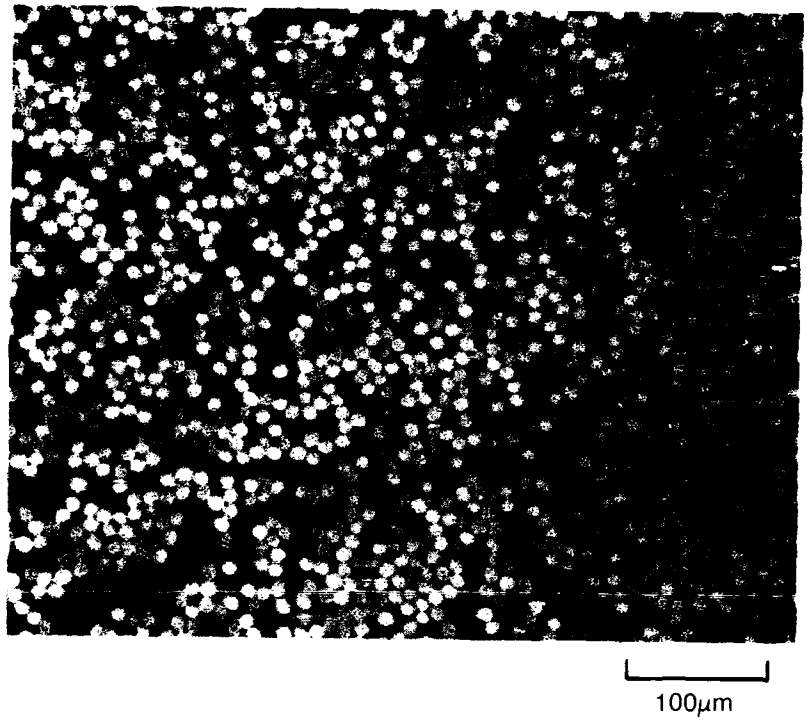

Fig. VI-3 (a). Microstructure of As-Fabricated P-100/LAS-I Composite

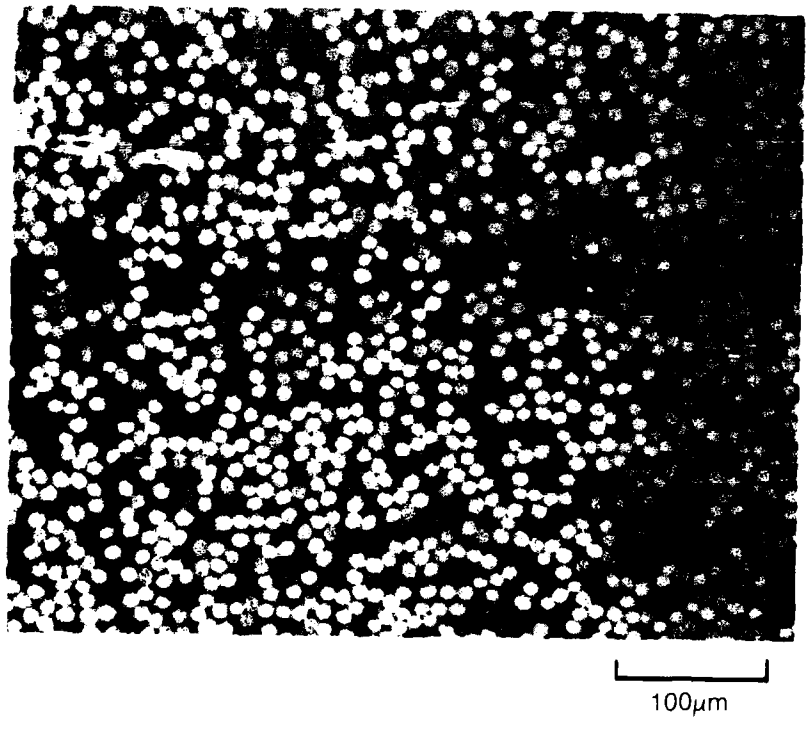

Fig. VI-3 (b). Microstructure of Ceramed P-100/LAS-I Composite

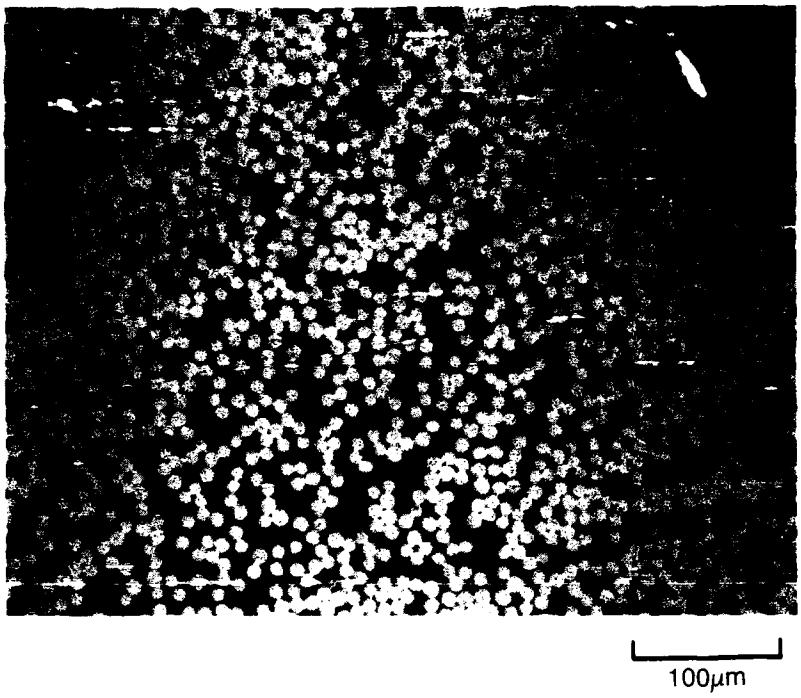

Fig. VI-4 (a). Microstructure of As-Fabricated P-100/BMAS Composite

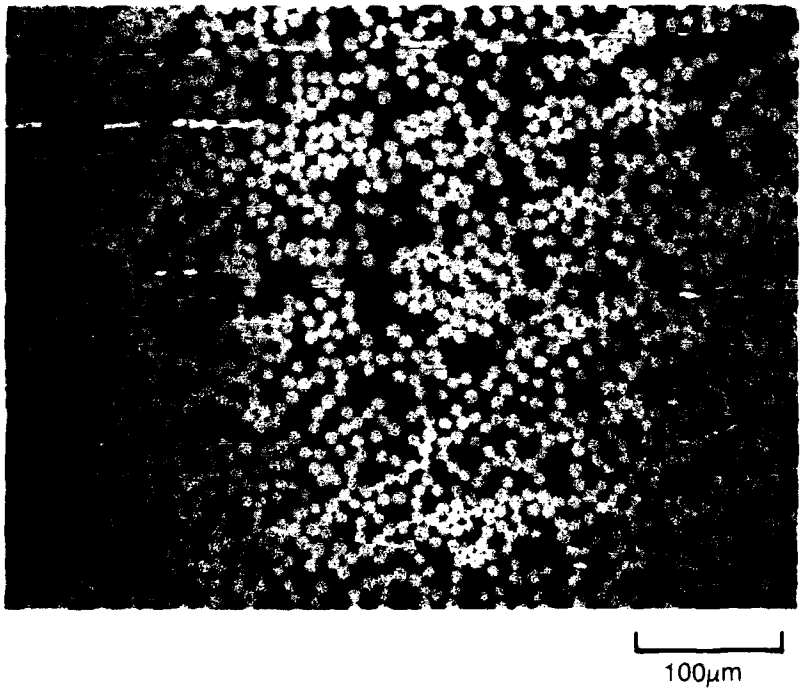

Fig. VI-4 (b). Microstructure of Ceramed P-100/BMAS Composite

89—7—50—21

Fig. VI-5 (a). Fracture Morphology of P-100/BMAS Composites

Fig. VI-5 (b). Tensile Fracture Surface of Ceramed P-100/BMAS Composite

89—7—50—22

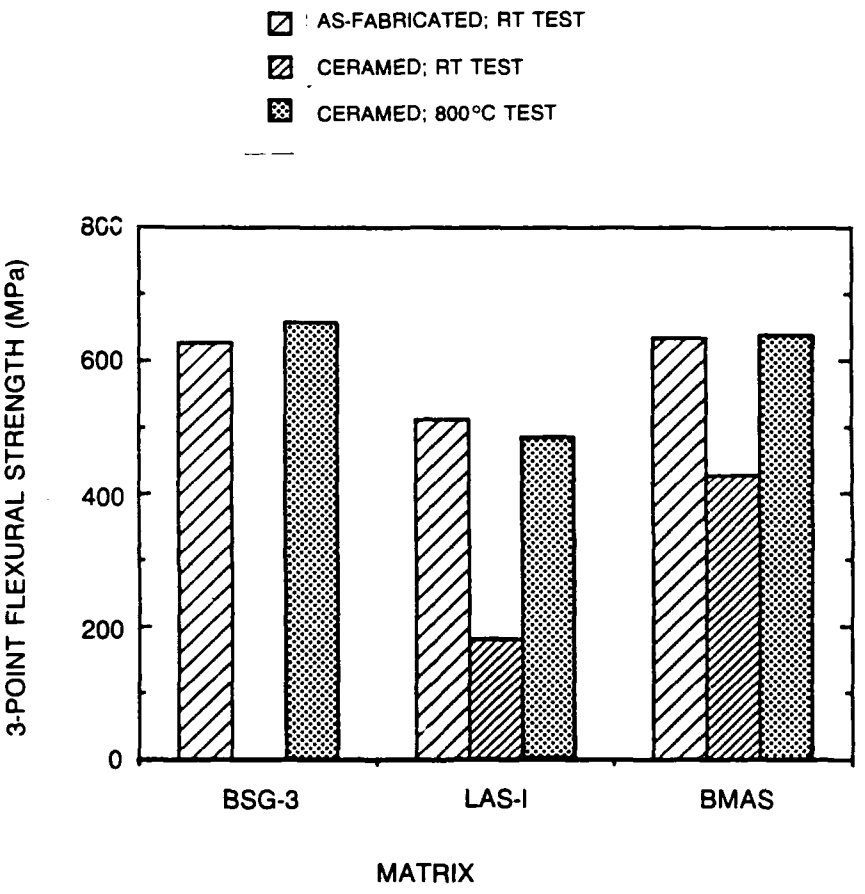

Fig. VI-6. Three-Point Flexural Strength for P-100 Fiber Reinforced Composites at Room Temperature (RT) and 800°C

89—7—50—12

VII. INTERFACE REACTIONS AND WETTING IN CARBON FIBER REINFORCED GLASS MATRIX COMPOSITES

C. G. Pantano, G. Chen and D. Qi
Department of Materials Science and Engineering
The Pennsylvania State University
University Park, PA 16802

A. Introduction

The fiber/matrix interfaces in carbon-fiber reinforced glass matrix composites are created during their high temperature fabrication. Due to the very low surface energy of carbon (fibers), the molten glass is non-wetting. Thus, the pressure employed in hot-pressing the composite plays an important role not only in the composite densification, but also in the development of intimate solid/liquid interfaces and in penetration ot the liquid into irregularities along the fiber surfaces. Of course, the final characteristics and stability of this interface depends upon any chemical reactions which occur at elevated temperature, and further, upon the stresses which develop during cooling. Nevertheless, it seems likely that the intrinsic wetting and spreading of the glass matrix phase are fundamental to the overall interface evolution. To be sure, the absence of any significant adherence between the carbon fibers and glass matrix is responsible for the high-fracture toughness of these composites [1], and this is certainly related to the limited wettability in this system.

The primary objective of this study was to evaluate effects of the glass matrix composition upon wetting and spreading of the glass on Pitch- and PAN-based carbon fibers. A secondary objective was to observe the relationship between wetting and any associated degradation of the carbon fibers. Two different methods were developed to study these interactions. In one case, hot-pressed composites were heated in an inert atmosphere at temperatures in excess of the softening point. This caused the glass matrix phase to *de-wet* the fibers, and thereby, to expose the fiber surfaces and to form micro-sessile drops on the fiber surfaces. In the other method, thin glass coatings were deposited on single filaments and on fiber tows using a sol/gel technique. These *model fiber/glass interfaces* have been used to study the interface reactions and wetting directly. The advantages of this method are that the glass composition can be easily varied using sol/gel synthesis, and that the carbon fiber surfaces - with a thin coating of the matrix glass - can be readily observed and characterized.

The effects of B_2O_3, Na_2O and variable valence transition metal oxides (Nb_2O_5 and MoO_3) in the glass matrix composition were of primary interest. The oxidation of carbon fibers is inhibited in the presence of B_2O_3 [2-4], and it is catalyzed in the presence of Na_2O and many other

metal oxides [5-9]. MoO_3 is also an exceptional oxidation catalyst for carbon, whereas no catalytic effect of Nb_2O_5 has been reported [6]. In addition, the variable valence transition metal oxides influence the local redox equilibria at the fiber matrix interface, and thereby, can lead to gaseous and solid phase *interphase* reaction products. Here, Nb_2O_5 and MoO_3 were chosen for study because their effect upon the interface thermochemistry and composite properties have already been reported [10, 11]. The experiments were carried-out on both Pitch and PAN based fibers to evaluate any differences in their surface chemical and structural characteristics. Here, too, it has already been reported [12] that the mechanical performance of Pitch- and PAN-based fiber composites are different, and in some cases, this could be attributed to interface effects. Finally, the effects of inert versus reducing atmospheres upon the interface reactions were examined.

B. Experimental Procedure

The primary variables in this study were the glass matrix composition and the type of carbon fiber. Table I presents the various glass compositions, and the type of specimen in which they were evaluated. The carbon fibers were either PAN-based HMU[a] , or Pitch-based P-100[b] .

The hot-pressed composites were supplied by United Technologies Research Center (UTRC). Uniaxial, continuous fiber composites were fabricated by hot-pressing pre-pregged tapes which were made by using the glass frit slurry infiltration technique [1]. The glass compositions used in these hot-pressed composites were CGW 7740 ($81SiO_2$, $13B_2O_3$, $4Na_2O$ and $2Al_2O_3$) and some special sodium borosilicate (NBS) melts where the Al_2O_3 was eliminated or where 1% Nb_2O_5 or 1% MoO_3 was added. In the case of these hot-pressed composites, fracture surfaces were examined after a heat-treatment in high-purity argon at 1200°C and 1300°C. This heat treatment caused *de-wetting* of the glass matrix, and thereby, sessile drops were created and the carbon fiber surfaces were exposed.

The glass thin film coatings were prepared using a sol/gel method. Most of the raw materials were organometallic compounds: tetraethoxysilane (TEOS), trimethyl borate, aluminum sec-butoxide, sodium acetate, niobium ethoxide and molybdenum dichloride dioxide. These compounds were mixed and hydrolyzed stepwise in an ethanol solution. In all cases, a transparent solution could be obtained. The use of these solutions to fabricate glass matrix composites has already been reported [13]. Here, the solutions were used to dip-coat 10 cm long carbon-fiber filaments or yarns. These carbon fibers were obtained directly from the manufacturers without any sizing applied. The fibers were held in the solution for 10 seconds, slowly withdrawn, and then dried in air at room temperature. The coated fibers were heated in air at 400°C for 30 minutes to remove residual organics and water. Finally, the fibers were heated at 1200°C or 1300°C in argon

[a] Hercules, Magna, UT 84044

[b] Amoco Performance Products, Inc., Ridgefield, CT 06877

(~>ppm O_2) or in carbon monoxide for 30 to 45 minutes. The fibers were then examined in the scanning electron microscope (SEM).

C. RESULTS

C. 1. Transition-Metal Oxide Effects

The SEM micrographs in Figure 1, show the effects of MoO_3 and Nb_2O_5 upon the fiber/matrix interaction in HMU/7740 composites. The composites were fractured along the fiber direction, and then were heated in argon for two hours at 1300°C to cause the glass matrix phase to de-wet the fiber surfaces. The micrograph in Figure 1a shows that little or no degradation of the fibers is apparent, whereas in Figures 1b and 1c, the influence of MoO_3 and Nb_2O_5 – even at the 1% level – is evident. The reactions that caused most of this degradation probably occurred during both the initial hot-pressing of these composites, although some additional reaction is likely during the de-wetting. (The de-wetting was carried out at 1200°C also, and the extent of degradation was comparable.) It seems certain that the fiber degradation is responsible for the poor mechanical performance reported in these transition-metal doped systems [11].

Figures 2, 3 and 4 show a similar set of micrographs, except in these cases, the interaction occurred between thin sol/gel glass coatings and the fiber surfaces. In general, the extent of degradation is less than in the case of the hot-pressed composites. This is due to differences in thermal history of the two specimens. The coated fibers (in Figures 2, 3 and 4) were held in argon at 1000-1200°C for only 45 min, whereas the composites (in Figure 1) were hot-pressed at 1200-1300°C, and then later, heated further at 1200°C or 1300°C to de-wet the fibers. Nevertheless, the effects of the matrix compositions are consistent. Namely, the fibers which were coated with glasses containing Nb_2O_5 or MoO_3 show definite pitting and attack of the surface, whereas the undoped borosilicate composition shows no obvious attack of the fibers. The micrographs in Figures 2, 3 and 4 also show the difference between HMU versus P-100 carbon fibers. It is evident that the type of fiber influences the morphology of the attack. The P-100 fibers are pitted preferentially along the grooves in the corrugated surface structure, and moreover, the grooves are elongated. In contrast, the HMU fibers show rounded pits which are more randomly distributed over the fiber surfaces.

The micrographs in Figure 2 show that the contact angle between the oxide glass and carbon fiber is different for P-100 (Pitch) versus HMU (PAN) carbon fiber. This effect of the carbon fiber type upon the contact angle was also observed in the hot-pressed composites The contact angle is usually greater than 90° on the HMU fibers, and less than 90° on the P-100 fibers. In most cases, the sessile drops were smaller and more numerous on the P-100 fibers. The presence of Nb_2O_5 or MoO_3 did not significantly influence the observed contact angle, but it is shown below that the B_2O_3/Na_2O concentration ratio exhibits a big effect upon the wetting.

C. 2. Influence of Na_2O and B_2O_3

The SEM micrographs in Figures 5 and 6 show the effect of the B_2O_3/Na_2O ratio upon the contact angle. These specimens were prepared using the sol/gel glass coating method. All of the glass compositions which contained Na_2O (see Table I) exhibited contact angles of the order 90° or greater. There was a trend that with increasing B_2O_3/Na_2O rations, the contact angle first increases and then decreases, but the effect was not dramatic. However, in the absence of Na_2O, a significant decrease in the contact angle could be observed. The micrographs in Figure 6 show the exceptional wetting exhibited by the binary $B_2O_3 \cdot 3SiO_2$ composition. It was also observed that the extent of carbon fiber degradation was minimal in the Na_2O-free composition.

The difference in surface morphology which develops on the Pitch and PAN fibers due to the interface reaction with glass is most obvious. Figure 7 shows more clearly that in the case of HMU fiber, a uniform microporosity develops in the fibers. Moreover, a cratering of the fibers occurs in those regions where the molten glass droplets were in contact with the fiber. In contrast, the extent of cratering on the P-100 fibers is virtually nonexistent. Rather, preferential etching along the fiber axis occurs. The size and orientation of the etch grooves on the P-100 fibers may account for the slightly lower contact angles observed on P-100 versus HMU for all the compositions. That is, the difference in wetting behavior between these two fiber types may be due more to differences in surface roughness than in chemistry.

C. 3. Atmosphere Effects

The reaction between oxide glasses and carbon generates CO and CO_2 [10]. This suggests that the presence of a high CO activity in the atmosphere during the initial development of the fiber/glass interface could limit degradation of the fibr surfaces. This hypothesis was examined using the ternary sodium borosilicate sol/gel coatings. All of the glass coating compositions listed in Table I were deposited and pre-treated (in air at 400°C) in a manner identical to those already described. In this case, t! ough, the coated fibers were heat-treated in CO at 1300°C. The most important observation made in these experiments was the absence of any significant degradation of the fibers after the heat-treatment in CO. Figure 7b (heat-treated in CO) can be compared directly to Figure 7a (heat-treated in Ar). The microporosity and cratering observed on the HMU fibers after the treatment in Ar is not observed after the treatment in CO. In the case of the P-100 fibers, the extent of preferential etching of the corrugated microstructure is much less prevalent. These differences were observed for all of the glass compositions.

These experiments also suggested a relationship between the wetting and extent of fiber degradation. This effect was especially prevalent in the case of the P-100 fibers. The apparent contact angle is measurably higher on all of the P-100 fibers heat-treated in CO. Again, this points

to the role of surface roughness in wetting and spreading of the oxide glass or the carbon fibers. The only exception to this is the sodium-free binary borosilicate where the spreading was substantial in CO. This was also observed in Ar. It should also be recalled that in argon, the sodium-free composition did not yield any obvious etching or cratering of the fibers – in spite of the coverage of the carbon fibers. Altogether, these observations reveal that sodium catalyzes a reaction between the glass and carbon fiber surface. The reaction is limited if a high activity of CO is maintained in the atmosphere during the initial contact between the glass and fiber, or if sodium is eliminated in the glass composition. Finally, it shows that one effect of the interface reaction is the development of surface roughness which influences the contact angle, spreading, and probably, adhesion of the glass on the fiber surface.

C. 4. Interfaces in Composites

In general, the chemical effects at the interfaces in carbon fiber/borosilicate glass composites are minimal, and this probably accounts for the high contact angles observed in these systems. Figure 8 presents some Auger microanalyses obtained on the fracture surface of a PAN-based carbon-fiber/borosilicate glass composite. Most of the surfaces on the fiber pullouts are pure carbon. Nevertheless, regions where the glass matrix is still adherent to the fibers can always be found. The analyses obtained in the matrix troughs (not shown) were largely representative of the glass phase, although some carbon could be detected there. It is emphasized that the carbon Auger signal on the surface of the matrix trough was significantly greater than the background level found on a fractured region of the glass matrix. The possible formation of silicon-carbide and/or silicon-oxycarbide was specifically investigated by analysis of the trough surfaces using Auger (carbon line-shape analysis) and x-ray photoelectron spectroscopy (XPS), but the presence of these compounds could not be verified. Thus, it is likely that the carbon found on the surface of the trough represents CO or CO_2 diffusion into the glass phase and/or adherent microcrystallites of the carbon fibers. Altogether, these surface analyses are consistent with easy debonding of the carbon/glass interface. The micrographs presented below suggest that the limited adherence which is observed in this system is due to the presence of localized interphase reaction products (associated with specific impurities or dopants) and/or morphological discontinuities in the interface.

Figure 9 compares the fracture surfaces of the P-100 and HMU fiber composites. It is obvious that the morphology of the interfaces is very different. The extent of debonding and fiber-pullout is more prevalent in HMU fiber composites than in P-100 fiber composites, and this can probably be attributed to the smoother interfaces in the HMU system. This, in turn, accounts for the higher fracture toughness reported for the HMU composites [12]. In the P-100 composite, the corrugated interface increases the interfacial area, and thereby, influences the interfacial shear strength. Moreover, the mechanical interlocking of the glass matrix phase and the corrugated fiber surface further increases the interfacial shear strength.

The interface morphologies observed on the composite fracture surfaces correlate directly with the interface reactions observed in the wetting and de-wetting studies. The comparison in Figure 9 shows clearly that the interface morphology in the composites is analogous to the surface morphology on the de-wetted fibers (Figure 1) and the sol/gel coated fibers (Figure 2). Figure 10 compares HMU carbon fiber pullouts in composites prepared with and without the MoO_3 additions. Here, too, the interfaces are analogous to the surfaces in Figure 1a (the un-doped composite) and Figure 1b (the MoO_3-doped composite). The effects of the reaction products upon the interfacial shear strength are easy to understand after observing the lower micrograph in Figure 10. The interfacial shear strength (measured using a fiber push-out test) was 16 MPa in the undoped-matrix, and 38 MPa in the MoO_3-doped matrix [12]. These reaction products were identified as Mo_2C using transmission electron microscopy (TEM) and x-ray diffraction (XRD) [11]. The consequences of these reaction products upon the fiber surface, itself, are more clearly seen in Figure 1b. The corresponding effect of this interface reaction upon the fiber strength has not been determined, per se, but it is probably the most important factor in control of the composite mechanical performance.

The micrographs in Figure 11 present another view of the interfaces in these composites. Here, an interlaminar fracture surface was created in the Nb_2O_5-doped composite. This exposed a trough in the matrix where the presence of pores can be seen. These pores were not observed in the matrix troughs of the undoped composites. They may be associated with particulate reaction products on the fiber surface, but more likely are due to the gas evolution which accompanies the interface reactions in composites doped with transition metal-oxide.

D. DISCUSSION

The interface reactions which occur between glass matrices and carbon fibers have already been evaluated using a thermochemical model [10]. Primarily, they reveal that the generation of CO and CO_2 gas is fundamental to the interaction. Thus, the local activity of CO and CO_2 at the interface will influence the extent and nature of the reaction. The calculations indicate that SiC will form only if the CO/CO_2 activity at the interface is low. The fact that neither silicon carbide nor silicon oxycarbide could be found at the interface via Auger microanalyses of the matrix trough) suggests that the reaction of carbon and glass leads to high local pressures of CO and CO_2 whose transport away from the interface is limited. On the other hand, the reduction of Nb_2O_5 and MoO_3 occurs readily at the carbon fiber/matrix interface, and therefore, the CO/CO_2 pressures can be even higher in these systems than at interfaces where these variable valence dopants are not present. But in these doped systems, carbide and oxycarbide reaction products are stable at high CO/CO_2 pressures. It has already been reported [11], and was further demonstrated here, that these Mo- and Nb-carbide reaction products are present at the interfaces in doped composites. It was also reported that the strength of the composites was significantly reduced when these dopants

were included. Here, the fiber surface reaction coating studies showed that the loss of mechanical strength is probably due to the effect of these reactions on the integrity of the fibers. These fiber surfaces were etched, pitted, and rather grossly degraded through the addition of these oxides. But in the presence of an external CO atmosphere, these reactions are limited, and the associated fiber degradation and interphase reaction products are not observed.

It was also found that the contact angle between the glass matrix phase and carbon fibers is influenced by the B_2O_3 to Na_2O concentration ratio. It is to be expected that increases in B_2O_3 content will reduce the surface tension of a silicate glass, and this probably accounts for the slight reduction in contact angle in the composition rante Na_2O/B_2O_3 = 1.5 to .33. Nevertheless, the abrupt and obvious decrease in the contact angle when Na_2O is eliminated in the glass phase suggests a more specific effect. The fact that Na_2O catalyzes the oxidation of carbon reveals a potential chemical effect of Na_2O. But the unique effects of B_2O_3 cannot be overlooked. It is well known that B_2O_3 *wets* graphite, and further, *limits* the oxidation of carbon [2-4]. It is for this reason that B_2O_3 additions are used in the fabrication of carbon-carbon composites. The reason for the compatibility of B_2O_3 and carbon surfaces has never been rigorously explained, but is probably associated with the molecular structure of the boron oxide liquid. In pure B_2O_3, planar $[BO_3]$ triangles and $[B_3O_6]$ boroxyl rings constitute the liquid structure. The preferred orientation of these planar species at surfaces and interfaces is energetically favorable. And in this orientation, they can more readily wet the low energy carbon fiber surface. However, in sodium-borate and sodium-borosilicates, the so-called *boron-oxide anomaly* leads to a change in the coordination of boron to create $[BO_4]$ tetrahedra. It is proposed here that this accounts for the abrupt change in contact angle of the binary B_2O_3-SiO_2 glasses, relative to the ternary Na_2O-B_2O_3-SiO_2 compositions.

These studies also demonstrated an effect of the carbon fiber upon the interface reactions. There are a number of reasons to expect the interface chemistry and structure to depend upon the carbon fiber type; (i) the graphitic microcrystallites which constitute the Pitch fibers may nucleate crystals in the glass matrix near the interface, (ii) the oxide functional groups (C=O and COOH) on the fiber surfaces may differ in concentration and activity, (iii) Pitch fibers are more oxidation resistant than PAN fibers, and thereby, limit the thermochemical reactions and local CO pressure during hot pressing, and (iv) the morphology which develops due to oxidation of the fiber surface by the glass matrix may differ due to differences in the internal structure of the two fiber types. The SEM micrographs obtained in the matrix troughs have, on occasion, suggested the presence of crystallized glass at the fiber/glass matrix interface. But, the prevalence of this phenomena does not show a measurable dependence upon fiber type. Nevertheless, this local crystallization may play an important role in determining the interface adhesion, in general. The Auger microanalyses have not revealed any significant difference in the surface composition of carbon fiber pullouts between HMU and P-100; in fact, except for adherent extracts of the glass matrix, oxide has never been detected on either of the carbon fiber types! These observations further indicate that

differences in the interfacial shear strength between Pitch- and PAN-based carbon fiber composites are associated with the morphology differences shown in Figure 9. Since both fiber types are oxidized to a certain extent by the glass matrix during processing, the difference in interface morphology is probably related to the internal microstructure of the fiber. This creates a unique surface structure during oxidative etching of the fibers by the molten matrix phase. This effect is evident at the interfaces in the composites (Figure 9), as well as on the surface of the de-wetted and glass coated fibers (Figures 2-7). The enhanced wetting of the P-100 fibers by the glass matrix occurs due to roughness effects, and not necessarily to chemical differences at the interface.

E. SUMMARY

The contact angle of the borosilicate glass matrix phase on the carbon fibers is of the order 90-150°. The primary reaction creates gaseous reaction products whose high local activity and limited diffiusivity eliminates the possible formation of solid interphase reaction products. The gaseous reaction products probably contribute toward the creation of a weak bonding layer in the final composite, although localized etching and/or reactions with impurities may cause some adherence. This is consistent with the rather clean interfacial debonding observed in this system.

The interface reactions were significantly enhanced when the matrix phase was doped with small concentrations of reducable transition metal oxides. In this case, degradation of the fibers was most apparent, but in addition, the formation of interphase reaction products could be clearly observed. These effects led to a significant reduction in the mechanical properties of the composites. The observed influence of these dopants provides insight to the interface reactions, but perhaps of more significance, they suggest that impurities in the matrix and/or fibers can lead to localized reactions at the interface.

Finally, some of the effects of glass matrix composition and carbon fiber type were demonstrated. The wetting was greatly enhanced in the case of binary borosilicate compositions, but it remains to be determined whether enhanced wetting influences the final properties of the composite. The creation of distinct interface morphology and rugosity was most prevalent in the Pitch-based fibers. The rough, corrugated surface on the P-100 fibers is intrinsic to their internal structure which is exposed during oxidation by the matrix. The enhanced wetting or adhesion due to roughness is consistent with the high interfacial shear strength, as well as the limited debonding and fiber pull-out, exhibited by the P-100 composites.

ACKNOWLEDGEMENT

The authors gratefully acknowledge the Office of Naval Research (ONR N00014-55-C-0332 and N00014-87-K-0247) for their support of this research.

REFERENCES

1. K. M. Prewo, J. J. Brennan and G. K. Layden, "Fiber Reinforced Glass and Glass-Ceramics for High Performance Applications," *Am. Cer. Soc. Bull.*, **65** (2), 305-313, 322 (1986).

2. D. W. McKee, C. L. Spiro and E. J. Lamby, "The Effect of Boron Additives on the Ocidation Behavior of Carbons," *Carbon*, **22** (6), 507-511 (1984).

3. P. Ehrburger, P. Baranne and J. Lahaye, "Inhibition of the Oxidation of Carbon-Carbon Composite by Boron Oxide," *Carbon*, **24** (4), 495-499 (1986).

4. D. W. McKee, "Borate Treatment of Carbon Fibers and Carbon/Carbon Composites for Improved Oxidation Resistance," *Carbon*, **24** (6), 737-741 (1986).

5. P. L. Walker, Jr., M. Shelef and R. A. Anderson, "Catalysis of Carbon Gasification," in Chemistry and Physics of Carbon, P. L. Walker, Ed., Vol. 4, 287-383 (1968).

6. D. W. McKee, "Metal Oxides as Catalysts for the Oxidation of Graphite," *Carbon*, **8**, 623-635 (1970).

7. D. W. McKee and D. Chaterji, "The Catalytic Behavior of Alkali Metal Carbonates and Oxides in Graphite Oxidation Reactions," *Carbon*, **13**, 381-390 (1975).

8. B. P. Jalan and Y. K. Rao, "A Study of the Rates of Catalyzed Boudouard Reactions," *Carbon*, **16**, 175-184 (1978).

9. Y. K. Rao and A. A. Adjonolo, "Catalysis of the Boudouard Reactions," *High Temperature Science*, **19**, 51-77 (1985).

10. P. M. Benson, K. E. Spear and C. G. Pantano, "Thermochemical Analyses of Interface Reactions in Carbon-Fiber Reinfored Glass Matrix Composites," in Ceramic Microstructures '86, J. A. Pask and A. G. Evans, Ed., Plenum Press, New York, 415-425 (1987).

11. K. M. Prewo, W. Tredway and C. G. Pantano, "Carbon Fiber Reinforced Glass Matrix Composites for Space Based Applications, UTRC Report R87-917470-1, ONR Annual Report, August 30, 1987.

12. W. Tredway, K. M. Prewo and C. G. Pantano, to appear in *Carbon*, 1989.

13. D. Qi and C. G. Pantano, "Sol/Gel Processing of Carbon-Fiber Reinforced Glass Matrix Composites," in Ultrastructure Processing of Advanced Ceramics, J. D. Mackenzie and D. R. Ulrich, Ed., John Wiley and Sons, Inc., 635-649 (1988).

Table I

Sample Specifications

Glass Frits: Hot-Pressed Composites

- $81SiO_2$, $13B_2O_3$, $4Na_2O$, $2Al_2O_3$ (CGW 7740)
- $83SiO_2$, $13B_2O_3$, $4Na_2O$ (NBS)
- $82SiO_2$, $13B_2O_3$, $4Na_2O$, $1Nb_2O_5$ (NBS + 1% Nb_2O_5)
- $82SiO_2$, $13B_2O_3$, $4Na_2O$, $1MoO_3$ (NBS + 1% MoO_3)

Sol/Gel Glass Coating Composites: Glass Coatings on Fibers

- $83SiO_2$, $13B_2O_3$, $4Na_2O$ + 2,4% Al_2O_3
- $83SiO_2$, $13B_2O_3$, $4Na_2O$ + 2,4% Nb_2O_5
- $83SiO_2$, $13B_2O_3$, $4Na_2O$ + 2,4% MoO_3
- $74SiO_2$, $0B_2O_3$, $26Na_2O$
- $74SiO_2$, $5B_2O_3$, $21Na_2O$
- $73SiO_2$, $11B_2O_3$, $15Na_2O$
- $73SiO_2$, $16B_2O_3$, $11Na_2O$
- $73SiO_2$, $21B_2O_3$, $6Na_2O$
- $72SiO_2$, $28B_2O_3$, $0Na_2O$

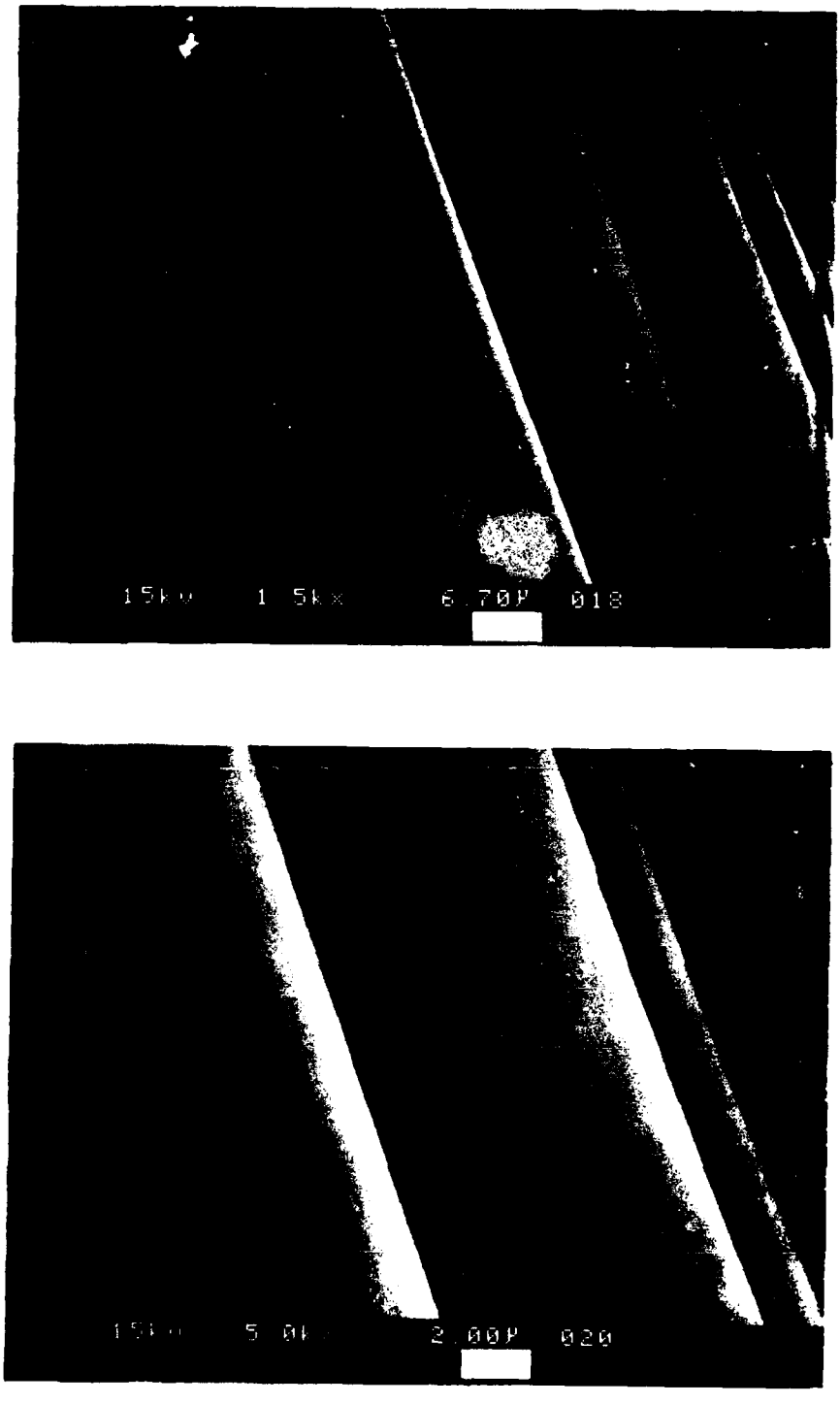

Fig. 1a. The Fiber Surfaces Exposed in a Hot-Pressed HMU/NBS Composite After De-Wetting in Argon

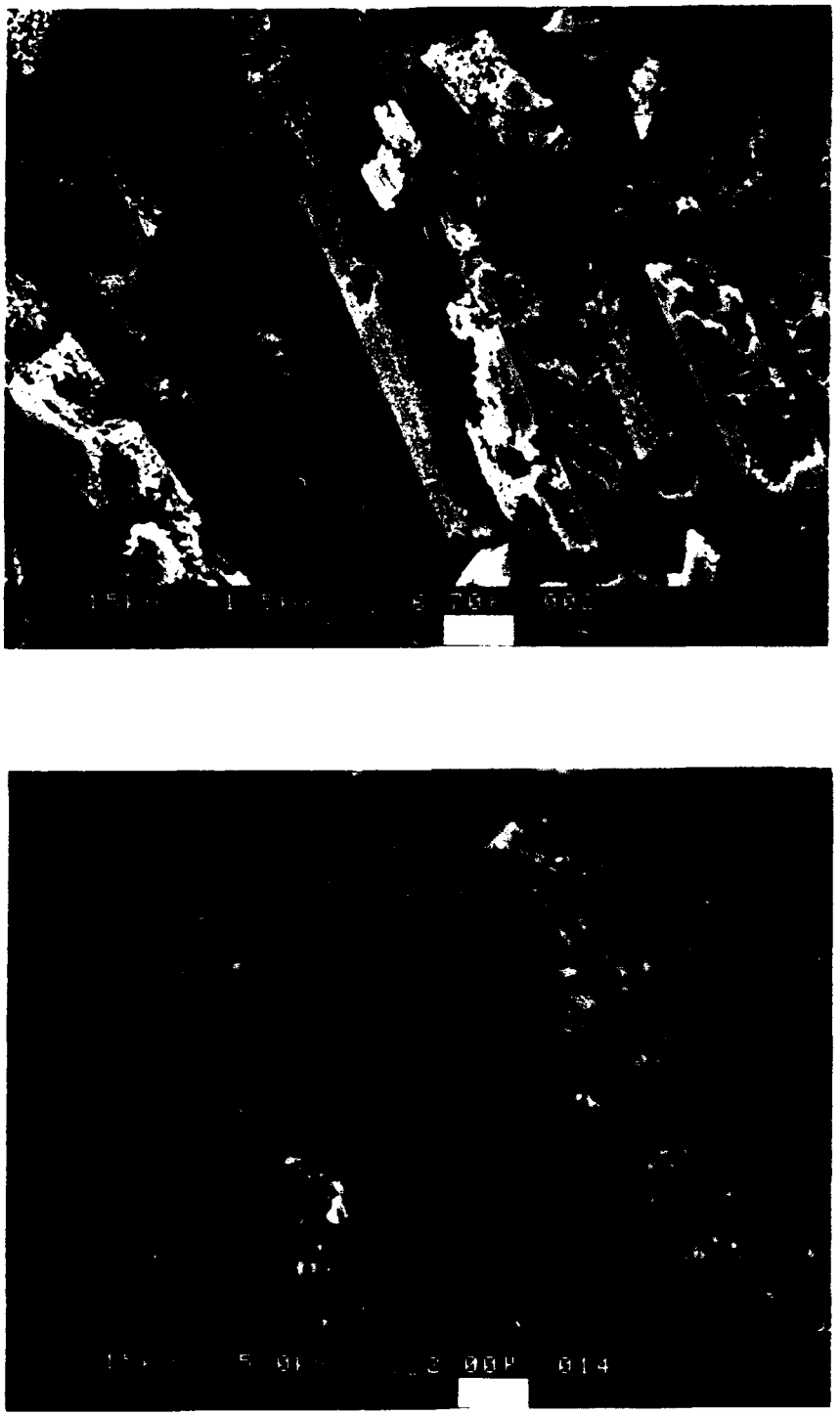

Fig. 1b. The Fiber Surfaces Exposed in a Hot-Pressed HMU/NBS + 1% MoO_3 Composite After De-Wetting in Argon

89—7—50—24

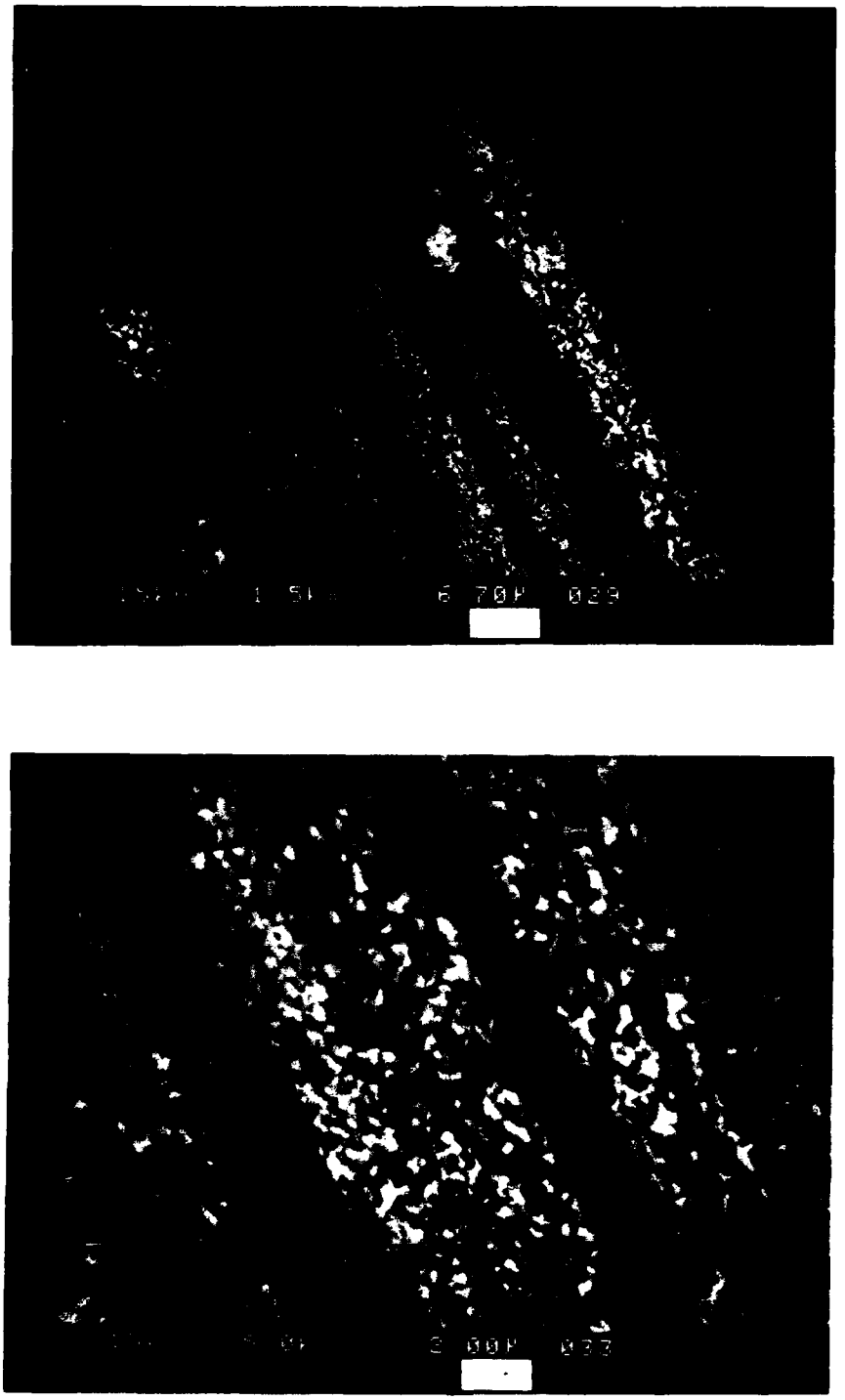

Fig. 1c. The Fiber Surfaces Exposed in a Hot-Pressed HMU/NBS + 1% Nb_2O_3 Composite After De-Wetting in Argon

89—7—50—25

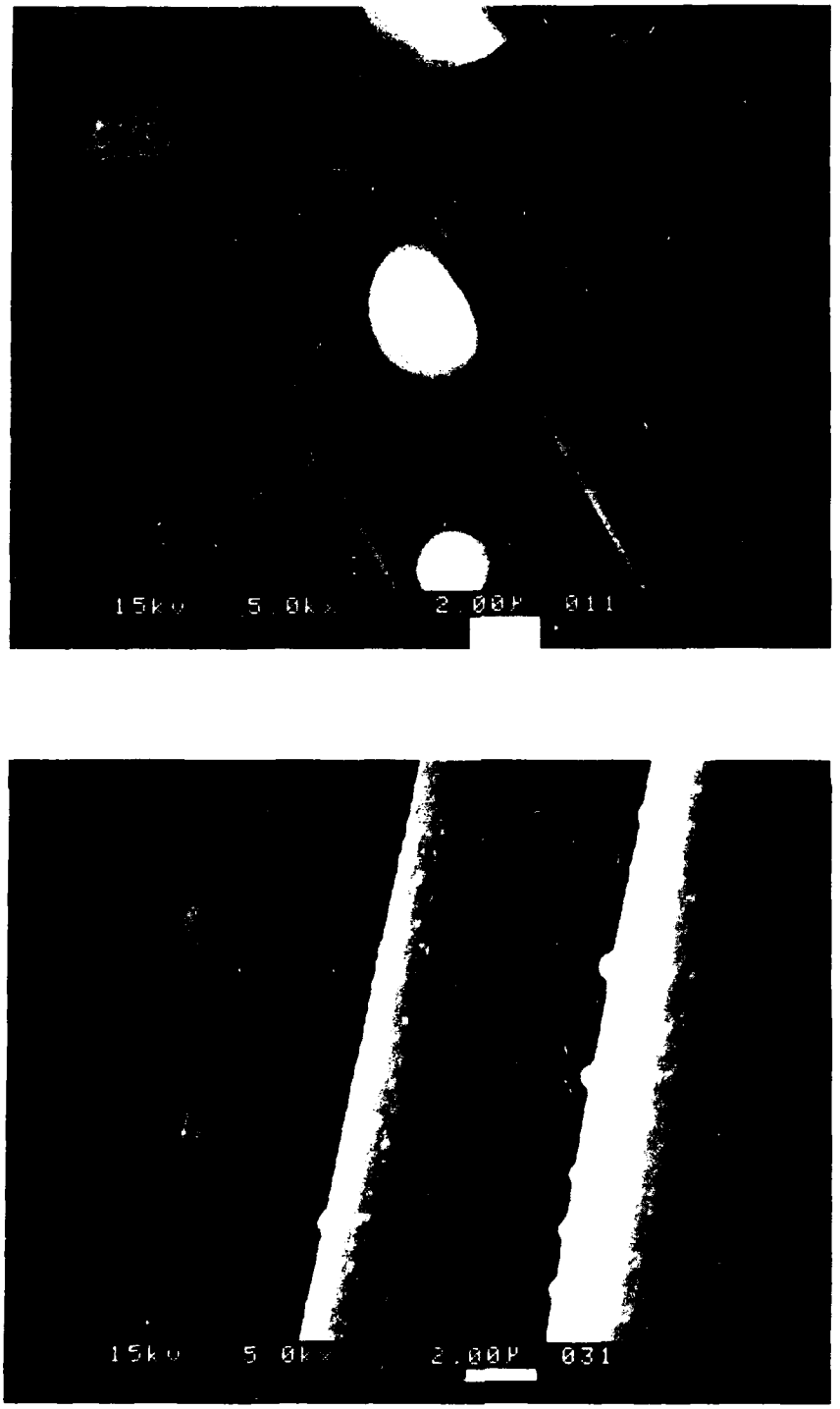

Fig. 2. Sol/Gel Glass Coated Carbon Fibers After a Heat-Treatment in Argon at 1000°C; Sodium-Borosilicate (NBS) on HMU Fibers (Upper) and P-100 Fibers (Lower)

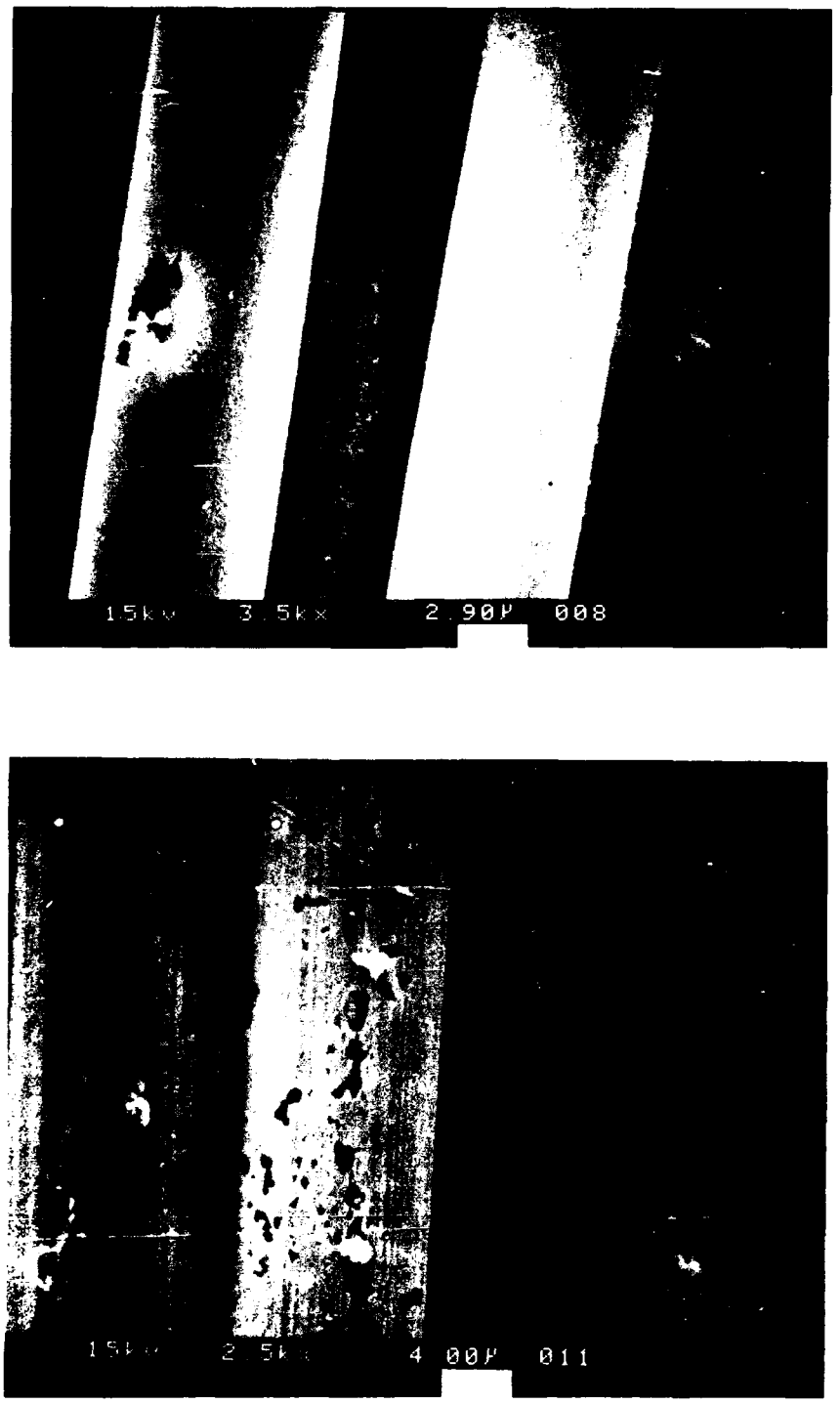

Fig. 3. Sol/Gel Glass Coated Carbon Fibers After a Heat-Treatment in Argon at 1200°C; Sodium-Borosilicate (NBS) Plus 4% MoO_3 on HMU Fibers (Upper) and P-100 Fibers (Lower)

89—7—50—27

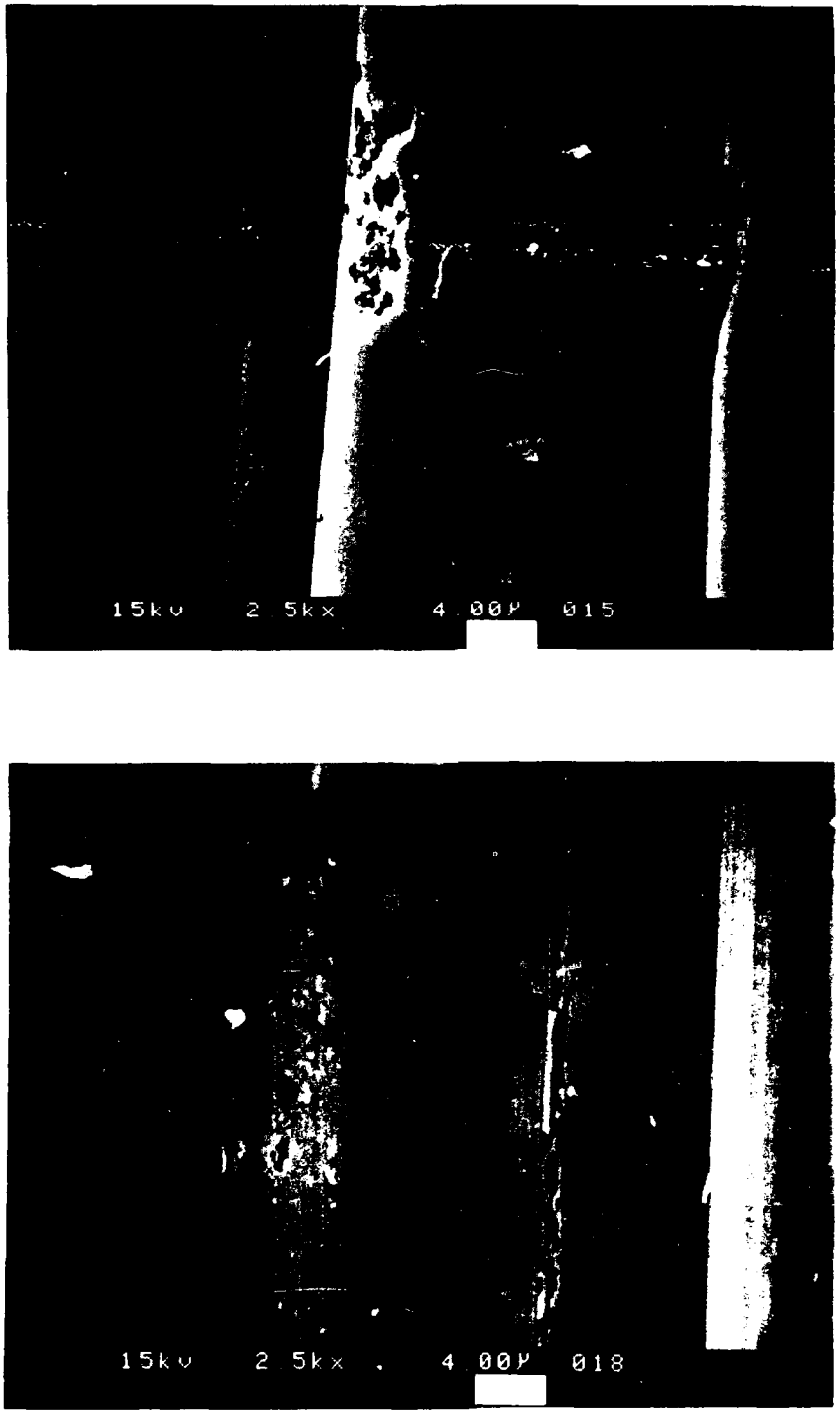

Fig. 4. Sol/Gel Glass Coated Carbon Fibers After a Heat-Treatment in Argon at 1200°C; Sodium-Borosilicate (NBS) Plus 4% Nb_2O_3 on HMU Fibers (Upper) and P-100 Fibers (Lower)

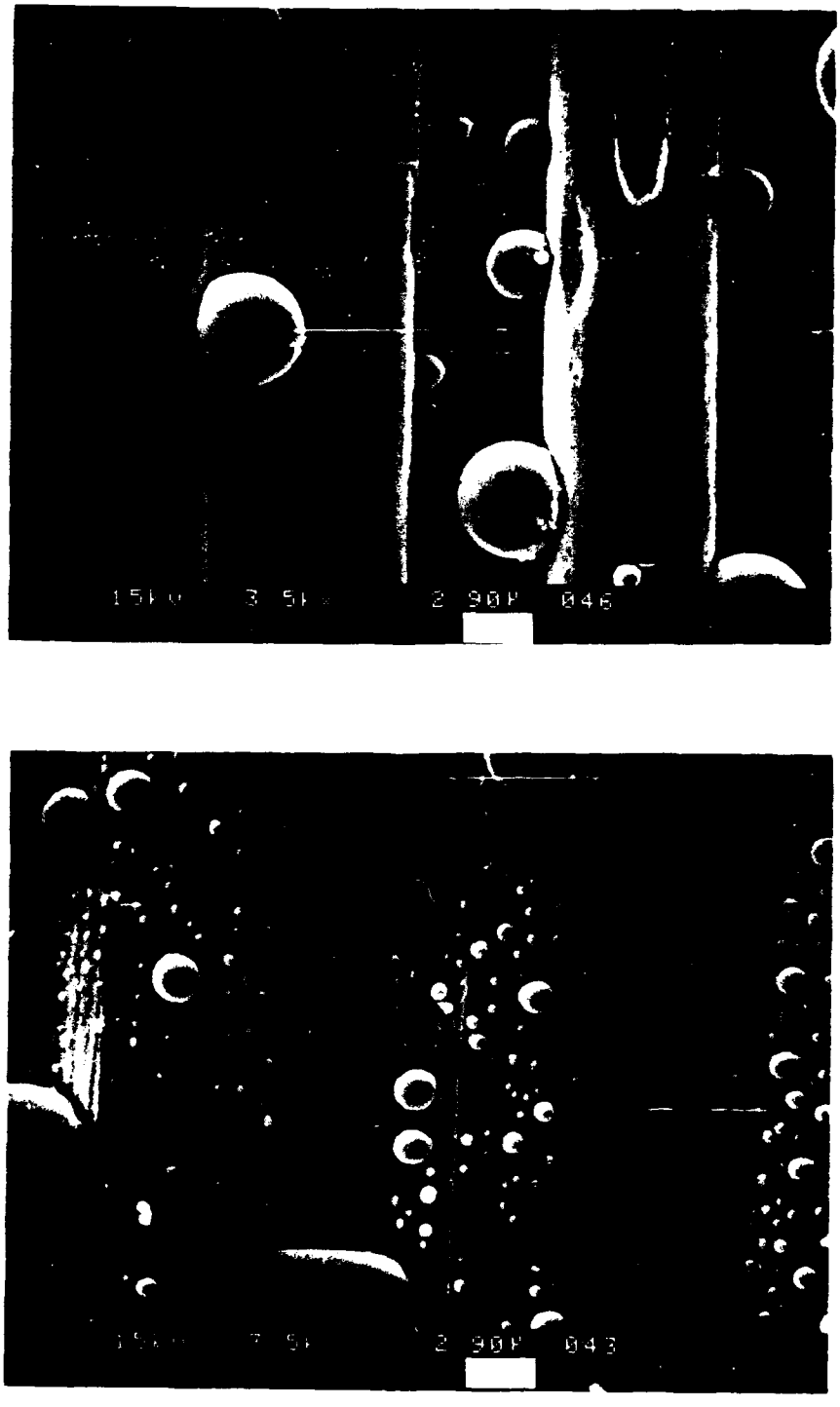

Fig. 5. The Wetting Behavior of a 75% SiO_2, 10% B_2O_3, 15% Na_2O Glass on HMU Fiber (Upper) and P-100 Fiber (Lower)

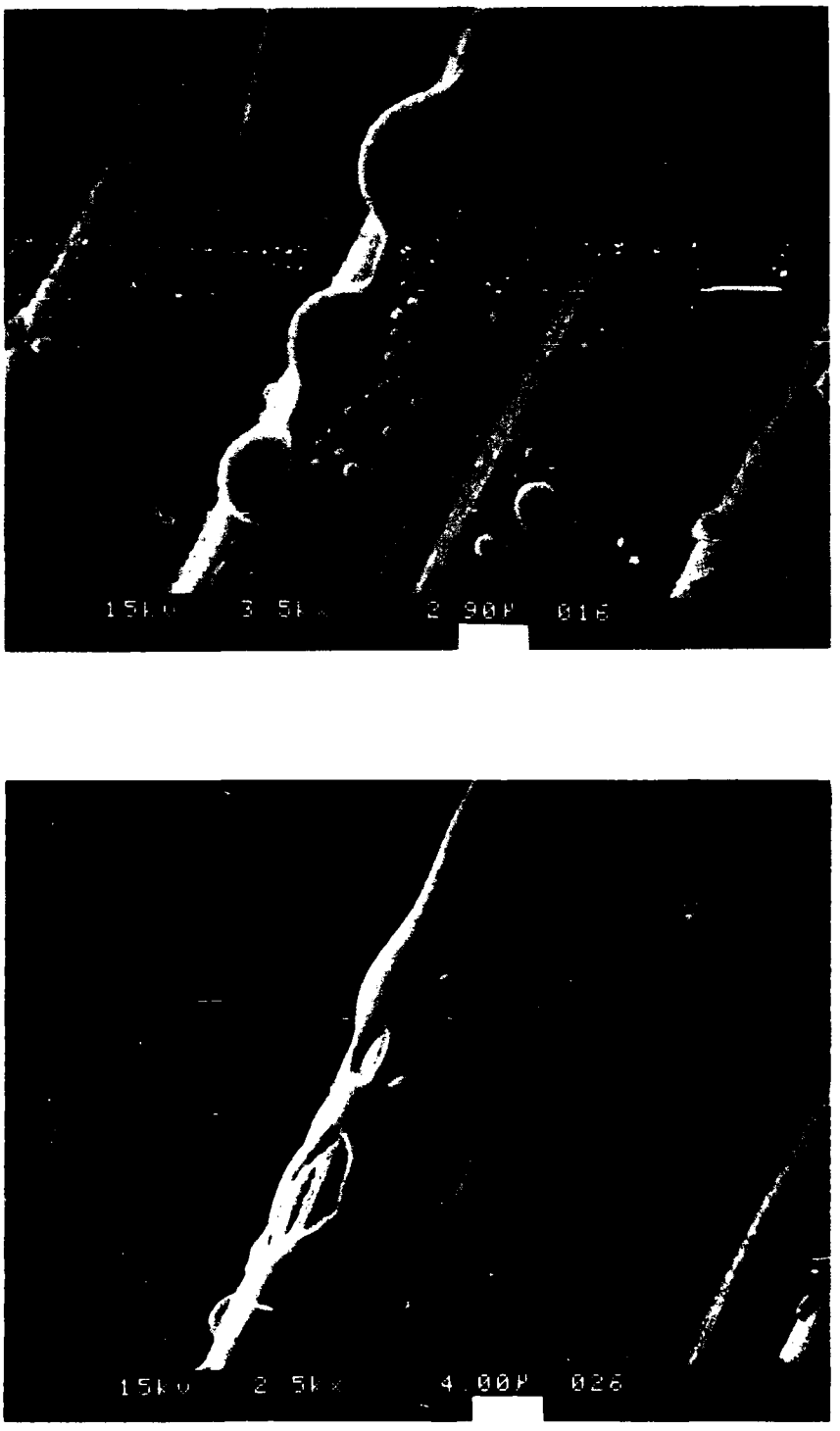

Fig. 6. The Wetting Behavior of a 75% SiO_2, 25% B_2O_3 Glass on HMU Fiber (Upper) and P-100 Fiber (Lower)

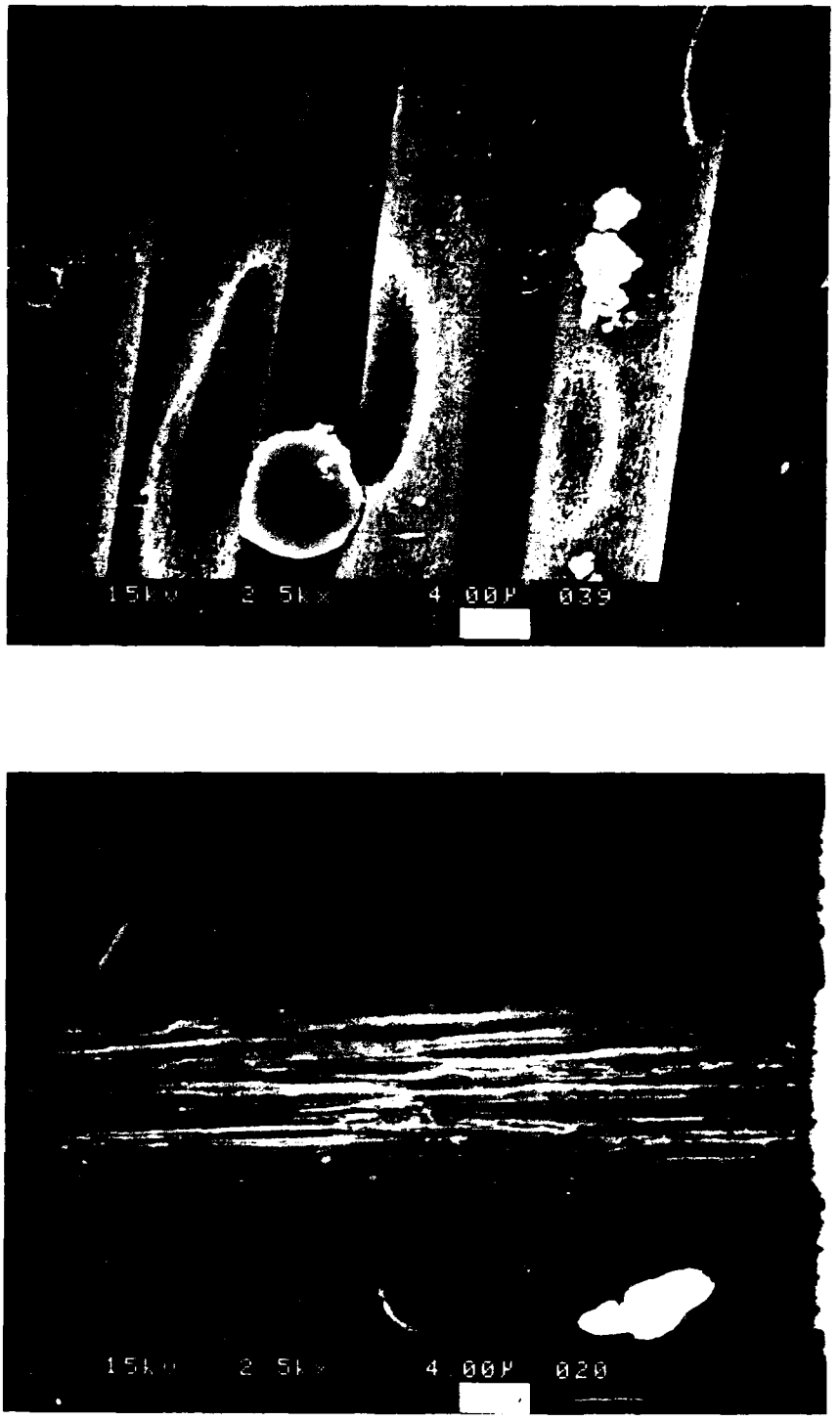

Fig. 7a. The Effects of Contact Between the 73% SiO_2, 16% B_2O_3, 11% Na_2O Glass and HMU Fiber (Upper) and P-100 Fibers (Lower); 1300°C in Ar

89—7—50—31

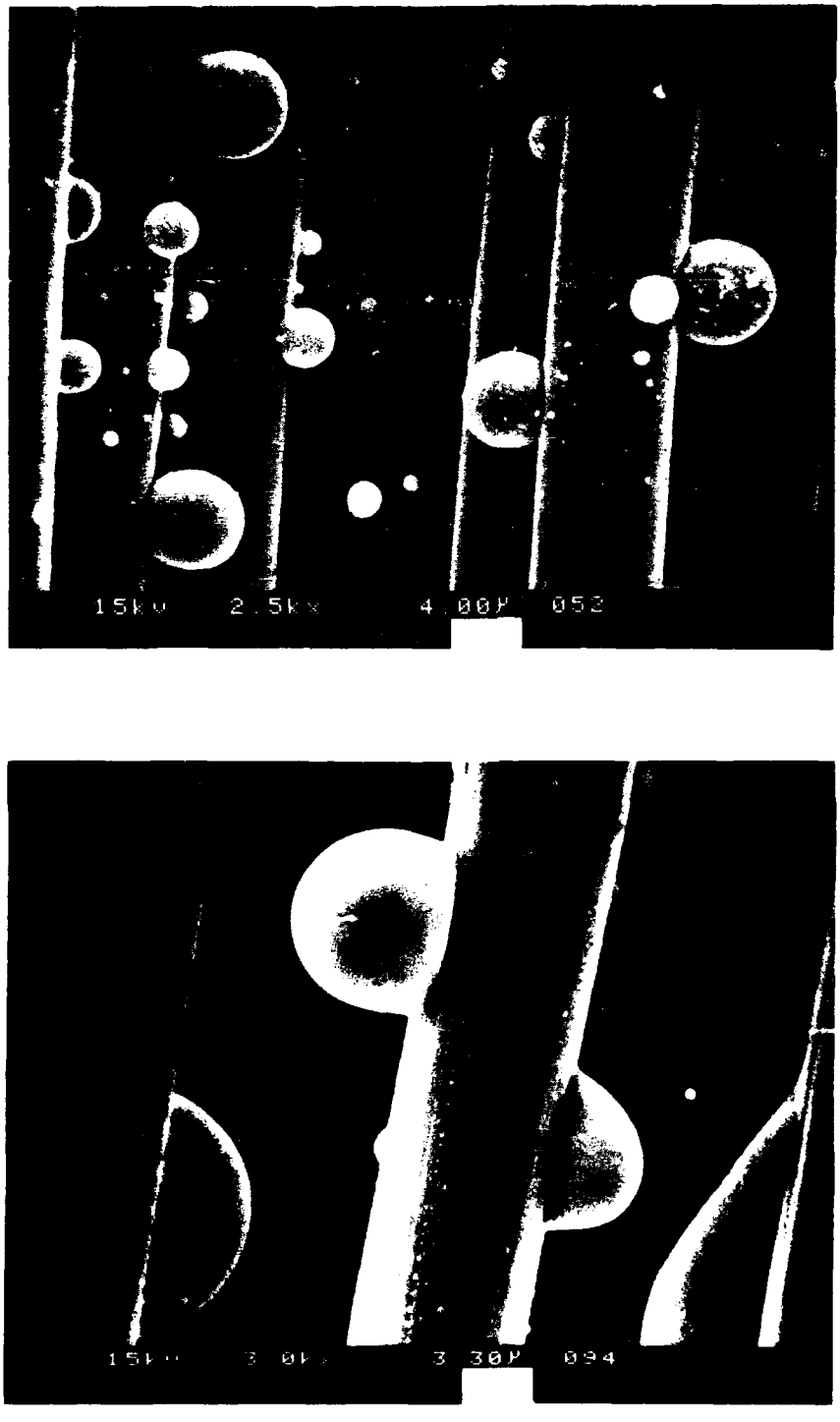

Fig. 7b. The Effects of Contact Between the 73% SiO_2, 16% B_2O_3, 11% Na_2O Glass and HMU Fiber (Upper) and P-100 Fibers (Lower); 1300°C in CO

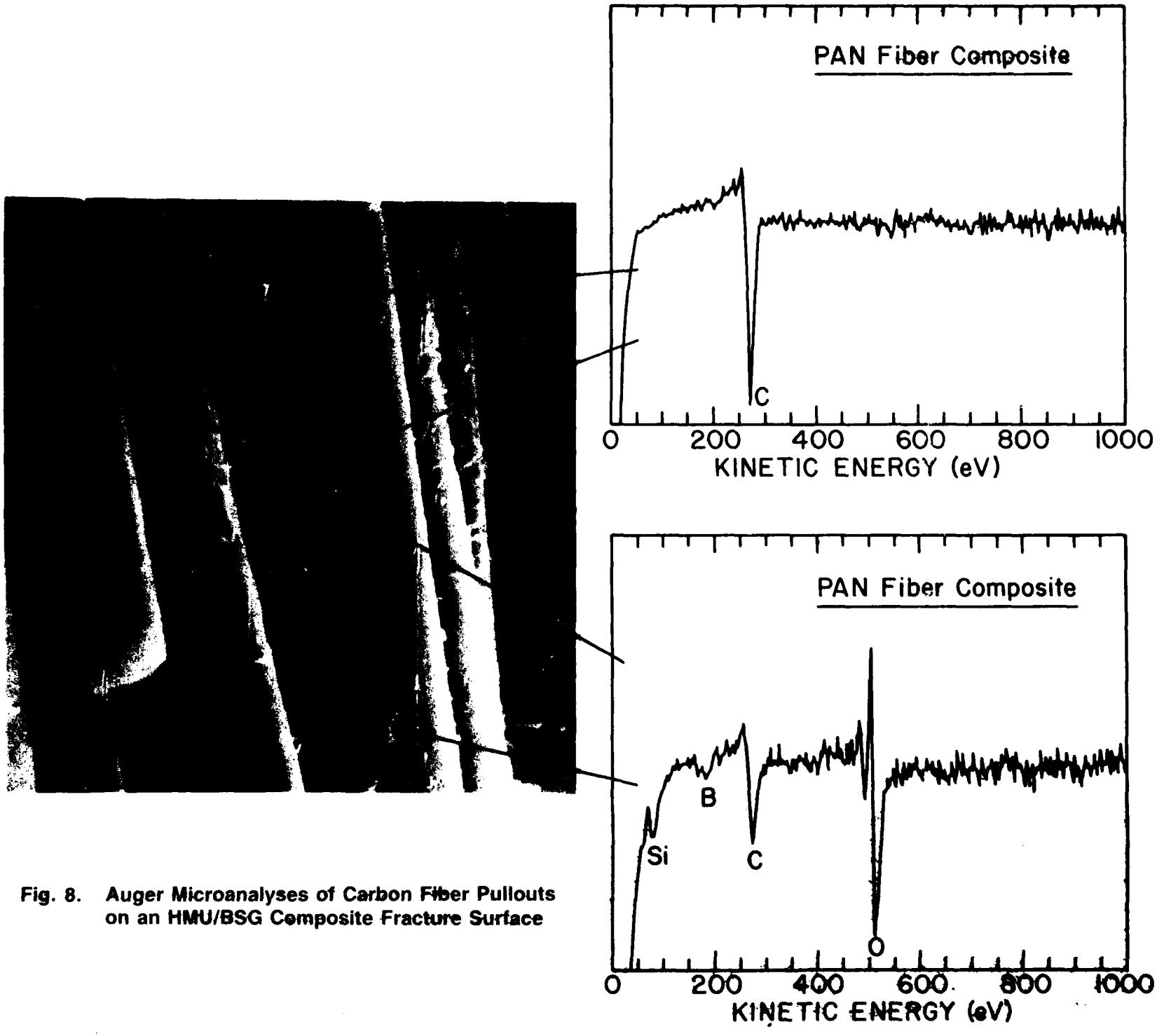

Fig. 8. Auger Microanalyses of Carbon Fiber Pullouts on an HMU/BSG Composite Fracture Surface

R89-917704-1

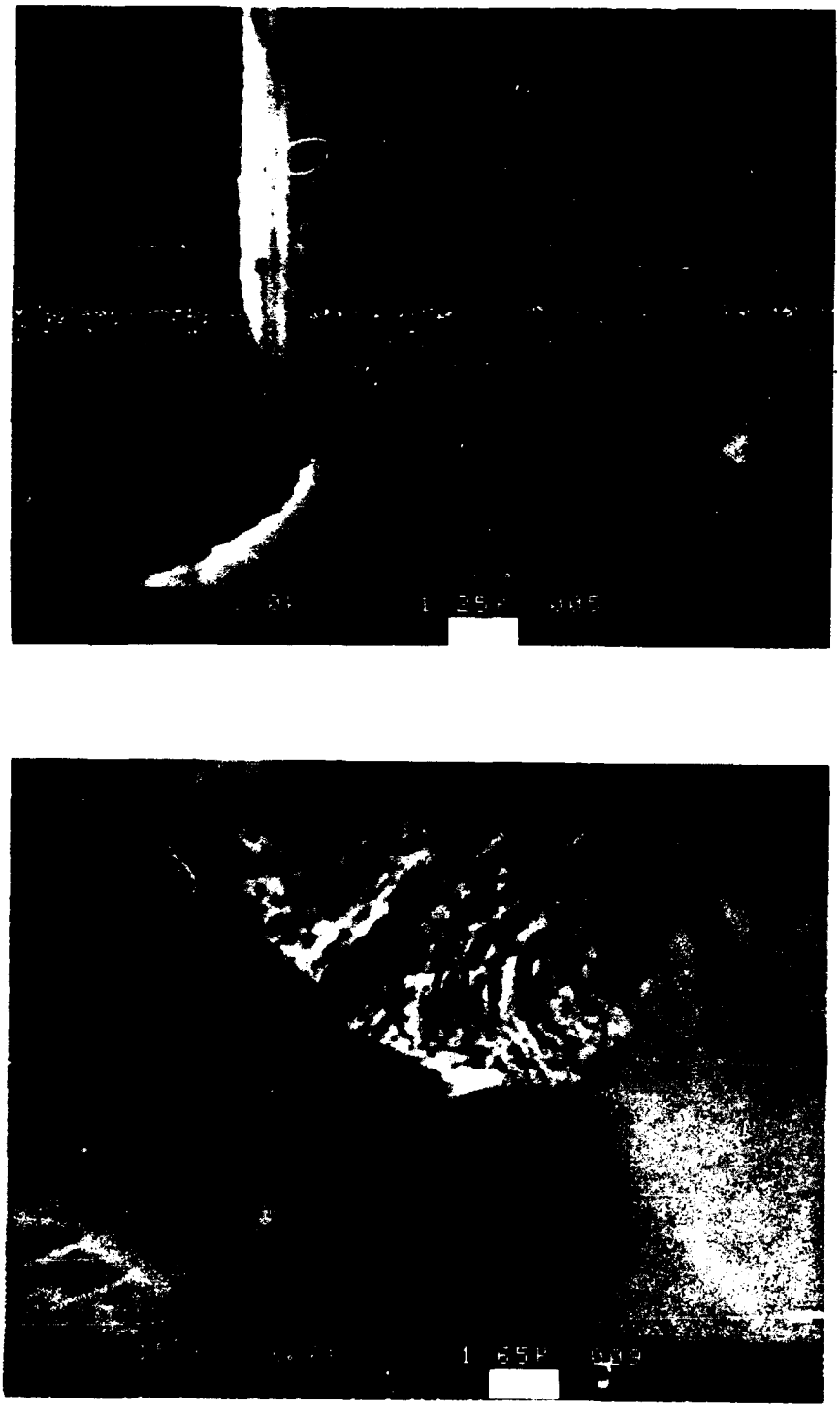

Fig. 9. The Fracture Surfaces of a HMU/NBS Composite (Upper) and a P-100/NBS Composite (Lower)

89—7—50—34

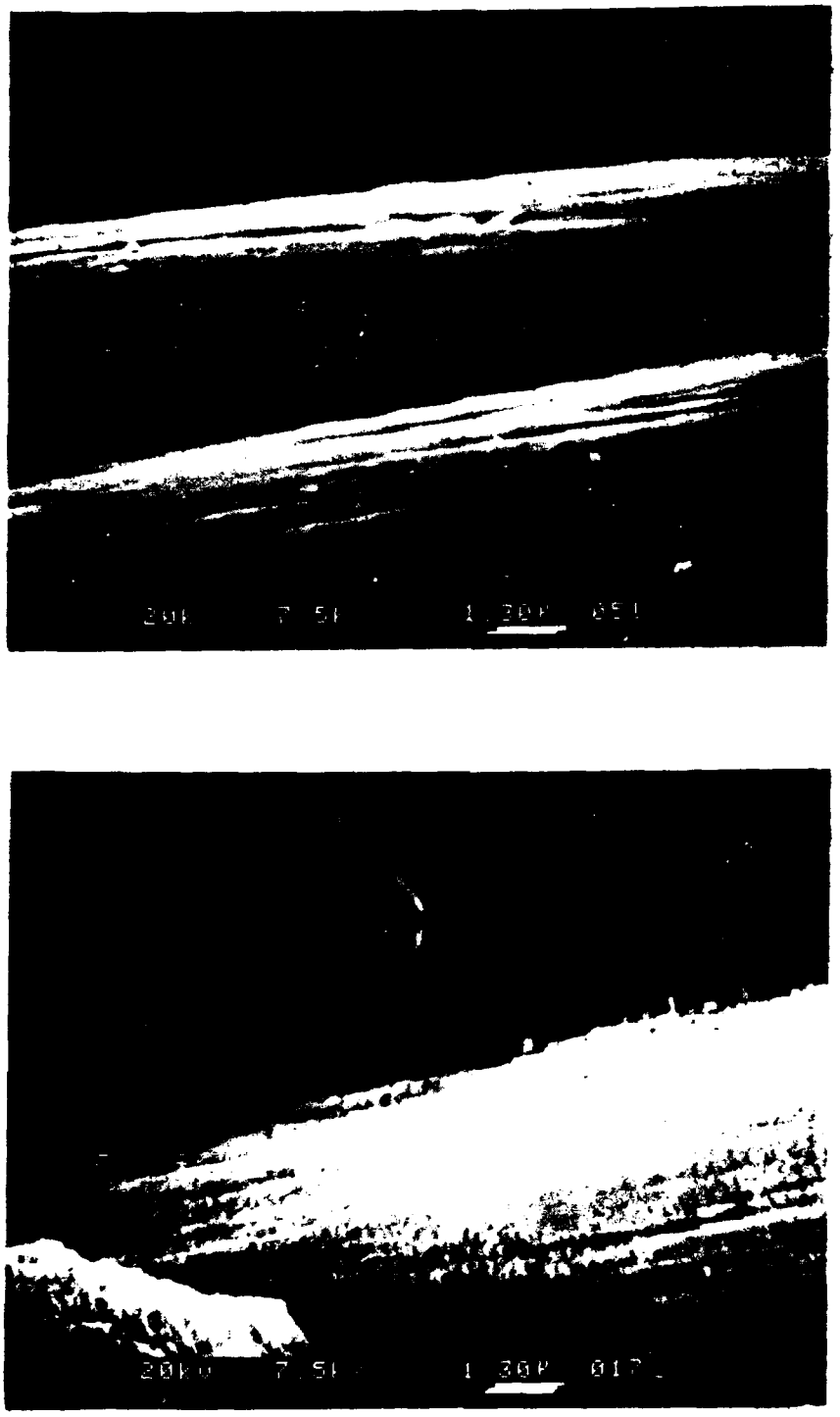

Fig. 10. The Carbon Fiber Pullouts on the Fracture Surfaces of HMU/NBS (Upper) and HMU/NBS + 1% MoO_3 (Lower) Composites

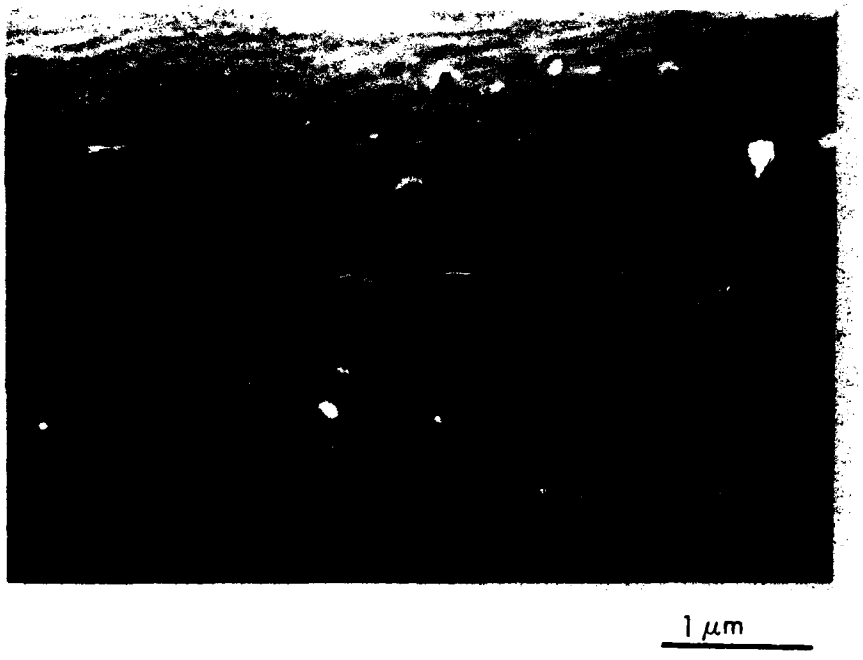

Fig. 11. The Matrix Trough on the Interlaminar Fracture Surface of an HMU/NBS + 1% Nb_2O_5 Composite

89—7—50—35

VIII. SOL/GEL PROCESSING OF OXYCARBIDE GLASSES AND GLASS MATRIX COMPOSITES

H. Zhang and C. G. Pantano
Department of Materials Science and Engineering
The Pennsylvania State University
University Park, PA 16802

A. Introduction

In earlier studies, the thermochemical interactions between carbon fibers and silicate glass matrices were evaluated [1]. It was found that at high temperatures, the predominant reactions between the glass matrix and carbon fibers produce CO, CO_2 and SiO gases. These reactions are greatly enhanced if the glass matrix composition contains reducible oxides such as Nb_2O_5 or MoO_3. In these cases, it could be shown that significant degradation of the fiber surfaces occurs, and moreover, solid phase reaction products including Nb-carbide and Mo-carbide eventually form at the interface [2]. If excessive, these interphases lead to a measurable increase in the interfacial shear strength, and correspondingly, a decrease in the strength and fracture toughness of the composite.

On the basis of these observations, it is proposed that the interface reactions can be limited if *chemically-reduced* glass matrices are used in the composite fabrication; that is, glasses whose redox potential has been equilibrated with carbon. In this way, a great deal of latitude would exist in the time and temperature schedule for composite processing. Moreover, the high temperature strength of the composite could – for a variety of reasons – be improved. The limited interface reactivity should prevent degradation of the fibers during service at elevated temperatures. Also, the carbon-coating glass matrix would oxidize to a degree, and thereby, limit the oxidation rate of the fibers. And finally, the presence of carbon and/or carbide in the glass matrix will reduce the crystallization rate of the glass. In general, though, the ability to control the interfaces through the redox potential of the glass matrix phase would represent a new approach to tailoring the interface properties in composites. One way to reduce the oxidation state of the glass is to substitute carbon for oxygen in the silicate network; i.e., to create an *oxycarbide* network.

We have already developed a sol/gel method for the synthesis of ternary silicon-oxycarbide (Si-O-C) glasses [3]. The solutions are prepared using organometallic silanes which contain one unhydrolyzable alkyl group. In this way, carbon can be retained in the gel, and most importantly, it is covalently bonded to silicon. The gel can then be processed in an inert atmosphere to create a carbon-containing x-ray amorphous *black glass*. In the case of SiO_2, it has been shown that up to

18% carbon can be incorporated into the dense glass. ^{29}Si magic angle spinning-nuclear magnetic resonance (MAS-NMR) verifies that 50-60% of the silicon atoms in the glass are bonded directly to one [$SiCO_{3/2}$] or two [$SiC_2O_{2/2}$] carbon atoms. ^{13}C NMR reveals that there is also some free carbon in the glass. But the creation of the oxycarbide network is the significant observation. Although other investigators have discussed the synthesis of carbon-containing glasses [4-7], this study provided the first direct verification of Si-C ligands in the dense *black glass*.

The sol/gel approach is certainly advantageous, and perhaps critical, to the synthesis of oxycarbide glass. But the gelation and hot pressing characteristics of the ternary Si-O-C system are not yet suitable for carbon fiber reinforced composite fabrication. On the other hand, we have a well developed sol/gel method for the synthesis of borosilicate glasses and carbon fiber reinforced borosilicate glass composites [8], and further, possess a data base of microstructural, interface and mechanical properties. Thus, it is ideally suited for evaluating the effects of carbon additions to the matrix glass composition. In this paper, the synthesis and characterization of these borosilicate/ oxycarbide glasses is described, and the temperature-dependent strength behavior of carbon fiber reinforced *borosilicate/oxycarbide* glass composites is reported.

B. Synthesis of Glasses and Composites

The borosilicate glass is nominally of the Pyrex® (CGW 7740) composition: $81SiO_2$, $13B_2O_3$, $4Na_2O$ and $2Al_2O_3$. The alkoxide precursors used in the sol/gel syntheses of the *oxide* glass are tetramethoxysilane (TMOS), trimethyborate, aluminum sec-butoxide and sodium acetate. In the oxycarbide, carbon is introduced by replacing one-half of the tetra-methoxysilane with methyl-trimethoxysilane. An equimolar mixture of these two silanes are hydrolyzed for two hours at 60°C in methanol which contains one-third the water required for complete hydrolysis of the methoxy groups. Subsequently, stepwise additions of the B, Al and Na precursors are added. Then, an excess of water is introduced to drive the hydrolysis to completion. The resulting solution is clear and is typically of pH 5. The gelation of this solution requires about four hours at 80°C. They are aged and dried further at 80°C to obtain clear, stiff gels. The *black* glass is obtained after a heat-treatment of the gel at 800°C in argon.

Although the sol and gel can be processed to yield a glass frit for conventional composite fabrication, the solutions were used to pre-preg carbon fiber paper directly [8]. It was found that these solutions exhibited a strong tendency to wet and impregnate the carbon fiber paper. The carbon fiber paper (Celion-International Paper Co.) was cut and stacked in a mold, and then a measured volume of solution was introduced. An independent measure of the effective glass yield (after processing the solution through to a dense glass) permits a reasonably accurate control of the volume fraction of fiber in the final composite.

Here, composites with 25 volume percent fibers were fabricated. The molds containing the fiber paper and solution were covered and held overnight at 80°C to effect the gelation. These preforms were then aged and dried at 80°C for eight days. Before hot pressing, the preforms were heat-treated at 600°C in argon for 30 min. The hot pressing was accomplished in vacuum at 1200°C under 1000 psi pressure. The heat-treated preforms were stacked in the die, and after reaching ~800°C, the pressure was applied. The composites were then heated rapidly, and held for only a very short time at the maximum temperature of ~1250°C. The pressure was maintained until the system cooled to <700°C.

C. Characterization of the Glasses

The carbon contents of the solution, gel and glass are presented in Table I; the data obtained for a ternary silicon oxycarbide [3] is shown for comparison. It can be seen that the methyl groups are, in fact, retained in the gel. This is further verified by the ^{29}Si MAS-NMR spectra in Figure 1a. It shows the presence of methyl groups bonded directly to Si, and the absence of Si-methoxy groups. These peak assignments are based upon the study of simpler Si-O-C gels [3] (Figure 2), and NMR spectra published in the literature [9]. In the ternary silicon-oxycarbide gel, there is one methyl group for every silicon atom (lines at ~50 and 60 ppm). This is because methyl-trimethoxysilane was the only silica precursor and the methyl ligand is not susceptible to hydrolysis/polymerization. In the case of the borosilicate, additional lines due to silica and/or silicate are observed at 90, 100 and 110 ppm. The silica precursor in the borosilicate was a 50-50 mixture of methyl-trimethoxysilane and tetramethoxysilane. Thus, one-half of the silicon atoms have a methyl group and three oxygens (the lines at 50-70 ppm) and the other half of the silicon atoms are bonded to four oxygens (the lines at 90-110 ppm). The integrated intensity ratio of these two sets of lines is consistent with the initial 50-50 solution composition. The deconvolution of these peaks reveals whether the oxygens bonded to the silicon are bridging or hydroxylated. It should be noted that the line at ~100 ppm could be due to $CH_3O\underline{Si}O_{3/2}$ or $OH\underline{Si}O_{3/2}$, but ^{13}C NMR spectra verified the absence of any methoxy groups (CH_3O) in the gels.

Figure 1b shows the ^{29}Si NMR spectra of the borosilicate/oxycarbide glass. The presence of Si-C ligands in the glass is indicated by the line at ~70 ppm. But in contrast to the Si-O-C glasses (Figure 2), Si atoms with only one carbon ligand ($CSiO_{3/2}$) are observed. The ternary glasses showed the additional presence of Si atoms with two carbon ligands ($C_2SiO_{2/2}$) at ~35 ppm. Moreover, the carbon analyses in Table 1 reveal a substantial loss of carbon – approximately 65% - during conversion of the borosilicate gel to glass. In contrast, the ternary Si-O-C gels lost only 15% of the carbon during the gel-to-glass conversion. It is likely that the other constituents in this glass (B_2O_3, Al_2O_3 and Na_2O) catalyze the oxidation of the Si-C bonds, and thereby, lead to the evolution of CO or CO_2 – even in the argon atmosphere.

Figure 3 compares the densification behaviors of the borosilicate *oxide* and the borosilicate *oxycarbide* gels. The expected density of the borosilicate glass is approximately 2.2 g/cm^3. It can be seen that this value is reached after a one hour heat-treatment of the gel at 650°C. At higher temperatures, bloating of the glass occurs due to the water trapped in the gel. The borosilicate/oxycarbide gel requires a higher temperature to exhibit any densification. The theoretical density of the borosilicate/oxycarbide glass is not known, but is expected to be slightly less than 2.2 g/cm^3 because of the carbon substitution for oxygen. More importantly, though, bloating is not observed in the oxycarbide-at least at temperatures up to 1200°C. These observations are consistent with effects of a carbon substitution in the glass network.

The most important influence of the carbon observed in this study concerned the crystallization behavior. Figure 4a shows the x-ray diffraction patterns of the borosilicate and borosilicate/oxycarbide glasses after heat-treatments at 900°C and 1100°C for one hour in argon. There is no measurable crystallization of the oxycarbide, whereas the oxide glass is almost completely devitrified at 1100°C. A semi-quantitative analysis (using the method of internal standards) showed that the oxide begins to crystallize at 800°C, whereas the onset of the crystallization in the oxycarbide is shifted to >1100°C. The rate of cystallization is considerably greater for the borosilicate than for the borosilicate/oxycarbide; this is shown in Figure 4b. Chi [5] and Larsen [6] also observed an effect of carbon upon the crystallization of silica glasses. The mechanism through which the carbon additions influence the crystallization behavior is not fully understood. There is certainly an effect of viscosity upon the kinetics, but the thermodynamic effects of the carbon substitution are unknown.

Finally, the contact angle of the borosilicate and borosilicate/oxycarbide glasses on the carbon fibers was measured. The carbon fibers were dip-coated in the solutions, and then heat-treated in argon at ~1200°C to create micro-sessile drops. SEM micrographs show a clear difference in the wetting behavior of the oxide and oxycarbides. The borosilicate is essentially non-wetting, and exhibits a contact angle of ~90°. The borosilicate/oxycarbide spreads on the fibers, and exhibits a contact angle of $\leq$45°.

D. Strength Behavior of Oxycarbide Matrix Composites

The room temperature mechanical properties of the oxycarbide matrix composites were somewhat inferior to the standard oxide matrix materials. The data in Table 2 shows a two- to three-fold decrease in the flexural strength and fracture toughness. It was expected that a loss of room temperature fracture toughness would occur in this system. The better wetting of oxycarbide glass on the carbon fibers enhances the fiber/matrix adhesion, and this limits debonding and fiber pullout. But the magnitude of the effect was far greater than expected. It was suspected that volatiles in the composite preforms – which could not be removed during the argon treatment at 600°C – were responsible, in part, for the poor performance. Any volatiles which can oxidize the

fibers will cause a decrease in their strength. Thus, additional composites were prepared and these were heat-treated at 300°C in air before the 600°C argon treatment. It can be seen (Table 2) that this led to a nearly two-fold improvement in the room temperature properties. It is not yet known how much further improvement in the room temperature properties can be expected. Larsen, et al [6] used a *black glass* matrix in SiC fiber reinforced composites, and they also found the room temperature properties to be very sensitive to the processing. More expereince in the processing of these highly reduced glasses is required.

The SEM micrographs in Figure 5 show the fracture surfaces of the oxycarbide matrix composites tested at room temperature. Most obvious is the absence of any significant degree of fiber pullout. Nevertheless, the higher magnification images show that fiber/matrix debonding does occur, and further, that the fibers have not been etched or degraded in any way due to interactions with the glass matrix. But in many regions, a granular residue associated with the matrix phase adheres to fiber surfaces. This is generally not observed in the oxide matrix composites. This undoubtedly contributes to an increase in the interfacial shear strength. If the enhanced adhesion in this system occurs without any degradation of the fiber strength, one would expect an increase in the composite strength at the expense of fracture toughness. This was the effect anticipated, but clearly, an increase in strength has not yet been realized.

On the other hand, the use of an oxycarbide matrix in these composites does enhance the high temperature performance of the composites. Figure 6 compares the flexural strength of the borosilicate composites and the borosilicate/oxycarbide composites. The tests were performed in argon over the temperature range 700-1000°C. It is clear that the oxide matrix composite undergoes a significant loss in strength in this temperature range. The borosilicate/oxycarbide glass appears to retain its strength – albeit low – up to 1000°C. The fractured specimens were examined in the SEM, and the differences could be attributed – directly – to the crystallization resistance of the borosilicate/oxycarbide.

E. Summary

It has been shown that borosilicate/oxycarbide glass can be synthesized using a sol/gel approach. The resistance of the glass to bloating and crystallization is increased by the carbon incorporation, and this enhances the high-temperature strength behavior of carbon-fiber reinforced composites. This is the most advantageous effect of the oxycarbide matrix. But whereas 80-90% of the carbon in ternary silica-oxycarbide gels is retained during the gel-to-glass conversion, only 30-40% is maintained in the borosilicate. This suggests that other glass compositions, or the ternary Si-O-C, should be developed to increase the oxycarbide content of the glass matrix in composites. Moreover, further study of the interface chemistry of these oxycarbide glasses with carbon, fibers and with silicon carbide fibers, is warranted.

ACKNOWLEDGEMENT

The authors gratefully acknowledge the Office of Naval Research (ONR N00014-55-C-0332 and N00014-87-K-0247) for their support of this research.

REFERENCES

1. P. Benson, K. E. Spear and C. G. Pantano, "Thermochemical Analysis of Interface Reactions in Carbon Fiber Reinforced Glass Matrix Composites," in Ceramic Microstructures '86, J. A. Pask and A. G. Evans, Eds. (Plenum, New York, 1987), pp. 415-426.

2. W. K. Tredway, K. M. Prewo and C. G. Pantano, "Fiber Matrix Interfacial Effects in Carbon Fiber Reinforced Glass Matrix Composites," to appear in Carbon, 1989.

3. H. Zhang and C. G. Pantano, "Synthesis and Characterization of Si-O-C Glasses," submitted to J. Am. Ceram. Soc., 1989.

4. C. F. Smith and W. B. Crandall, "Method of Making Carbon Containing Glasses," U.S. Patent No. 3,378,431 (1968).

5. F. K. Chi, "Carbon Containing Monolithic Glasses via the Sol/Gel Process," Ceramic Sci. and Eng. Proc., 4, 704-717 (1983).

6. D. C. Larsen, et al., "Silicon Carbide Fiber Reinforced Black Glass Matrix Composites," AFWAL-TR-83-4134.

7. J. Homeny and G. G. Nelson, "Oxycarbide Glasses in the Mg-Al-Si-O-C System," J. Am. Ceram. Soc., 71[5], 386-390 (1988).

8. D. Qi and C. G. Pantano, "Sol/Gel Processing of Carbon Fiber Reinforced Glass Matrix Composites," in Ultrastructure Processing of Advanced Ceramics, J. D. MacKenzie and D. R. Ulrich, Eds. (Wiley, New York, 1988), pp. 635-649.

9. J. Lipowitz, H. A. Freeman, R. T. Chen and E. R. Prack, "Composition and Structure of Ceramic Fibers Prepared from Polymer Precursors", Advanced Ceramic Materials, 2(2), 121-128 (1987).

Table 1

Carbon Contents+ of Solutions, Gel and Glass

	Borosilicate	Silica
Total Carbon in Solution (calculated)	14.7%	35%
Carbon in Gel (calculated)*	7.2%	16%
Carbon in Gel (measured)	9.2%	14%
Carbon in Glass (measured)	3.2%	12%

+ LECO carbon analyzer
* assumes all methoxy groups are hydrolyzed

Table 2

Room Temperature Mechanical Properties of Carbon Fiber Reinforced Glass Composites*

	3-point Flexural Strength (MPa)		Fracture Toughness $MPa \cdot m^{1/2}$	
	flatwise	edgewise	flatwise	edgewise
borosilicate	336	350	7.28	9.15
borosilicate/oxycarbide • w/o heat-treatment in air	112.5	103.4	2.69	3.03
borosilicate/oxycarbide • w/300°C heat treatment in air	196.3	172.2	5.57	4.98

* all composites contain 25% v/o Celion fiber

R89-917704-1

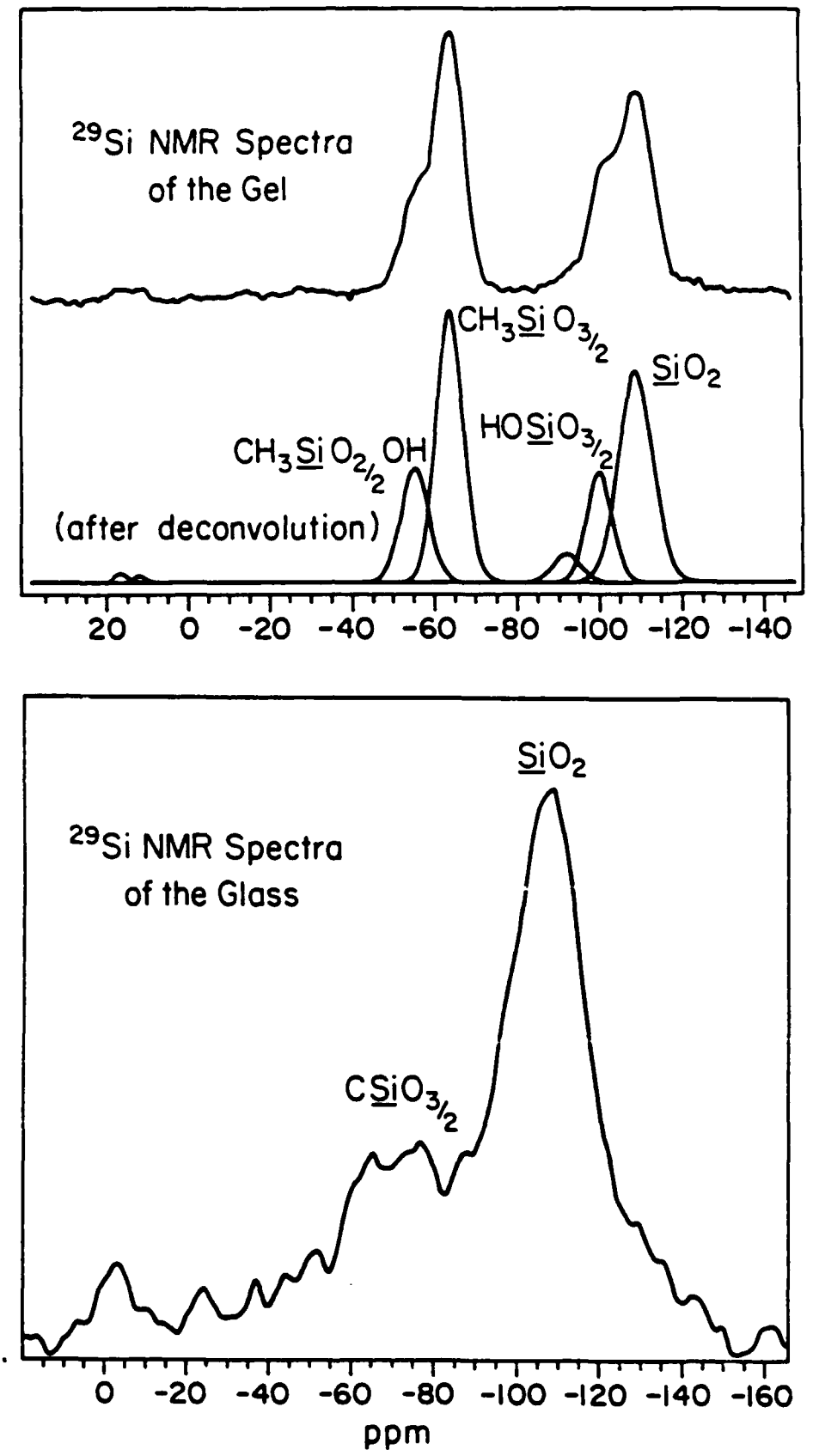

Figure 1. ^{29}Si MAS-NMR spectra of the (a) borosilicate/oxycarbide gel and, (b) borosilicate/ oxycarbide glass obtained after an 800°C heat-treatment of the gel in argon.

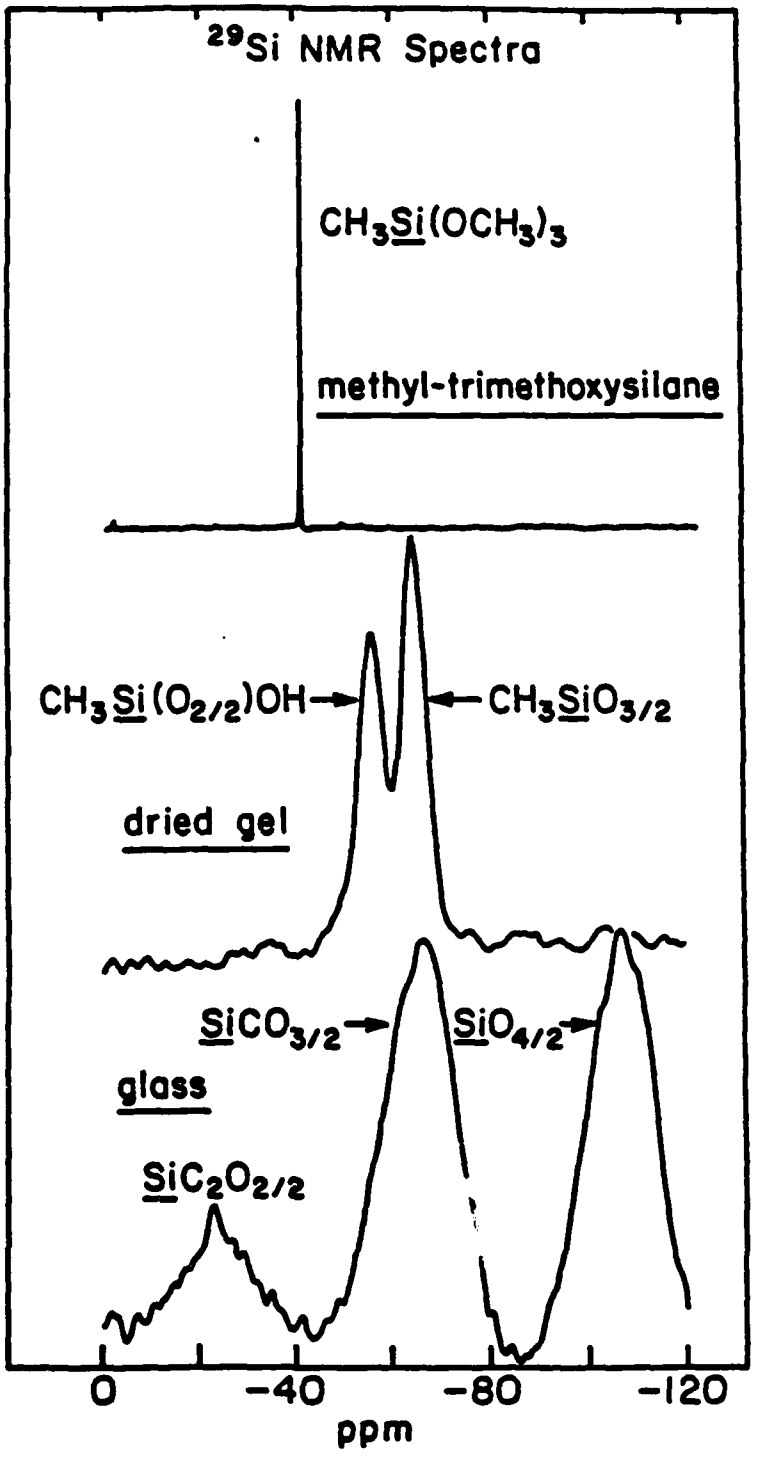

Figure 2. ^{29}Si MAS-NMR spectra of a ternary (Si-O-C) silicon oxycarbide prepared using a methyltrimethoxysilane precursor; the glass was obtained after a 900°C heat-treatment of the gel in argon.

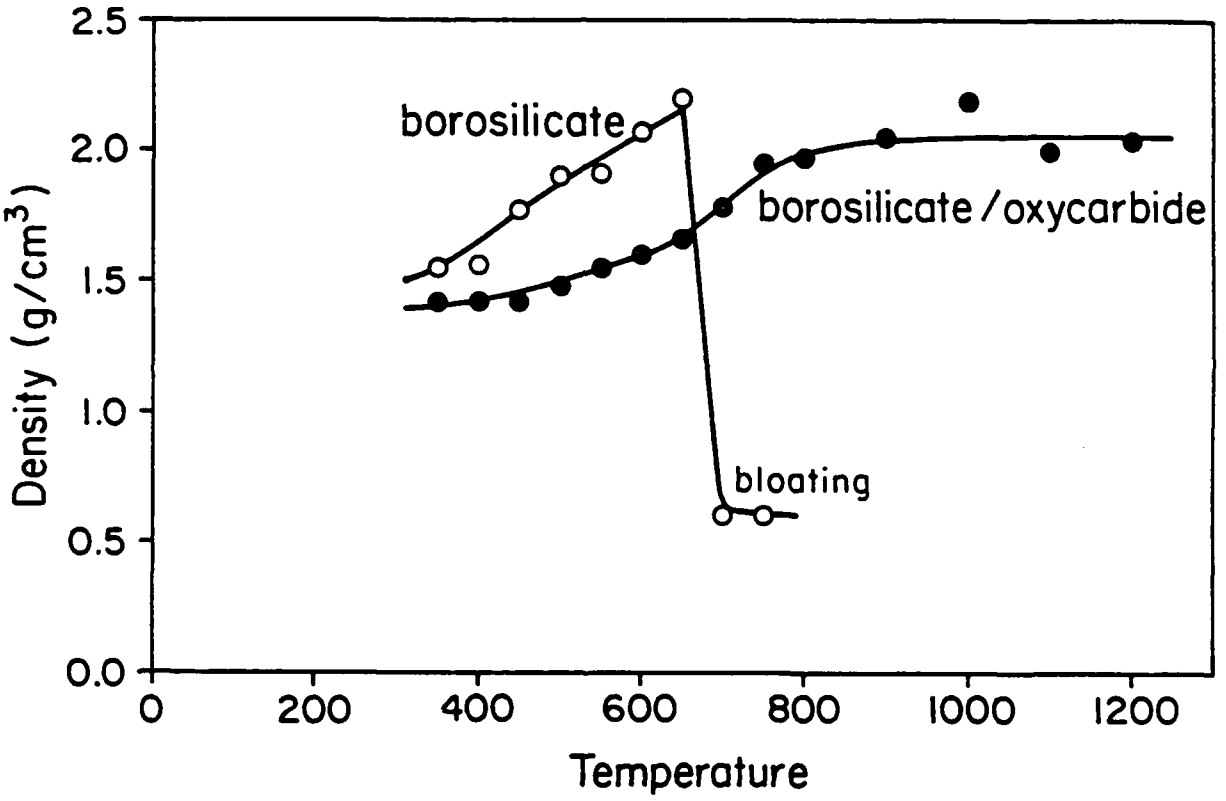

Figure 3. The densification behavior of borosilicate and borosilicate/oxycarbide gels in argon; each data point represents one hour of sintering.

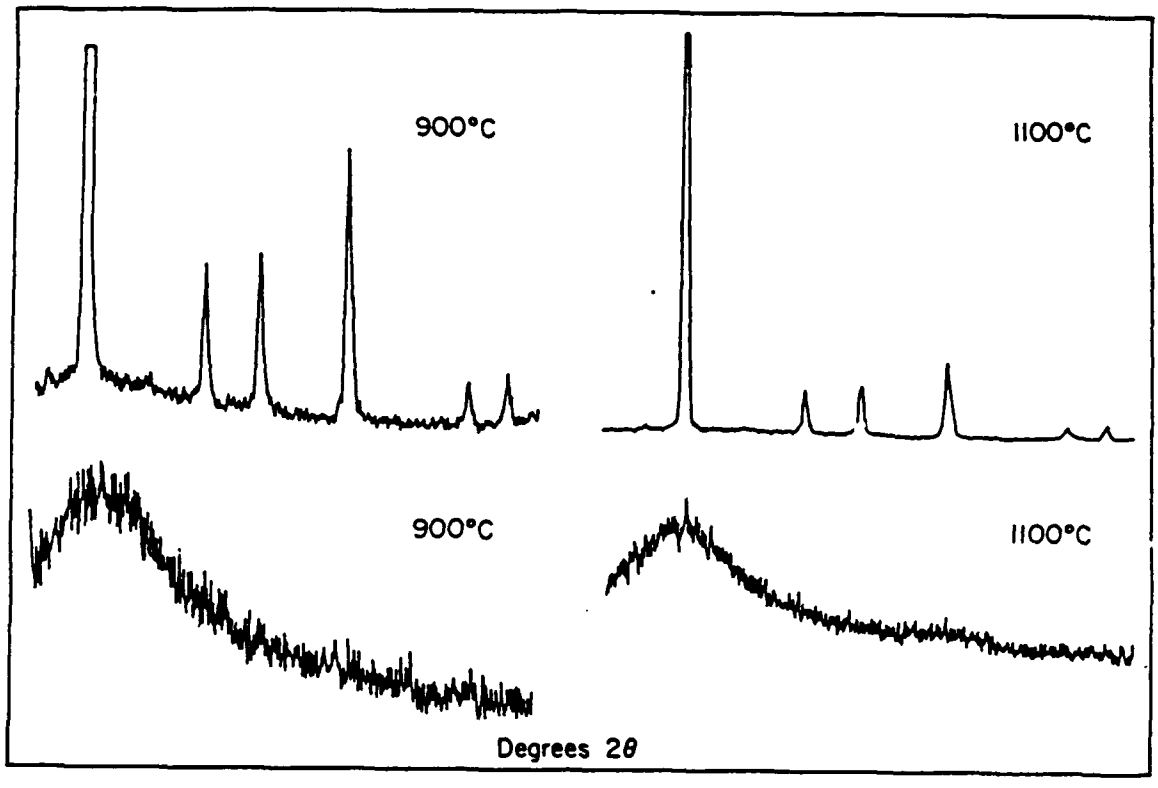

Figure 4a. X-ray diffraction patterns of the borosilicate (upper) and borosilicate/oxycarbide (lower) glasses after ~2 hours in argon.

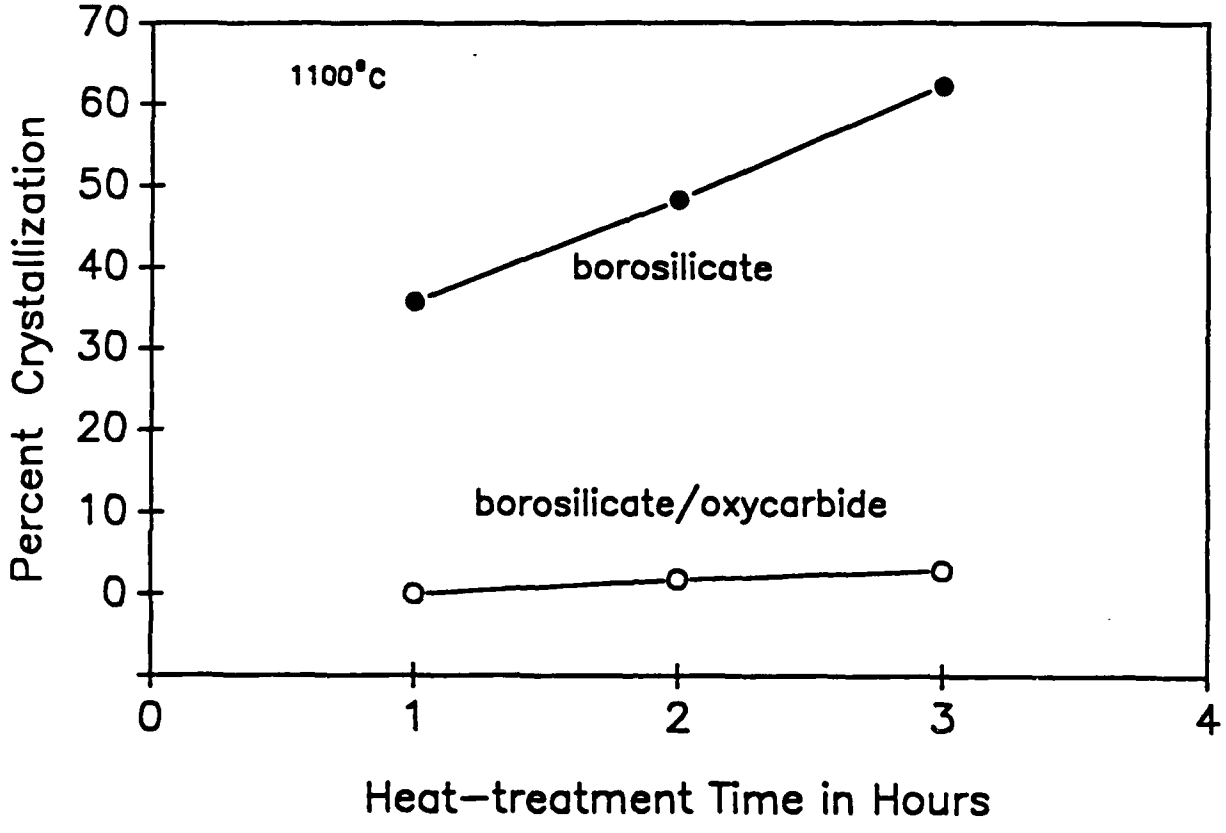

Fibure 4b. The kinetics of crystallization of the borosilicate and borosilicate/oxycarbide at 1100°C in argon; semi-quantitative analysis using the method of internal standards.

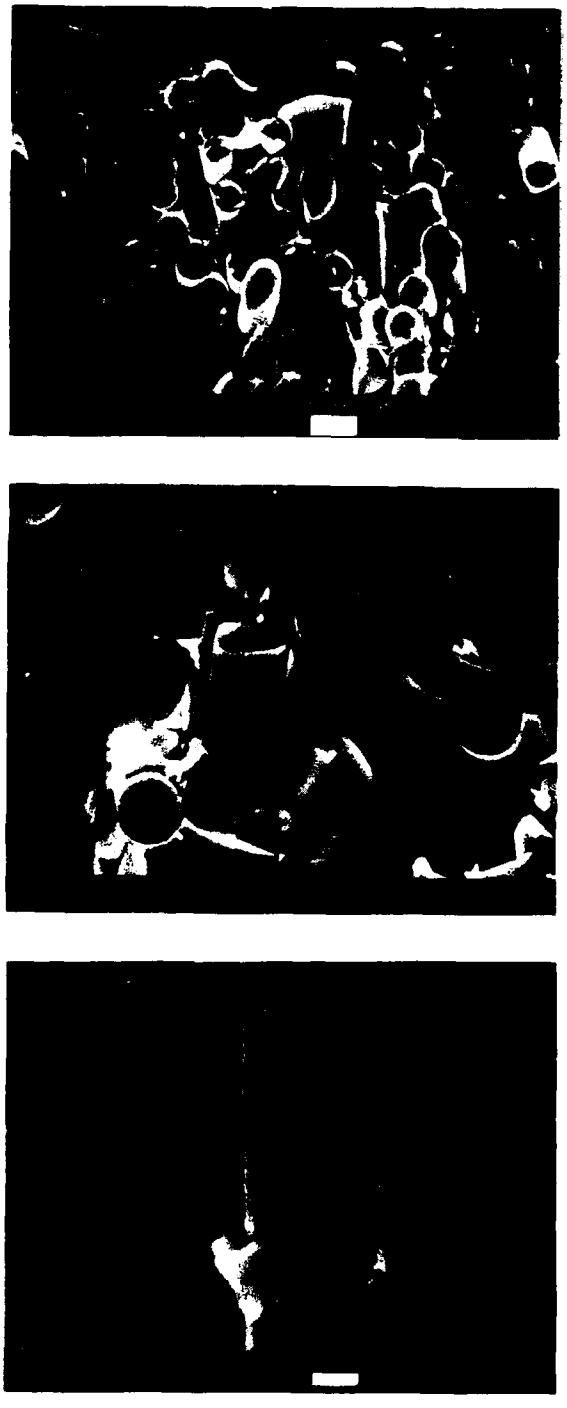

Fig. 5. SEM Micrographs of the Room Temperature Fracture Surface of a Carbon Fiber Reinforced Borosilicate/Oxycarbide Glass Matrix Composite

89—7—50—13

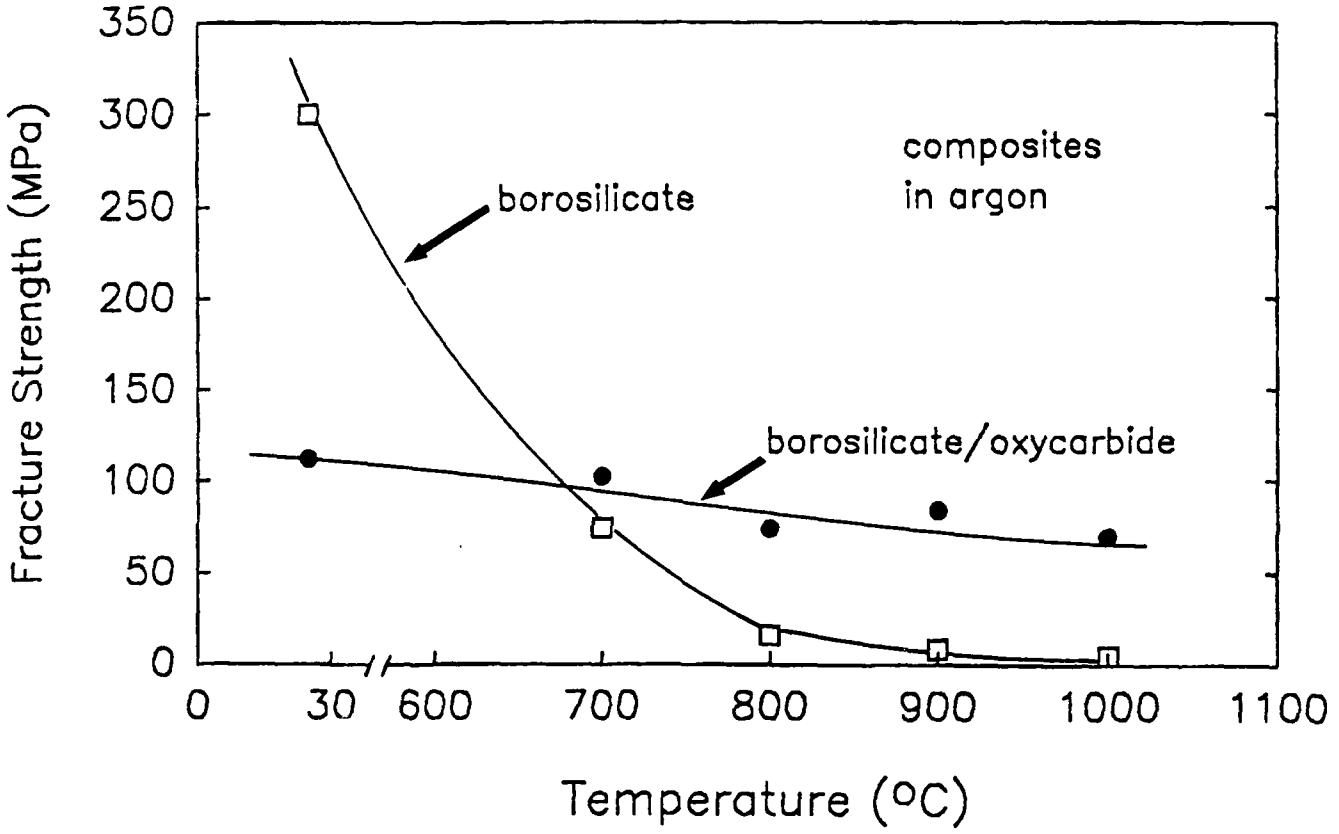

Figure 6. Temperature dependence of the 3-point flexural strength of carbon-fiber reinforced borosilicate and borosilicate/oxycarbide glass matrix composites in argon.

IX. DELIVERABLES

A set of four (4) 10 cm x 10 cm panels of unidirectional and [0/90] P-100 and HMU carbon fiber reinforced glass matrix composites was delivered to the contracting officer on December 20, 1988. The specific information pertaining to each composite is summarized in the table below. The P-100/BSG-2 composites were supplied in the form of impact samples for instrumented Charpy testing. Notched specimens were prepared in L-S, L-T, and T-L orientations for the [0/90] panel and in L-S and L-T orientations for the unidirectional panels. Ultrasonic C-scan evaluation was performed on the P-100/BSG-2 composites prior to sample preparation to ensure that the panels were of high quality. The only composite containing large regions of high attenuation was the composite containing carbon scrim cloth. These regions were located near the ends of the composite and were thought to correspond to either high fiber volume regions resulting from the loss of glass from the composite ends during fabrication or delaminated areas resulting from the use of the scrim cloth. These areas were avoided in the preparation of the impact samples.

UTRC Composite #	Fiber	Matrix	Orientation	Fiber Volume %	Thickness (mm)
626-88	P-100	BSG-2	[0/90]	35	11.8
627-88	P-100	BSG-2	0°	39	10.6
628-88	P-100 Scrim	BSG-2	0°	33 4	11.2
524-88	HMU	BSG-2	[0/90]	43	1.7

SUMMARY

Program Importance

The goal of this program is two-fold: (1) develop a fundamental understanding of the mechanisms controlling behavior in carbon fiber reinforced glasses and glass-ceramics, and; (2) use this information to improve this family of composite materials that is superior to any other in its combination of low density, strength, stiffness, toughness, and environmental stability. Glass and glass-ceramic matrices can withstand temperatures and environmental conditions far more severe than those tolerated by the more traditional matrices of polymers or metals. This characteristic combined with the high strength, stiffness, and toughness provided by carbon fibers results in a unique high performance composite material suited for critical applications. The easy formability of the glass matrix at high temperatures also permits the fabrication of a wide range of engineering shapes and sizes.

Approach

A variety of ultra-high elastic modulus pitch-based carbon fibers were combined with several different glass and glass-ceramic matrix compositions to produce unidirectionally reinforced composites. Composite performance was evaluated in several different areas, including tensile stress-strain behavior, flexural properties at both room and elevated temperature, thermal expansion, and fracture behavior. The importance of the fiber-matrix interface in the control of composite performance was central to the investigation.

Significant Progress

- Glass matrix composites with high strength (540-790 MPa) and high elastic modulus (300-350 GPa) and specific stiffness (135-165 x 10^7 cm) were fabricated by using ultra-high elastic modulus pitch-based carbon fibers as the reinforcement. Tensile stress-strain behavior was found to differ somewhat from that of HMU/Glass composites, particularly with respect to proportional limit (PL) stress and strain. Cyclic testing revealed that there was no loss in composite stiffness during cycles subsequent to being loaded to stress levels well above the PL, suggesting that severe matrix microcracking is not taking place at the PL. Fiber-matrix interfacial adhesion was found to be higher in composites containing pitch-based fiber relative to HMU fiber, which subsequently affected interlaminar shear strength and composite fracture behavior. This increased adhesion was believed to result primarily from the rougher surface of the pitch-based carbon fiber, with a possible contribution from the higher surface energy of pitch-based fiber relative of HMU.

- Residual matrix tensile stress (σ_m) resulting from differential thermal contraction between fiber and matrix was shown to have a strong influence on composite PL behavior. Reduction of σ_m by altering matrix composition resulted in significantly improved PL stress and strain in pitch fiber reinforced composites.

- Pitch/Glass composites were found to exhibit fairly linear coefficient of thermal expansion (CTE) behavior in the longitudinal direction over the temperature range of -150°C to +100°C, varying from approximately -0.75 ppm/°C to -1.0 ppm/°C. This CTE behavior was reproducible over several thermal cycles. The thermal strain behavior exhibited a hysteresis of less than 25 ppm over the entire thermal cycle.

- High temperature matrix compositions were developed which maintained the excellent tensile properties of pitch fiber reinforced composites while giving them the capability to preserve structural integrity up to temperatures of at least 800°C. The compositions providing the best composite mechanical properties were a high-SiO_2 glass and a glass-ceramic in the BMAS system.

- Composition was found to have a strong influence on the wetting behavior of glasses on carbon fibers. Gaining an awareness of the factors controlling wetting is important in understanding the influence of fiber-matrix adhesion on composite behavior. Among borosilicate glasses, it was found that the presence of Na_2O reduced the degree of wetting of carbon fibers by the glass. Glass compositions in the SiO_2-B_2O_3 binary system exhibited low contact angles and significant spreading on carbon fibers. Wetting behavior was also found to differ among HMU and pitch-based carbon fibers, primarily as the result of structural differences.

- A new glass system known as "oxycarbide glass" was developed using sol-gel processing techniques. The presence of carbon in the glass network in amounts up to 3.2% was found to have a significant effect on wetting behavior and thermal stability. Oxycarbide glasses demonstrated enhanced wetting behavior on carbon fibers as well as resisting devitrification at temperatures as high as 1100°C.

Future Plans

Work conducted on Contract N00014-85-C-0332 has been completed. Additional studies on the development of carbon fiber reinforced glass for structural applications in space are currently being performed on ONR Contract N00014-89-C-0046. This program is designed to enhance the readiness of C/Glass composites for implementation into structural components for space based systems, with particular emphasis on the use of high specific stiffness composite materials.

Acknowledgements

The authors gratefully acknowledge the support of the Innovative Science and Technology branch of the Strategic Defense Initiative Organization through the Office of Naval Research (Contract N00014-85-C-0332) with Dr. Steven Fishman as the contract monitor. They would also like to recognize Mr. William Kelley for composite fabrication, Ms. Judy Whitehead for carrying out for the SEM portions of the investigation, and the Mechanical Testing group at UTRC for performing the tensile and flexural testing.